

**TOWARDS FULL PRESERVATION OF
POLARIZATION OF PROTON BEAM IN THE
AGS**

Fanglei Lin

Submitted to the faculty of the Graduate School

in partial fulfillment of the requirement

for the degree

Doctor of Philosophy

in the Department of Physics

Indiana University

December 2007

Accepted by the Graduate Faculty, Indiana University, in partial fulfillment of the requirements for the degree of Doctor of Philosophy.

S. Y. Lee, Chairman, Ph.D.

M. H. Hess, Ph.D.

R. de Ruyter, Ph.D.

S. Setayeshgar, Ph.D.

M. Bai, Ph.D.

August 26th, 2007

Copyright ©2007 by
Fanglei Lin
ALL RIGHTS RESERVED

To Mom and Dad

You are my rock-firm supporters and make me truly believe I can conquer any difficulty and that tomorrow will be always better.

Acknowledgments

Many thanks to all the people who have helped and supported me during my graduate education. It might be difficult to name all of them here, but I sincerely appreciate the efforts of all who contributed to this work. There are a few people and groups that I would like to explicitly acknowledge.

Firstly, I would like to thank my thesis adviser professor S.Y.Lee in Indiana University Physics Department. I am feeling especially fortunate to be his student and get his earnest, constant guidance and encouragement all the time. Thanks to him for introducing me to work on spin physics and sending me to Brookhaven National Laboratory, where I made contact with many outstanding experts and got hands-on experience in the accelerator physics.

I am specially grateful to my supervisor Dr. M. Bai at Brookhaven Collider Accelerator Department for her sincere support and time she devoted to assisting me in many questions and my well being. I also sincerely thank Dr. T. Roser, Dr. H. Huang, Dr. A. U. Luccio, Dr. W. W. MacKay for their judicious advice and support. Their doors were always open to me to explain and discuss any problems of accelerator physics.

In addition, I would like to thank Dr. L. A. Ahrens, Dr. K. Brown, Dr. C. Gardner, Dr. E. D. Courant, J. W. Glenn, Dr. V. Ptitsyn, Dr. J. Takano, Dr. S. Tepikian, Dr. N. Tsoupas for all the help, discussions, suggestions and insights into various problems in spin physics, as well as in the practical skills for accelerator control in the Main Control Room where I was taking shifts in AGS. I also would like to thank John Woods and Roger Katz for always solving my computer related problems.

I thank all the operators, engineers and technicians who have contributed to the AGS polarized proton development at BNL. In particular, I acknowledge Dr. A. Zelenski for providing high and constant source polarization, K. Zeno for machine

tuning, Dr. Kin Yip and Seth Nemesure for polarimeter measurements. All of them made the machine run smoothly and made this thesis possible.

Again, I would like to thank my committee members Dr. Mark Harry Hess, Dr. Robert de Ruyter, Dr. Sima Setayeshgar for their suggestions and for taking time to attend my thesis defense. I am also indebted to all professors whose classes I took and enjoyed when I was at Bloomington, to the department secretaries Tracey Lynn Mc Gookey and June Karen Dizer who gave me their generous helps and assistances when I was off campus.

It is also my pleasure to thank all my friends and classmates, especially my best friends Weiming Guo and his family, Lin Wang and Jie Yang for their encouragement all the time. Their friendship will be deep in my heart forever.

Finally, I express my great gratitude to my parents for giving me life and also to the cares they have been giving to me. Thanks for their encouragement and support when I was in a low point of my life. This thesis would not exist at all without their love. Thanks to my little brother for the laughs and quarrels we had as we were together and to all of my relatives who care about me.

Abstract

Fanglei Lin

Towards Full Preservation of Polarization of Proton Beam in the AGS

As an injector to RHIC (Relativistic Heavy Ion Collider) at Brookhaven National Laboratory for spin program, the AGS (Alternating Gradient Synchrotron) is the bottleneck for preserving the polarization of proton beam from 2.4 GeV to 24 GeV. Because the spin tune ν_s is energy dependent, i.e. $\nu_s = G\gamma$ (G is the anomalous gyromagnetic g-factor, γ is the Lorentz factor), two major spin resonances, an imperfection resonance happening at $G\gamma = k$ and an intrinsic resonance happening at $G\gamma = k \pm \nu_y$ (k is integer and ν_y is the vertical betatron tune), can cause the beam to become depolarized completely during the acceleration. To overcome these resonances, local spin rotators called *Siberian snakes* are introduced to preserve the polarization of the proton beam in the AGS.

Two partial snakes (rotating the spin vector by an angle of less than 180°), a normal conducting helical dipole snake and a superconducting helical dipole snake, have been used in AGS 2006 polarized proton run. Separated by $1/3$ of the ring, the two partial snakes provide a spin tune gap that is wide enough to accommodate the vertical betatron tune ν_y so that both imperfection and intrinsic resonances are avoided. This configuration resulted in 65% polarization measured at the AGS extraction energy with a 82-86% polarization at the injection. However, there was still 20% polarization loss. Three possible reasons could explain the polarization loss: (1) horizontal intrinsic resonances happening at $\nu_s = k \pm \nu_x$ due to a non-vertical stable spin direction caused by the partial snakes, (2) residual vertical intrinsic resonances due to the low vertical tune at the beginning of the acceleration, (3) high order partial snake resonances.

Preliminary simulations using a simplified analytic model and spin tracking pro-

gram SPINK showed the existence of horizontal intrinsic resonances. With realistic AGS lattice parameters, acceleration rate, and partial snakes strengths, the results from both the simplified analytic model and multi-particle spin tracking agreed well when artificially removing the spin coherence (the spin components after one resonance are affected by the resonances they passed). The beam polarizations reach more than 10% loss from these simulations. Two kinds of experiments, horizontal polarization profile measurement and B-field scan, were carried out to explore the horizontal intrinsic resonance. Both results confirm the polarization loss. The horizontal intrinsic resonance strengths from the data fitting also agrees with the calculations from the simplified analytic model.

Because the vertical betatron tune was pushed to be inside the spin tune gap only after ramping past $G\gamma = 5$, leaving two weak intrinsic resonances in the acceleration cycle, the vertical motion could still cause depolarization. Therefore, vertical polarization profiles taken at the AGS extraction energy showed depolarization due to the vertical motion, which was consistent with the spin tracking simulations.

With high vertical betatron tunes inside the spin tune gap, modest depolarization can still be caused by high order partial snake resonances. Vertical betatron tune scans at several intrinsic resonance locations were also taken to explore these resonances experimentally. In addition, the vertical betatron tunes were close to integer 9 at the flat-top energies, the beam polarization was sensitive to the harmonic orbit correction. The measured polarization vs the 9th harmonic component of the orbit served as a merit of harmonic orbit correction. All of the simulation and experimental results are presented in this thesis. The properties of spin motion in the presence of partial snakes are also discussed.

_____	_____
_____	_____

Contents

1	Introduction	1
2	Spin Dynamics with Partial Siberian Snakes	5
2.1	General Spin Motion in a Synchrotron	5
2.2	Properties of Spin Motion with Partial Snakes	15
3	AGS Experimental Facility	19
3.1	AGS Configuration	19
3.2	Two Partial Siberian Snakes in the AGS	24
3.3	Coulomb-Nuclear Interference Polarimeter	29
4	Simulation and Experiment	33
4.1	Investigation of Horizontal Intrinsic Resonance	34
4.1.1	Simulation Results	34
4.1.2	Experimental Results	45
4.2	Investigation of Other Depolarizing Sources	56
4.2.1	Residual Vertical Intrinsic Resonances	56
4.2.2	High Order Partial Snake Resonances	65
4.2.3	Closed Orbit Distortion	72
5	Summary and Solution	77
5.1	Summary	77

5.2 Solution	81
A Transverse and Longitudinal Component of Magnetic Field with Re- spect to the Beam Direction	
85	
B Effective Froissart-Stora Formula for a Gaussian Distribution Beam	87
C Spinor Equation	89
D Horizontal Component of the Stable Spin Direction	91
E Spin Rotation for Spin Tracking	95

List of Tables

3.1	Locations of quadrupoles and multipoles in the AGS	21
3.2	Parameters of three CNI polarimeter targets.	30
4.1	Experimental data for horizontal polarization profile measurements with two partial snakes at 10% plus 5.9% and 14% plus 5.9%.	47
4.2	Fitted parameters from beam profiles. A is the normalized count rate at the beam center, x_0 is the beam center position, and σ is the hori- zontal rms beam size.	48
4.3	Fitted parameters from horizontal polarization profiles. P_i is the initial polarization at injection and $K = \frac{\epsilon(\gamma)}{\sqrt{\gamma}}$ is the energy independent factor.	49
4.4	Beam parameters used in the calculation of rms beam size σ_β due to the betatron motion.	51
4.5	Comparison of K values between the calculation and the fitting for two different partial snakes configurations.	51
4.6	Part of the B-field scan data.	54
4.7	Important parameters from four spin trackings with different vertical tune paths. Different colors represent different trackings as shown in Fig. 4.9.	63
4.8	Calculated strengths of the two intrinsic resonances from DEPOL with different vertical tune paths.	64

4.9	Strengths of four strong intrinsic resonances calculated by DEPOL in the bare AGS machine assuming particle at a normalized rms emittance 2.5 mm-mrad.	65
4.10	High order partial snake resonance locations for both 10% (2.1 T) cold snake plus 5.9% (1.53 T) warm snake and 14% (2.5 T) cold snake plus 5.9% (1.53 T) warm snake conditions.	69
4.11	AGS imperfection resonance strengths calculated using DEPOL with different closed orbit distortions and vertical tune close to 9 at $G\gamma = 36 + \nu_y$	74

List of Figures

2.1	The curvilinear coordinate system for a particle motion in a circular accelerator. \hat{x} , \hat{s} and \hat{y} are the unit basis vectors along the radially outward, the longitudinally forward and the vertically transverse directions and form a right-handed system.	7
2.2	Spin tune from Eq. (2.36) (top plot) and vertical component of the stable spin direction Eq. (2.39) (bottom plot) as a function of $G\gamma$ with two partial snakes separated by 1/3 of the ring in the AGS. The solid curves are for 10% cold snake and 5.9% warm snake; the dashed ones are for 14% cold snake and 5.9% warm snake.	17
3.1	Acceleration complex for polarized proton at Brookhaven National Laboratory.	20
3.2	AGS ramp rate of $\alpha = \frac{dG\gamma}{d\theta}$ as a function of time in an acceleration cycle.	22
3.3	Schematic drawing of the AGS polarized proton complex.	23
3.4	AGS warm snake spin rotation angle as function of γ	27
3.5	AGS cold snake spin rotation angle as function of γ	28

4.1	Simplified analytic model and multi-particle tracking with a Gaussian distribution in horizontal phase space. The upper plot is for 10% and 5.9% partial snakes; the lower one is for 14% and 5.9% partial snakes. Both simplified analytic model and simulation have the same normalized rms horizontal emittance, zero vertical emittance and 8.72 horizontal tune. The multi-particle tracking shows that the spin coherence results in less polarization loss comparing to the simplified analytic model.	42
4.2	Spin tracking from both simplified analytic model and multi-particle with Gaussian Distribution. The upper plot is for 10% and 5.9% partial snakes; the lower one is for 14% and 5.9% partial snakes. Both simplified analytic model and simulation have the same normalized rms horizontal emittance, zero vertical emittance and 8.72 horizontal tune. The spin coherence is artificially removed from the multi-particle tracking.	44
4.3	Horizontal polarization profiles (upper) and horizontal beam profiles (bottom) in the AGS for two different strength of the partial snakes. The solid curves are for 10% cold snake and 5.9% warm snake, and the dashed ones for 14% cold snake and 5.9% warm snake. The beam profile curves are fitted using Eq. (4.19) and polarization profile curves are fitted using Eq. (4.22) after crossing 82 isolated horizontal intrinsic resonances.	50
4.4	One B-field scan from the AGS 2006 polarized proton run. Black dots are for the calculated $G\gamma$ and red diamonds are for the calibrated $G\gamma$. The horizontal betatron tune was around 8.64.	55
4.5	Vertical polarization profile (upper) and vertical beam profile (bottom) in the AGS for the 10% cold snake and 5.9% warm snake configuration.	57

4.6	Fractional part of the measured vertical tunes (dots are connected by a dashed line) and spin tune with 10% cold snake and 5.9% warm snake as a function of $G\gamma$	58
4.7	Fractional part of the measured vertical tunes (dots connected by a line) and spin tune with 10% cold snake and 5.9% warm snake at the early part of the energy ramp.	59
4.8	Spin tracking through the first two weak intrinsic resonances with 10% (2.1 T) cold snake and 5.9% (1.53 T) warm snake. The polarization is obtained along the stable spin direction.	60
4.9	Spin trackings through the first two weak intrinsic resonances with different vertical tune paths. The polarization is obtained along the stable spin direction.	63
4.10	Vertical tune scan at $12 + \nu_y$ (weaker) and $36 + \nu_y$ (stronger) intrinsic resonance position for 14% (2.5T) cold snake plus 5.9% (1.53T) warm snake.	67
4.11	Vertical tune scan at $12 + \nu_y$ and $36 - \nu_y$ with 14% (2.5T) cold snake and 5.9% (1.53T) warm snake.	68
4.12	Spin tracking with constant vertical betatron tunes located at high order partial snake resonance locations with 14% (2.5T) cold snake and 5.9% (1.53T) warm snake.	70
4.13	Spin tracking with constant vertical betatron tunes located at high order partial snake resonance locations with 10% (2.1T) cold snake and 5.9% (1.53T) warm snake.	71
4.14	Measured polarization as a function of vertical $\sin 9\theta$ harmonic amplitude. 73	
4.15	Imperfection resonance strengths calculated using DEPOL as a function of different vertical $\sin 9\theta$ harmonic amplitude at $36 + \nu_y$	75

-
- 4.16 Comparison of the polarization vs. the vertical $\sin 9\theta$ harmonic amplitude while crossing the imperfection resonance at $G\gamma = 45$ between spin tracking and experiment. The vertical axis is the ratio of polarization after and before resonance, the horizontal axis is the vertical $\sin 9\theta$ harmonic amplitude. The locations of polarization dip agree well between the simulation and experiment. 76
- 5.1 A simple spin tracking by putting one single particle at the normalized rms emittance 2.5π mm-mrad ellipse in the horizontal phase space. The horizontal tune was set at 8.985 inside the spin tune gap generated by 10% (2.1 T) cold snake and 5.9% (1.53 T) warm snake. The tracking result shows no depolarization. 82
- 5.2 Spin tracking of 100 particles with Gaussian distribution in the vertical phase space. The normalized rms vertical emittance was set at 2.5π mm-mrad, and zero for the horizontal emittance. The upper plot is the vertical tune path. The bottom plot is the tracking result, which shows significantly less depolarization comparing to Fig.4.8. 84

Chapter 1

Introduction

Introduced by Uhlenbeck and Goudsmit to explain the result of Stern-Gerlach experiments, spin has become a fundamental concept and plays an important role in the interactions of elementary particles. To study spin interactions in the quark and gluon level, one employs collision of intense beams of polarized protons at high energy. The Relativistic Heavy Ion Collider (RHIC) at Brookhaven National Lab provides a unique facility for this study. Here, polarized protons can be brought into any energy for collisions from 50 to 500 GeV center of mass energy. The design calls for an intensity of 2×10^{11} proton/bunch with a polarization of 70%. As the injector to RHIC, the Alternating Gradient Synchrotron (AGS) is mostly the bottleneck to preserve polarization.

When polarized protons are accelerated in an accelerator, the spins of the particles will precess because of the spin interactions with the magnetic fields. In a perfect circular accelerator with only vertical guiding dipole magnetic fields, the spin vector precesses around the vertical direction called stable spin direction \hat{n}_{co} that is defined as the invariant spin vector after a complete orbit revolution for a given location in the accelerator. The number of spin precessions per orbital revolution is called spin tune ν_s . Horizontal magnetic fields can perturb the spin vector away from the

vertical, causing spin polarization loss when the spin precession frequency equals the frequency of the spin perturbing magnetic fields. Two main types of spin resonances are the imperfection resonances driven by the vertical closed orbit errors in dipoles and quadrupoles, and vertical intrinsic resonances driven by the vertical betatron motion in quadrupoles. For an accelerator with P superperiods of the lattice, the imperfection resonances happen at $G\gamma = n$ and the intrinsic resonances happen at $G\gamma = kP \pm \nu_y$, where $G = \frac{g-2}{2}$ is the anomalous gyromagnetic g-factor, γ is the Lorentz factor, $G\gamma$ is the unperturbed spin precession tune, n, k are integers, ν_y is the vertical betatron tune. In addition, there are also other higher-order depolarization resonances due to the linear horizontal and vertical betatron coupling, nonlinear magnetic fields provided by the higher order magnetic multipoles, and by synchrotron oscillations. However, the resulting depolarization due to the latter effects can be negligible if these high order spin resonances are much weaker than the two types of main spin resonances. In the AGS, the polarized proton beams are accelerated from 2.35 GeV to 24 GeV, passing 41 imperfection resonances and 7 strong intrinsic resonances from injection to extraction. These resonances can totally destroy the polarization of the proton beam.

In order to overcome the spin depolarizing resonances, Derbenev and Kondratenko proposed in 1978 to use a local magnet called *Siberian snake* to rotate the spin vector around a horizontal axis by 180° [1]. In the presence of the snake, the spin tune becomes $\frac{1}{2}$, and the perturbations of spin motion from the dipole errors are canceled in every two successive revolutions. Since the depolarizing resonance strength in the medium energy synchrotron is not strong, a partial snake [2, 3, 4] that rotates spin vector by less than 180° can be strong enough to overcome both imperfection and intrinsic resonances provided that the betatron tunes are placed within a range of resonance free gap called spin tune gap. For instance, two partial helical dipole snakes have been successfully commissioned in the AGS. The cold snake is a super conducting helical dipole snake with a maximum field of 3 Tesla [5, 6]. The warm snake is a normal

conducting helical dipole snake at 1.53 Tesla [7]. With the combination of the two partial snakes, high intensity (1.5×10^{11} proton/bunch) polarized proton beam (65% polarization) was achieved at the AGS extraction energy in the 2006 with 82-86% polarization at the injection.

With the two partial snakes in the AGS the stable spin direction is not vertical, therefore the perturbing fields that rotate the spin away from the stable direction have vertical as well as horizontal components. Particles undergoing horizontal betatron oscillation encounter vertical field deviations at the horizontal oscillation frequency. As a result, resonances with the spin tune are driven by the horizontal betatron oscillations, and will occur whenever the spin tune satisfies $\nu_s = n \pm \nu_x$. This type of resonance is called horizontal intrinsic resonance [8]. A proper understanding of the behavior of this type resonance is needed so that the full polarization transmission can be implemented for reaching the RHIC spin project goals.

This thesis studies ideas in achieving a full polarization for the AGS. Chapter 2 provides the general spin motion in a synchrotron and the spin dynamics with partial Siberian snake(s) dealing with the normal polarization issues. In Chapter 3, AGS experimental facilities for the investigation of polarization are described. Experimental results and analyses of the exploration of the polarization in AGS follow in Chapter 4. In this part, not only the horizontal intrinsic resonance but also other factors leading to beam depolarization are presented. Finally, the summary and conclusion are given in Chapter 5.

Chapter 2

Spin Dynamics with Partial Siberian Snakes

2.1 General Spin Motion in a Synchrotron

I Basic Spin Motion

For a beam with a large number of particles in an accelerator, the polarization is defined as the ensemble averaged spin vector in a classical picture. For a system of spin- $\frac{1}{2}$ particles, the degree of polarization is given as,

$$P = \frac{N_+ - N_-}{N_+ + N_-}, \quad (2.1)$$

where N_{\pm} are the numbers of particles in two spin state $|\frac{1}{2}, \pm\frac{1}{2}\rangle$ along a quantization axis. When the spin states of all particles are along one quantized axis, the beam is 100% polarized with $P = \pm 1$. Three parameters are needed to specify the polarization of spin- $\frac{1}{2}$ particles: two parameters for the quantized axis and one for N_+/N_- ratio. Therefore, the polarization of the spin- $\frac{1}{2}$ system is a vector characterized by a direction and a magnitude. The polarization is the ensemble average of the spin vector given by $\vec{P} = \frac{2}{\hbar} \langle \vec{S}_R \rangle = \langle \vec{\sigma} \rangle$ using the Pauli spin matrices $\vec{\sigma}$.

In the rest frame of a moving particle in a synchrotron, the motion of spin vector under the external electro-magnetic field is described by the Thomas-BMT equation [9, 10]

$$\frac{d\vec{S}}{dt} = \frac{e}{\gamma m} \vec{S} \times \left[(1 + G\gamma) \vec{B}_\perp + (1 + G) \vec{B}_\parallel + \left(G\gamma + \frac{\gamma}{\gamma + 1} \right) \frac{\vec{E} \times \vec{\beta}}{c} \right] \quad (2.2)$$

where the spin vector \vec{S} is in the particle rest frame and \vec{B}_\perp and \vec{B}_\parallel are the transverse and longitudinal components of the magnetic fields in the laboratory frame with respect to the particle's velocity $\vec{\beta}c$. γ is the Lorentz factor, $G = \frac{g-2}{2}$ is the anomalous gyromagnetic factor which has the value 1.7928 for proton, and the vector \vec{E} stands for the electric field.

The Thomas-BMT equation shows that the spin vector precesses around the transverse magnetic field at a rate $\frac{1}{\gamma}(1 + G\gamma)$, and around the longitudinal magnetic field at a rate $\frac{1}{\gamma}(1 + G)$. Typically, the terms involving \vec{E} is usually small comparing to those involving the magnetic fields \vec{B}_\parallel and \vec{B}_\perp . For most of our discussion of spin motion the electric field has been neglected for the simplification of the Thomas-BMT equation.

Since the particles of a beam bunch in an accelerator circulate around a reference orbit, the Thomas-BMT equation can be expressed around this reference orbit in the Frenet-Serret coordinate system following Courant and Ruth [11, 12] as shown in Fig. 2.1, where the three unit basis vectors along the radially outward \hat{x} , longitudinally forward \hat{s} , and vertically transverse \hat{y} . In a planar circular accelerator, we have

$$\frac{d\hat{x}}{ds} = \frac{\hat{s}}{\rho}, \quad \frac{d\hat{s}}{ds} = \frac{-\hat{x}}{\rho}, \quad \frac{d\hat{y}}{ds} = 0, \quad (2.3)$$

where ρ is the local radius of curvature of the reference orbit. A particle's motion in this coordinate system is given by

$$\vec{r} = r_0(s) + x\hat{x} + y\hat{y}, \quad (2.4)$$

$$\vec{v} = \frac{d\vec{r}}{dt} = \frac{ds}{dt} \left[x' \hat{x} + \left(1 + \frac{x}{\rho} \right) \hat{s} + y' \hat{y} \right], \quad (2.5)$$

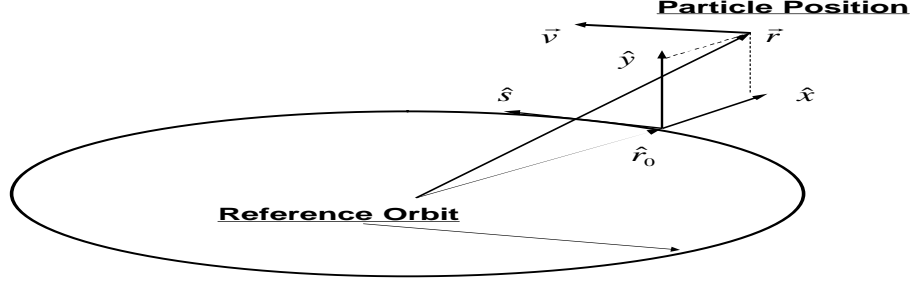


Figure 2.1: The curvilinear coordinate system for a particle motion in a circular accelerator. \hat{x} , \hat{s} and \hat{y} are the unit basis vectors along the radially outward, the longitudinally forward and the vertically transverse directions and form a right-handed system.

with \vec{r}_0 being the reference orbit and $\hat{s} = \frac{d\vec{r}_0}{ds}$.

The transverse and longitudinal component of the magnetic field can also be expressed under the Frenet-Serret coordinate system (See Appendix A),

$$\vec{B}_\perp = B\rho \left(1 - \frac{x}{\rho}\right) \left[\left(x'' - \frac{1}{\rho}\right) \hat{y} + \frac{y'}{\rho} \hat{s} - y'' \hat{x} \right], \quad (2.6)$$

$$\vec{B}_\parallel = (B_s + y' B_y) \hat{s} = -B\rho \left(\frac{y}{\rho}\right)' \hat{s}. \quad (2.7)$$

Here $B\rho$ standing $\gamma mv/e$ is the magnetic rigidity of the particle.

Then translating the time independent variable to the bending angle in a dipole by using $\frac{d}{dt} = \frac{v}{\rho+x} \frac{d}{d\theta}$, Eq. (2.2) becomes

$$\frac{d\vec{S}}{d\theta} = \vec{S} \times \vec{F}. \quad (2.8)$$

The vector F is

$$\begin{aligned}
\vec{F} &= F_1 \hat{x} + F_2 \hat{s} + F_3 \hat{y} \\
&= [-\rho y''(1 + G\gamma)] \hat{x} \\
&\quad + [(1 + G\gamma)y' - \rho(1 + G)(\frac{y}{\rho})'] \hat{s} \\
&\quad + [-(1 + G\gamma) + (1 + G\gamma)\rho x''] \hat{y}.
\end{aligned} \tag{2.9}$$

Introducing three θ -independent unit vectors $(\hat{e}_1, \hat{e}_2, \hat{e}_3)$ coinciding with $(\hat{x}, \hat{s}, \hat{y})$ at any azimuth in the ring, Eq. (2.8) can be expressed as

$$\frac{d\vec{S}}{d\theta} = \vec{n} \times \vec{S}, \tag{2.10}$$

where

$$\vec{n} = -[F_1 \hat{e}_1 + F_2 \hat{e}_2 - G\gamma \hat{e}_3]. \tag{2.11}$$

In an ideal planar accelerator with only the vertical bending magnetic fields ($F_1 = F_2 = 0$), the spin vector will precess around the vertical direction by $G\gamma$ per orbital revolution. The spin vector will stay in the vertical direction if it is set initially vertical. Any spin vectors of the particles not lying on the vertical direction will precess around the vertical direction with $G\gamma$ spin precession turns per revolution during the acceleration. Thus the vertical direction is called the stable spin direction or spin closed orbit, which means the spin vector comes back to the same direction at a certain azimuthal position after one revolution, and $\nu_s = G\gamma$ is the spin tune in such ideal planar accelerator.

II Spin Resonances

In most synchrotrons, the vertical direction has been considered as the polarization direction because of the vertical guiding dipole fields. The sources of depolarization for a vertically polarized beam come from the horizontal components of the magnetic fields \vec{B}_{\parallel} and \vec{B}_{\perp} . Since the accelerators are mainly composed of bending magnets

and quadrupoles, the horizontal magnetic field components due to dipole rolls and quadrupoles can precess the spin away from the vertical direction. Additionally, perturbing fields can also come from multipoles and the synchrotron motion. Based on the sources of depolarization, the spin resonances can be classified to imperfection resonance, intrinsic resonance and high-order resonance.

The imperfection resonances are driven by the vertical closed orbit displacement from the center of a quadrupole due to the dipole rolls or quadrupole misalignments. Since the field errors perturb the spin vector in every revolution, the imperfection resonances happen at each $G\gamma = \text{integer}$, where $G\gamma$ is the spin tune and the resonance strength is proportional to the vertical closed orbit distortion. The intrinsic resonances are driven by the vertical betatron motion in quadrupoles, where the horizontal focusing magnetic fields are present. For an accelerator with P superperiods of the lattice, the intrinsic resonances happen at $G\gamma = kP \pm \nu_y$, where k is integer and ν_y is the vertical betatron tune. The high-order resonances are driven by other different mechanisms. For instance, the synchrotron sideband resonances come from the synchrotron motion modulation (energy oscillations) around the primary spin resonances. Coupling spin resonances arise from the linear coupling of the horizontal and vertical betatron motion.

Using the Thomas-BMT equation, the spin resonance strength can be given by [10]

$$\epsilon_K = \frac{1}{2\pi} \oint [(1 + G\gamma) \frac{\Delta B_x}{B\rho} + (1 + G) \frac{\Delta B_{\parallel}}{B\rho}] e^{iK\theta} ds. \quad (2.12)$$

Here ΔB_x is the radial perturbing field, ΔB_{\parallel} is the longitudinal perturbing field. The spin resonance strength can also be expressed in terms of particle coordinates

$$\epsilon_K = \frac{-1}{2\pi} \oint [(1 + G\gamma)(\rho z'' + iz') - i\rho(1 + G)(\frac{z}{\rho})'] e^{iK\theta} d\theta, \quad (2.13)$$

where ρ is the local orbit curvature, z is the vertical displacement of the beam from the center of a quadrupole, and K is the resonance spin tune.

III Froissart-Stora Formula

Under a constant resonance crossing rate $\alpha = \frac{d(G\gamma)}{d\theta}$, the final polarization of a beam after passing through an isolated spin resonance ϵ is given by the Froissart-Stora formula [13],

$$\left\langle \frac{P_f}{P_i} \right\rangle = 2e^{-\pi \frac{|\epsilon|^2}{2\alpha}} - 1. \quad (2.14)$$

The effect of the resonance on the polarization is determined by the ratio of $\pi \frac{|\epsilon|^2}{\alpha}$. For a weak resonance, the polarization can be preserved if the resonance is crossed with a high speed that produces $\pi \frac{|\epsilon|^2}{\alpha} \ll 1$. On the other hand, a strong resonance can be overcome by a full spin flip with the condition $\pi \frac{|\epsilon|^2}{\alpha} \gg 1$. For example, 99% polarization can be maintained if $\epsilon \leq 0.056\sqrt{\alpha}$, and 99% spin flip can be obtained if $\epsilon \geq 1.8\sqrt{\alpha}$.

A beam bunch is composed of particles with different betatron amplitudes and phases, the beam polarization is the ensemble average of spin vectors of particles in the bunch. Therefore, given a beam distribution $\rho(I)$ as a function of the emittance, the polarization after passing through a resonance is given by

$$\left\langle \frac{P_f}{P_i} \right\rangle = \int_0^\infty [2e^{-\pi \frac{|\epsilon|^2}{2\alpha}} - 1] \rho(I) dI, \quad (2.15)$$

with

$$\int \rho(I) dI = 1. \quad (2.16)$$

Here P_i and P_f are the polarization before and after crossing the resonance. Normally, the intrinsic resonance strength is proportional to the square root of the particle emittance I ,

$$|\epsilon(I)|^2 = |\epsilon(I_0)|^2 \frac{I}{I_0}, \quad (2.17)$$

where I_0 is the rms emittance of the beam, $\epsilon(I_0)$ is the rms value of resonance strength. For a beam with Gaussian distribution $\rho(I) = \frac{1}{2I_0} e^{-\frac{I}{2I_0}}$ in the phase space, we have

(See Appendix B)

$$\left\langle \frac{P_f}{P_i} \right\rangle = \frac{1 - \frac{\pi |\epsilon(I_0)|^2}{\alpha}}{1 + \frac{\pi |\epsilon(I_0)|^2}{\alpha}} \quad (2.18)$$

IV Siberian Snake

In order to maintain polarization in a synchrotron, an effective approach, proposed by Derbenev and Kondratenko, is to use Siberian snakes [1]. Siberian snakes are local spin rotators that cause the spin vector to precess by an angle of less than or equal to 180° around an axis in the horizontal plane.

A full Siberian snake, rotating the spin vector by an angle of 180° , forces the spin tune to be $\frac{1}{2}$, independent of energy. Any perturbation on the spin from the magnetic field errors in the accelerator lattice can be canceled in successive turns. Therefore, a full snake is strong enough to overcome all type of spin resonances. A partial Siberian snake rotates the spin vector by an angle of less than 180° . The resulting spin tune is energy dependent. A partial snake can overcome weak imperfection resonance by shifting the spin tune away from the integers. It can also overcome the intrinsic resonances if betatron tunes are located in the spin tune gap. The details of spin dynamics with partial Siberian snake(s) will be discussed in the next section.

The full and partial Siberian snakes have their own virtues and shortcomings. A full snake can overcome all type spin resonances but need a long straight space to accommodate its magnet(s). For instance, each of four full Siberian snakes in RHIC is 10.4 meters long. A partial snake does not need a long straight section in the machine lattice. However, it can overcome the imperfection resonances by shifting the spin tune away from the integers. For a medium energy accelerator, a strong enough partial snake can overcome both imperfection and intrinsic resonances with a proper accommodation of vertical betatron tunes. For example, two 3 meters partial snakes are used in the AGS due to the limitation of the available straight section. Therefore, considering the cost and space constraints, the full snake is necessary for

the high-energy accelerator and partial snake is a practical solution for the medium energy accelerator.

V Spinor Equation

Generally, a spin $\frac{1}{2}$ particle occupies one of the two eigenstates or a mixture of them with a certain probability distribution. The spin state of the spin $\frac{1}{2}$ particle is expressed by a two-component spinor wave function $\Psi = \begin{pmatrix} u \\ d \end{pmatrix}$. Here u and d are the probabilities of the particle in the two pure spin states. Therefore, the spin vector \vec{S} with three components (S_1, S_2, S_3) can be expressed by the two-component spinor as

$$S_i = \langle \Psi | \sigma_i | \Psi \rangle = \Psi^\dagger \sigma_i \Psi, \quad (2.19)$$

where σ_i , $i = 1, 2, 3$ are the Pauli matrices,

$$\sigma_1 = \begin{pmatrix} 0 & 1 \\ 1 & 0 \end{pmatrix}, \quad \sigma_2 = \begin{pmatrix} 0 & i \\ -i & 0 \end{pmatrix}, \quad \sigma_3 = \begin{pmatrix} 1 & 0 \\ 0 & -1 \end{pmatrix}. \quad (2.20)$$

From the Thomas-BMT equation

$$\frac{d\vec{S}}{d\theta} = \vec{S} \times \vec{F}, \quad (2.21)$$

the spin equation can be represented for the spinor (See Appendix C)

$$\frac{d\Psi}{d\theta} = \frac{-i}{2}(\vec{\sigma} \cdot \vec{n})\Psi = \frac{-i}{2}H\Psi = \frac{-i}{2} \begin{pmatrix} G\gamma & -\xi \\ -\xi^* & -G\gamma \end{pmatrix} \Psi, \quad (2.22)$$

where H is the spin precessing kernel and $\vec{\sigma}$ is the Pauli spin matrices. Equation (2.22) is equivalent to Eq. (2.2) and Eq. (2.10) in describing the spin motion in a synchrotron. The three components of spin vector are obtained using the spinor Ψ by

$$S_1 = u^*d + ud^*, \quad S_2 = -i(u^*d - ud^*), \quad S_3 = |u|^2 - |d|^2. \quad (2.23)$$

The off-diagonal matrix element of $\xi(\theta) = F_1 - iF_2$ produces spin mixing between the up-down components of the spinor Ψ . For an accelerator with no snake, $\xi(\theta) = F_1 - iF_2$ causes the spin depolarization due to the vertical motion. Because of the periodic or quasi-periodic betatron motion of particles, the depolarization driving term $\xi(\theta)$ can be expanded in Fourier series

$$\xi(\theta) = \sum_K \epsilon_K e^{-iK\theta}. \quad (2.24)$$

The Fourier amplitude ϵ_K is called the resonance strength, the corresponding frequency K is called the spin resonance tune.

With an artificially introduced snake to overcome the spin resonances by precessing the spin vector less than or equal to 180° locally, $\xi(\theta) = F_1 - iF_2$ becomes more complicated because of the revised three components of vector F . Simplifying the analytic model, the snake will be treated as a local spin rotator: kicking the spin vector around the snake axis by a certain angle but no effect on the transverse motions in the rest of the machine lattice. This results in the spinor equation Eq. (2.22) not being altered in the whole synchrotron except at the snake location, where the artificial spin rotation is introduced.

The spin motion equation throughout the snake location θ_s still has the same form

$$\frac{d\vec{S}}{d\theta} = \vec{S} \times \vec{F}, \quad (2.25)$$

but the integral should be from θ_s^- to θ_s^+ locally. Depending on the snake axis, the three components of \vec{F} will be given differently. Assuming the snake strength ζ , two basic snake axis conditions are considered here.

1. For the snake axis in a horizontal plane with $\hat{n}_s = \cos \phi_s \hat{e}_1 + \sin \phi_s \hat{e}_2$, it has

$$\begin{aligned} F_1 &= -\rho z''(1 + G\gamma) + \zeta \delta(\theta - \theta_s) \cos \phi_s \\ F_2 &= (1 + G\gamma)z' - \rho(1 + G)\left(\frac{z}{\rho}\right)' + \zeta \delta(\theta - \theta_s) \sin \phi_s \\ F_3 &= -(1 + G\gamma) + (1 + G\gamma)\rho x''. \end{aligned}$$

Then the spinor equation still has

$$\frac{d\Psi}{d\theta} = \frac{-i}{2} \begin{pmatrix} G\gamma & -\xi \\ -\xi^* & -G\gamma \end{pmatrix} \Psi, \quad (2.26)$$

except that the off-diagonal matrix element ξ becomes

$$\xi(\theta) = \zeta\delta(\theta - \theta_s) + \sum_K \epsilon_k e^{-iK\theta}. \quad (2.27)$$

The snake is located at the θ_s azimuthal angle in the ring with value of ζ resonance strength. The Fourier amplitude ϵ_K is the resonance strength arising from the spin perturbing fields in the whole ring, K is the resonance tune.

2. For the snake axis in vertical plane with $\hat{n}_s = \cos\phi_s\hat{e}_1 + \sin\phi_s\hat{e}_3$, it has

$$\begin{aligned} F_1 &= -\rho z''(1 + G\gamma) + \zeta\delta(\theta - \theta_s)\cos\phi_s \\ F_2 &= (1 + G\gamma)z' - \rho(1 + G)\left(\frac{z}{\rho}\right)' \\ F_3 &= -(1 + G\gamma) + (1 + G\gamma)\rho x'' + \zeta\delta(\theta - \theta_s)\sin\phi_s. \end{aligned}$$

Then the spinor equation becomes

$$\frac{d\Psi}{d\theta} = \frac{-i}{2} \begin{pmatrix} G\gamma - \zeta\delta(\theta - \theta_s)\sin\phi_s & -\xi \\ -\xi^* & -(G\gamma - \zeta\delta(\theta - \theta_s)\sin\phi_s) \end{pmatrix} \Psi, \quad (2.28)$$

where the off-diagonal matrix element ξ has

$$\xi(\theta) = \zeta\delta(\theta - \theta_s)\cos\phi_s + \sum_K \epsilon_k e^{-iK\theta}. \quad (2.29)$$

ϕ_s is the angle of snake axis with respect to the vertical direction.

By introducing an additional δ function, the spinor equations describe the spin motion with a snake at the location θ_s . The spinor wave function Ψ can be obtained by solving the spinor equation. And the propagation of the spinor wave function can be tracked using the spin transfer matrix (STM) $t(\theta_f, \theta_i)$ as

$$\psi(\theta_f) = t(\theta_f, \theta_i)\psi(\theta_i). \quad (2.30)$$

Because the polarization vector is real, the matrix elements of the STM satisfy

$$t_{22} = t_{11}^*, \quad t_{21} = -t_{12}^*, \quad (2.31)$$

and

$$t^\dagger t = I, \quad (2.32)$$

where I is the unit matrix.

For an accelerator, the magnetic fields are mostly piecewise constant, the final spinor wave function is given by the product of STM,

$$\psi(\theta_f) = \prod_{j=1}^N t(\theta_{j+1}, \theta_j) \psi(\theta_i). \quad (2.33)$$

A one turn map (OTM) for the stable spin direction is obtained by multiplying the spin transfer matrices in one revolution around the accelerator, which can be expressed as

$$t(\theta_i + 2\pi, \theta_i) = e^{-i\pi\nu_s \hat{n}_{co} \cdot \vec{\sigma}}. \quad (2.34)$$

Here ν_s is the spin tune, defined as the number of spin precession around the stable spin direction per revolution, \hat{n}_{co} is the stable spin direction on the closed orbit, which is the direction along the spin vector under OTM.

2.2 Properties of Spin Motion with Partial Snakes

In a perfect accelerator, the spin tune ν_s equals $G\gamma$ and the stable spin direction \hat{n}_{co} is vertical. The introduction of snake(s) revises the spin tune and stable spin direction, resulting in the resonance condition never being met. Therefore, a snake is a good approach to overcome spin resonances.

For the convenience of discussion, the configuration of two partial snakes in the AGS machine is considered in the following description. The two partial snakes, separated by 1/3 of the ring, are used to overcome the spin resonances in the AGS,

one is called the cold partial snake and the other the warm partial snake. Both of the snake rotation axes are along the longitudinal direction. Given χ_c and χ_w , the spin rotation angles caused by cold and warm snakes respectively, the closed orbit of OTM of the spin transfer matrix becomes

$$T = e^{-i\frac{1}{2}G\gamma(2\pi-\frac{2\pi}{3}-\theta)\sigma_3} e^{-i\frac{\chi_w}{2}\sigma_2} e^{-i\frac{1}{2}G\gamma\frac{2\pi}{3}\sigma_3} e^{-i\frac{\chi_c}{2}\sigma_2} e^{-i\frac{1}{2}G\gamma\theta\sigma_3}, \quad (2.35)$$

where θ is the orbital angle between the measurement location and the cold partial snake. Identifying the OTM to Eq. (2.34), the spin tune ν_s and spin closed orbit $\hat{n}_o = \cos\alpha_1\hat{e}_1 + \cos\alpha_2\hat{e}_2 + \cos\alpha_3\hat{e}_3$, where $(\cos\alpha_1, \cos\alpha_2, \cos\alpha_3)$ are the spin closed orbit directional cosines along the radially outward, longitudinally forward and vertically transverse axes respectively, are given by (See Appendix D)

$$\begin{aligned} \nu_s &= \frac{1}{\pi} \arccos \left(\cos \frac{\chi_c}{2} \cos \frac{\chi_w}{2} \cos [G\gamma\pi] - \right. \\ &\quad \left. \sin \frac{\chi_c}{2} \sin \frac{\chi_w}{2} \cos [G\gamma\frac{\pi}{3}] \right), \end{aligned} \quad (2.36)$$

$$\begin{aligned} \cos\alpha_1 &= \frac{-1}{\sin\pi\nu_s} \left(\cos \frac{\chi_w}{2} \sin \frac{\chi_c}{2} \sin [G\gamma(\pi - \theta)] + \right. \\ &\quad \left. \sin \frac{\chi_w}{2} \cos \frac{\chi_c}{2} \sin [G\gamma(\frac{\pi}{3} - \theta)] \right), \end{aligned} \quad (2.37)$$

$$\begin{aligned} \cos\alpha_2 &= \frac{1}{\sin\pi\nu_s} \left(\cos \frac{\chi_w}{2} \sin \frac{\chi_c}{2} \cos [G\gamma(\pi - \theta)] + \right. \\ &\quad \left. \sin \frac{\chi_w}{2} \cos \frac{\chi_c}{2} \cos [G\gamma(\frac{\pi}{3} - \theta)] \right), \end{aligned} \quad (2.38)$$

$$\begin{aligned} \cos\alpha_3 &= \frac{1}{\sin\pi\nu_s} \left(\cos \frac{\chi_w}{2} \cos \frac{\chi_c}{2} \sin [G\gamma\pi] - \right. \\ &\quad \left. \sin \frac{\chi_w}{2} \sin \frac{\chi_c}{2} \sin [\frac{G\gamma}{3}\pi] \right). \end{aligned} \quad (2.39)$$

Equations (2.36) to (2.39) show that the spin tune ν_s and stable spin direction \hat{n}_{co} at azimuthal location θ depend on energy $G\gamma$ as well as two snake rotation angles χ_c and χ_w . Figure 2.2 shows the spin tune and vertical component of the stable spin direction as functions of $G\gamma$. Two conditions of snakes are presented, one for a 14% cold snake and a 5.9% warm snake, one for a 10% cold snake and a 5.9% warm snake. The quoted percentage of snake strength is given as the fraction of the snake rotation

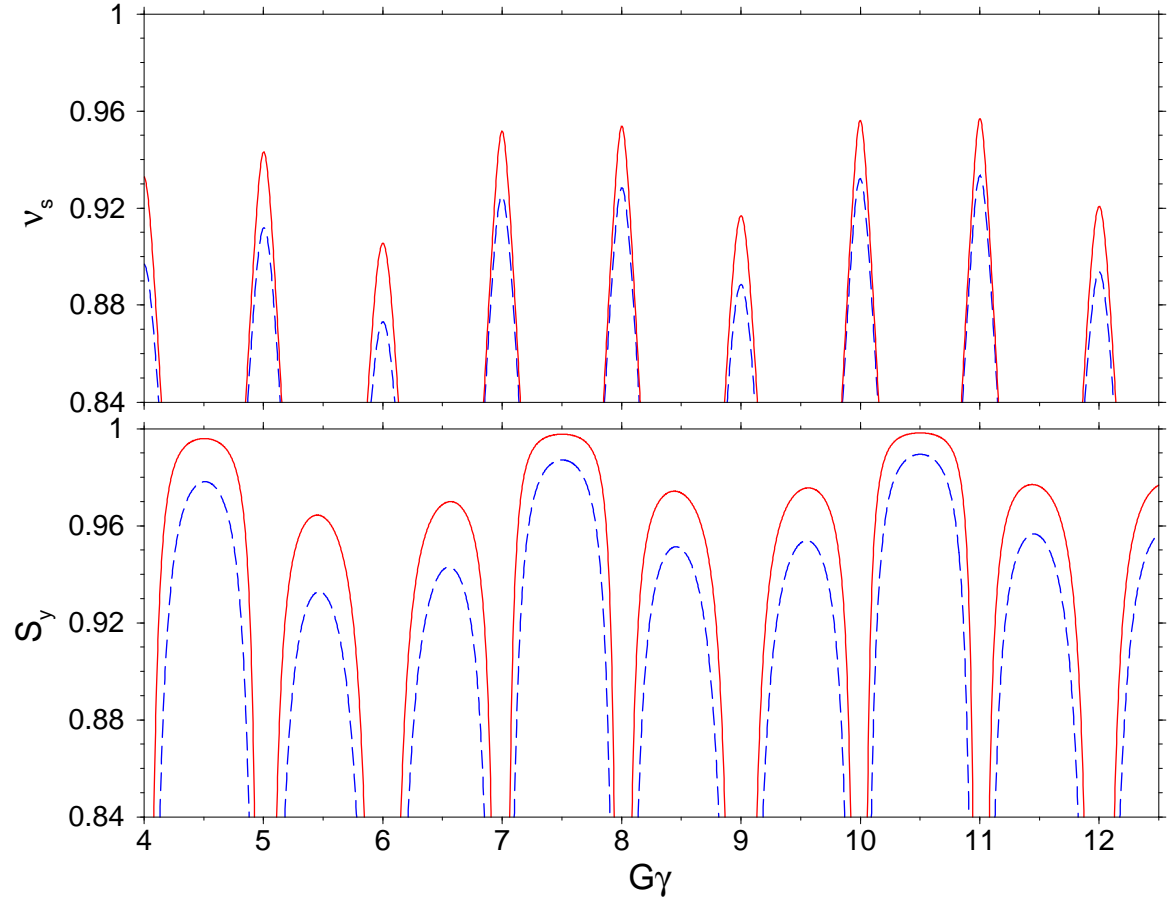


Figure 2.2: Spin tune from Eq. (2.36) (top plot) and vertical component of the stable spin direction Eq. (2.39) (bottom plot) as a function of $G\gamma$ with two partial snakes separated by $1/3$ of the ring in the AGS. The solid curves are for 10% cold snake and 5.9% warm snake; the dashed ones are for 14% cold snake and 5.9% warm snake.

angle to that of a full snake, i.e. χ/π . The deviation of spin tune from an integer reaches its maximum every $G\gamma = 3n$, where n is an integer, and the tilt of the stable spin direction away from vertical direction reaches its minimum at $G\gamma = 3n + 1.5$. Since the AGS has a super-periodicity of 12 and the vertical betatron tune is close to integer 9, this feature provides the maximum space for placing the vertical betatron tune in the prohibited region of spin tune (as known as spin tune gap) at all the strong vertical intrinsic resonances. The spin tune gap at all the other integers is large enough to avoid all weak vertical intrinsic resonances.

With the two partial snakes the stable spin direction is not vertical. Therefore the perturbing fields that rotate the spin away from the stable direction have vertical as well as horizontal components. Particles undergoing horizontal betatron oscillations encounter vertical field deviations at the horizontal oscillation frequency. As a result, resonances with the spin tunes driven by the horizontal betatron oscillations will occur whenever the spin tunes satisfied $\nu_s = k \pm \nu_x$. This type of resonance is called a horizontal intrinsic resonance [8]. To study the effect of horizontal resonances on the polarization, simulation works, both from a simplified analytic model and from multi particles spin tracking, were performed. Measurements were also carried out in the AGS to explore the horizontal intrinsic resonances.

Chapter 3

AGS Experimental Facility

3.1 AGS Configuration

The Alternating Gradient Synchrotron (AGS) is the polarized proton injector to the Relativistic Heavy Ion Collider (RHIC) at Brookhaven National Laboratory. The polarized H^- beam is originally produced by the optically pumped polarized ion source (OPPIS) [14] with $500\ \mu A$ in a single $400\ \mu s$ pulse, which corresponds to 12.5×10^{11} polarized H^- ions. Then the polarized H^- ions are accelerated to 200 MeV in the LINAC. The pulse of H^- ions is injected through a thin stripping foil and captured into a single bunch of about 4×10^{11} polarized protons in the AGS Booster. The single bunch of polarized protons is accelerated in the Booster to 1.5 GeV kinetic energy and then transferred to the AGS, where it is accelerated to 23.8 GeV total energy for final injection into RHIC. Figure 3.1 shows the whole acceleration complex for the polarized proton.

The AGS lattice is made up of 12 super-periods named from A to L starting from the injecting point. Each super-period has twenty combined function dipole magnets of long and short lengths, numbered 1 to 20 in each superperiods. The space between two adjacent magnets is a straight section, named for instance the A3 straight section

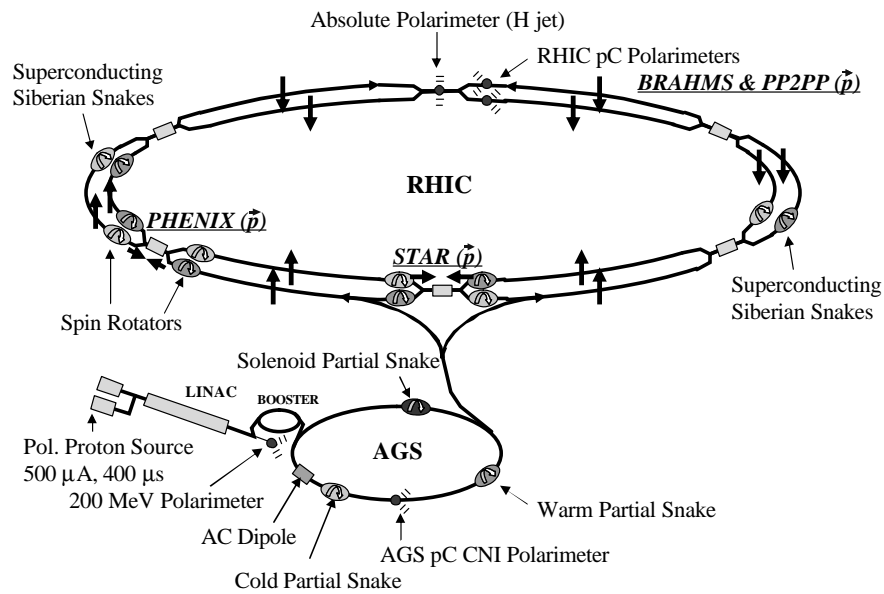


Figure 3.1: Acceleration complex for polarized proton at Brookhaven National Laboratory.

Table 3.1: Locations of quadrupoles and multipoles in the AGS

Equipments	Straight Section
12 vertical tune quadrupoles	A3, B3, C3 ... L3
12 horizontal tune quadrupoles	A17, B17, C17 ... L17
12 vertical sextupoles	A7, B7, C7 ... L7
12 horizontal sextupoles	A13, B13, C13 ... L13th
12 polarized proton quadrupoles	A3, B3, C3 ... L3 next to vertical tune quadrupoles
6 gamma transition quadrupoles	A17, C17, E17, G17, I17, K17 next to the horizontal tune quadrupoles
6 skew quadrupoles	B17, D17, F17, H17, J17, L17 next to the horizontal tune quadrupoles

after the 3rd magnet in the A super-period. A few quadrupoles and other multipoles for machine tuning are installed in these straight sections as shown in Table 3.1.

The circumference of the “design” orbit in AGS is 807.09 m (average radius of to 128.4526 m), which is essentially at the center of the quadrupoles. At the extraction energy, the circumference of the closed orbits is increased to 807.12 m (radius equals to 128.45798 m), 3 cm larger than the “design” value, to match the injection frequency of RHIC. The AGS machine operates at the harmonic number of 12 and nominal betatron tune 8.75 in both horizontal and vertical planes. To accelerate the polarized proton from 2.35 GeV/c to 23.8 GeV/c in the AGS 2006 run, the particle revolution frequency sweeps from 340.73 kHz to 371.18 kHz. After injection, the pulsed rectifier bank of the main magnet power supply is turned on to rapidly increase the magnet’s field to the desired current. Then the current is reduced by the flat-top rectifier bank to the precise final field. The whole process results an varied acceleration rate of α in the AGS as shown in Fig. 3.2 of the ramping rate as a function of time in one acceleration cycle.

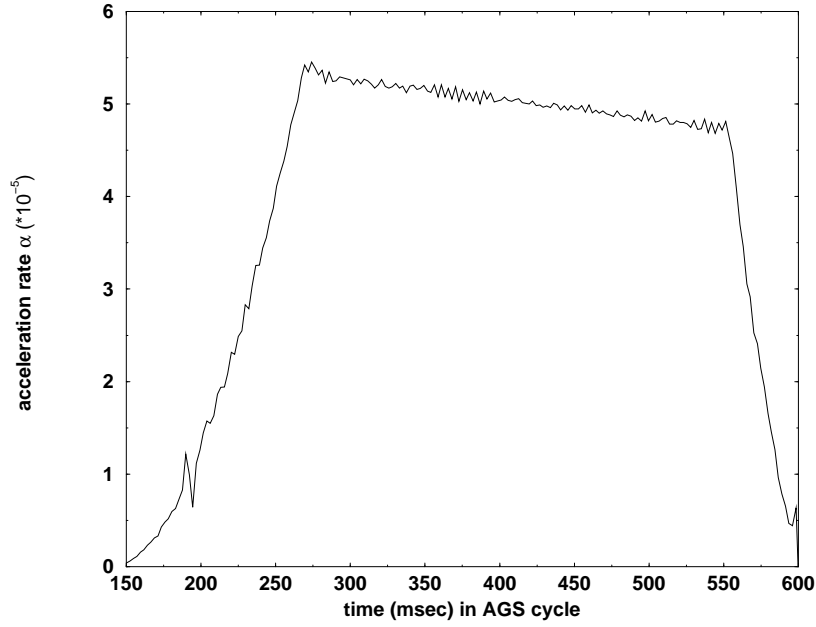


Figure 3.2: AGS ramp rate of $\alpha = \frac{dG\gamma}{d\theta}$ as a function of time in an acceleration cycle.

In order to overcome the spin depolarizing resonances and measure the beam polarization, a few important instruments have been installed. Figure 3.3 shows the schematic drawing of the AGS polarized proton complex.

In 1995, a 5% solenoid partial Siberian snake was installed in the I10 straight section to overcome the imperfection resonances, and tune-jump method [15] was used to overcome the intrinsic resonances. The 5% partial snake was operated by a 4.7 Tm solenoid with effective length 2.286 m, 3.8 million ampere turns and 1.5 MW power supply. An internal polarimeter [4] was installed in the C20 straight section to measure the circulating beam polarization during that time. Although this solenoid partial snake was good enough to overcome the imperfection resonances, the linear betatron coupling due to the solenoid magnet of the partial snake still led to modest polarization loss.

In 1998, in addition to the 5% solenoid partial snake, an AC dipole magnet in the

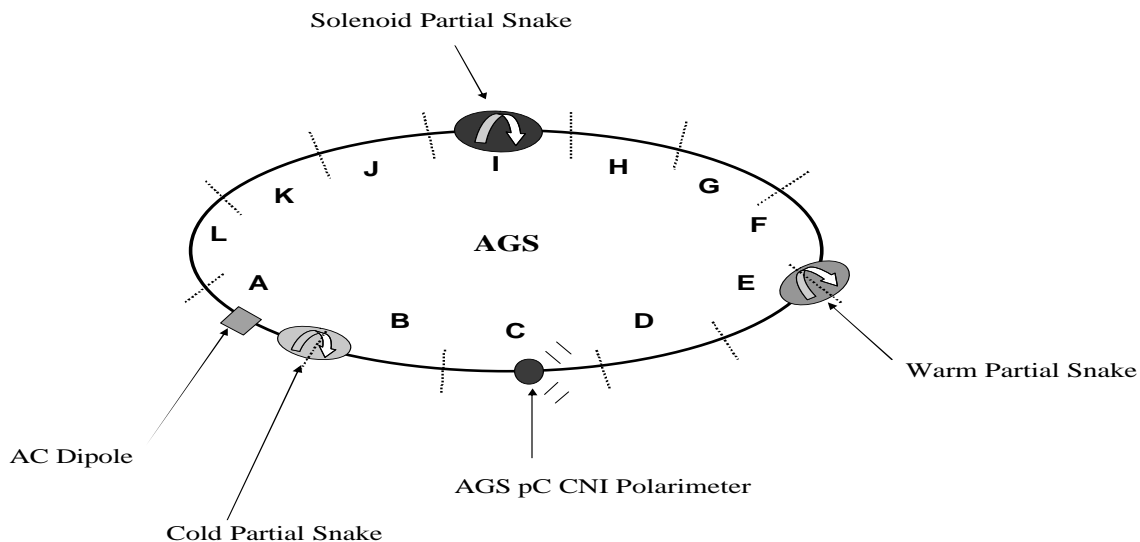


Figure 3.3: Schematic drawing of the AGS polarized proton complex.

A10 straight section was introduced to correct four strong intrinsic resonances in the AGS [16, 17]. The mechanism of using an AC dipole was to force all particles in the beam to coherently oscillate at a large amplitude and induce full spin flip. The AC dipole magnet is 81.28 cm long, 30.48 cm wide and 22.225 cm high with the resonance frequency tuned at 70 kHz for 10ms pulses for each spin resonance. The polarization of 40% was reached with this combination.

To reduce the transverse coupling resonances caused by the strong solenoidal field, a 5.9% normal conducting helical dipole partial snake (called warm partial snake) [7] was installed in the E20 straight section in 2004 to replace the 5% solenoid partial snake. With the combined operation of the warm snake and the AC dipole, 55% polarization was achieved at the AGS extraction energy.

However, the goal of full polarization transmission requires the correction of all the intrinsic resonances including the weak ones. In addition to the 5.9% warm partial

snake, a super-conducting helical dipole snake (called cold partial snake) [5, 6] with a maximum strength of 22% at the AGS extraction energy was added in the A20 straight section before the polarized proton run in 2005 to overcome all the imperfection and the intrinsic resonances. To eliminate the significant lattice distortion caused by the the two partial snakes, especially at low energy, four compensation quads were added for each of the two helical snake magnets. With this setup, the horizontal betatron tune was $\nu_x = 8.70$ and the vertical betatron tune ν_y was maintained just above 8.90 at injection and ramped up between 8.96 and 9 after $G\gamma = 5$. The vertical chromaticity was set close to zero to reduce betatron tune spread due to momentum spread. The combination of the 5.9% warm partial snake and 10% cold partial snake improved the polarization up to 65% with 1.5×10^{11} protons/bunch in AGS 2006 polarized proton run.

3.2 Two Partial Siberian Snakes in the AGS

The Siberian snakes are the only effective approach to maintain the polarization if the energy of the proton beam exceeds 30 GeV. Snakes can be constructed by using a constant longitudinal or transverse magnet individually. However, these schemes have been gradually discarded because of the betatron motion coupling caused by the longitudinal magnetic field or the large orbit excursion caused by the transverse magnetic field. In 1996, a design of the Siberian snake constructed from helical magnets was proposed by Ptitsyn and Shatunov for RHIC [18]. This idea was first realized in RHIC with four full superconducting Siberian snakes (two in each accelerating ring: Blue and Yellow ring), each of which was made of four 2.4 meter helical dipoles and built in 2002. With the commissioning of the four snakes (two in each ring), RHIC has maintained high polarization on the energy ramping and at top energy of 100 GeV.

However, the whole 10 meter long full snakes are not practical to be installed in

the AGS because the longest straight section is only 3 m. The new snake must be very compact with an arrangement of helical dipoles. After many studies of possibility, compact helical snakes, proposed by Thomas Roser [19], were adopted. The partial snake is composed of a single magnet with a sequence of three helices with different pitches. The design includes the compensation of the orbit excursion in the helix by putting steering magnets at the ends of the helix. This structure appears the most efficient in terms of spin rotation, orbit control and construction.

Two helical dipole partial snakes in the AGS, called warm partial snake [7] and cold partial snake [6], were developed and implemented at RIKEN Japan and at BNL USA, respectively. Except for the larger spin rotation produced by the cold snake, the differences between the two partial snakes are

1. the iron in the cold snake is saturated, resulting in the almost linear field scale with the current in the coils; while the field in the warm snake is not linear with the excitation.
2. the cold snake must be operated in DC; while the current in the warm snake may be varied in principle.

The warm partial snake is a normal conducting helical dipole partial snake, located at the E20 straight section in the AGS. The helical dipole field strength is designed at 1.5 Tesla with 2100 mm the whole length of iron yoke. The coil consists of three sections: the slow pitch of 0.196 deg/mm for 1320 mm in the center and the fast pitch of 0.4 deg/mm for 390 mm in each end. The cross-section of the coil is perpendicular to current flowing direction and always a rectangular shape. The pitches and lengths of each section are optimized to minimize the beam shift and deflection angle by using 3D field analysis and OPERA3D/TOSCA. The maximum orbital offset inside of the warm snake is approximately 18.77 mm in the horizontal plane, and 19.45 mm in the vertical plane at the injection energy of 2.4 GeV.

The cold partial snake is a super-conducting helical dipole partial snake, located at the A20 straight section in the AGS. The maximum field in the super conducting magnet is 3 T with 2100 mm the whole length of the iron yoke. The coil also consists of three sections with a pitch of 0.2017 deg/mm for 1208 mm in the center and a pitch of 0.4036 deg/mm for 446 mm in each end. In addition, a solenoid winding is built inside the main coils to compensate for the longitudinal component of the helical dipole field. Meanwhile, several corrector coils are placed on the same tube with the solenoid for the orbit correction.

In order to match the two snakes to the AGS lattice perfectly, four quadrupoles called compensation quadrupoles [20, 21], two on each side for each snake, have been added in to match the β functions at entrance and exit of the straight section containing snakes. The four compensation quadrupoles QCE17, QCE19, QCF1 and QCF3 are located in E17, E19, F1 and F3 respectively in the AGS for warm snake. Another four compensation quadrupoles QCA17, QCA19, QCB1 and QCB3 are located in A17, A19, B1 and B3 respectively for the cold snake. QCE17, QCF3, QCA17 and QCB3 are obtained by extra windings on the four existing tune quads QHFH and QHFV; QCE19, QCF1, QCA19 and QCB1 are newly fabricated quads of 0.35 m length. Since both snakes have focusing and coupling which are strongest at the lowest energy and become more and more transparent as beam energy ramps up, the operation of the four compensation quadrupoles is particularly important at low energies. The gradients of these compensation quadrupoles scale almost exactly as the reciprocal of the beam rigidity $B\rho = p/e$ squared because the transverse magnetic field on the orbit in the helical snake scales with the square of the orbit displacement that grows linearly with the inverse of the beam energy.

The two snakes run at constant fields, resulting in the snake strengths dropping as the beam energy ramps up due to energy dependent of spin rotation at low energies shown in Eq. (2.2). Both snakes have the maximum rotation at the lowest energy. Generally, the partial snake percentage quoted is the strength at the top energy.

Therefore, the warm snake is 5.9% partial snake that makes the spin rotation by 10.62 degrees at the flattop; the cold snake is 10% or 14% partial snake, rotating the spin direction by 18 degrees and 25.2 degrees, respectively at the flat top, based on the strength operated in the AGS 2006 run.

The snake field map is generated by Opera-3D [22]. The program SNIG [23] is used to track the particle trajectories through the field map. SNIG also calculates the spin evolution by integration of the BMT equation to give the 3×3 spin transfer matrices for different proton energies on the trajectories of particles. The spin rotation angles and axes can be obtained from the spin matrix. Figure 3.4 and 3.5 give the curves of the spin rotation angle as function of γ in AGS 2006 run during the acceleration cycle for the warm and cold snakes, respectively. The warm snake was always operated

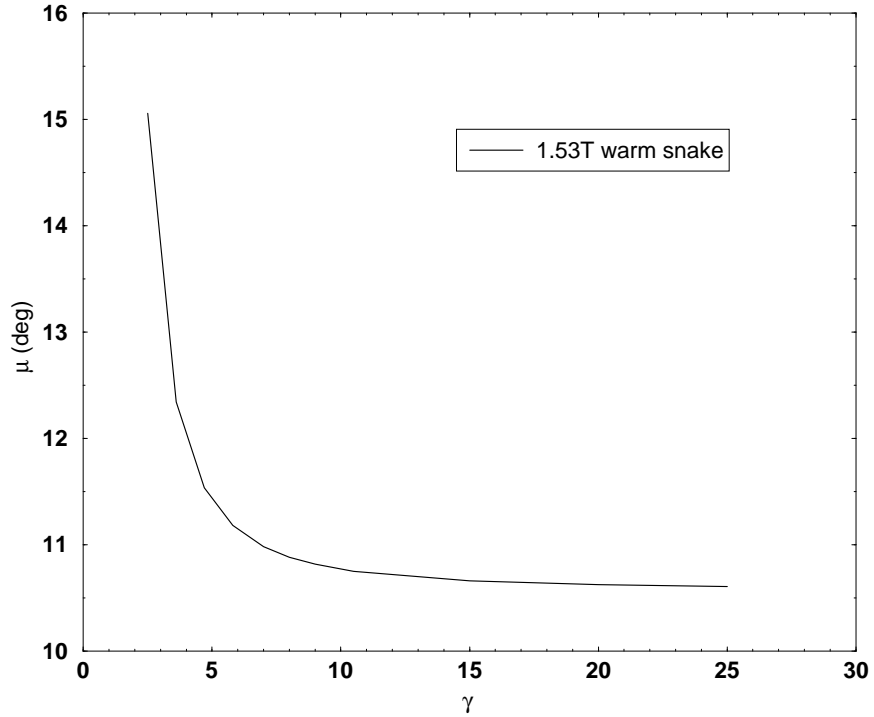


Figure 3.4: AGS warm snake spin rotation angle as function of γ .

at a constant magnetic field 1.53 T. The cold snake was run at 2.1 T (10%) constant magnetic field and 2.5 T (14%) constant magnetic field.

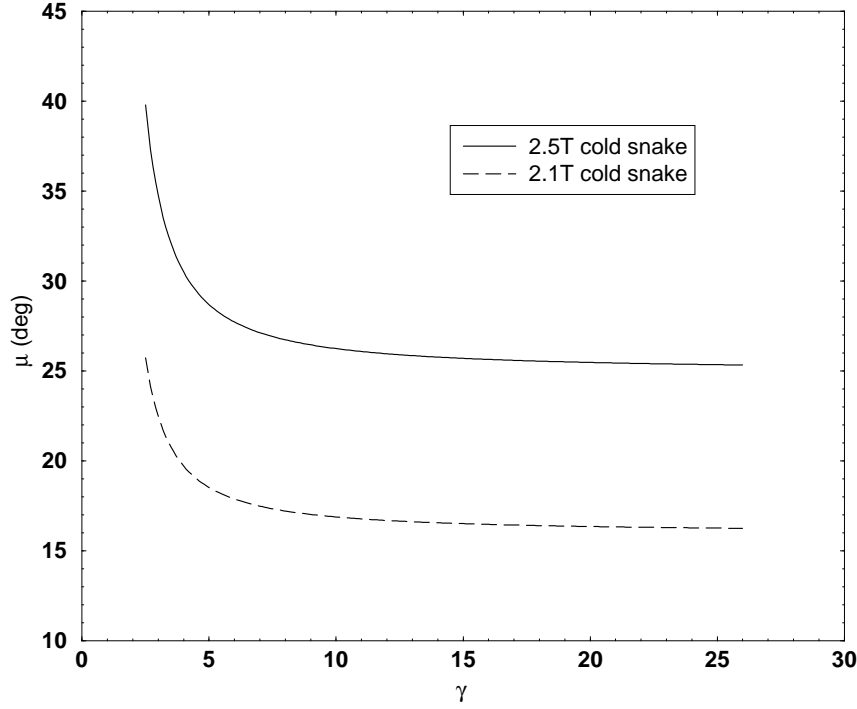


Figure 3.5: AGS cold snake spin rotation angle as function of γ .

The correlations between the spin rotation angle and the energy can be obtained by fitting the partial snake strength curves. Based on an analytical model of the field of a helix dipole in the Blewett-Chasman expression [24], the transverse magnetic field scales with the square of the orbit displacement. Because the orbit amplitude in a helical snake grows linearly with the energy, given a known $B_0 = 2.5$ the scaling law for the warm partial snake is [25],

$$\mu = \left(\frac{B}{B_0}\right)^2 \left(C_1 + \frac{C_2}{C_3 + \gamma^2}\right). \quad (3.1)$$

The fitting result gives

$$\begin{aligned} B &= 1.5307, \\ C_1 &= 28.2015, \\ C_2 &= 52.1787, \\ C_3 &= -1.8921; \end{aligned}$$

The scaling law for cold snake is,

$$\mu = \left(\frac{B}{B_0}\right)^2 \left(C_1 + \frac{C_2}{\gamma^2}\right). \quad (3.2)$$

Here for the 10% cold snake, the fitting result gives

$$\begin{aligned} B &= 3.4745, \\ C_1 &= 8.4147, \\ C_2 &= 29.5833, \end{aligned}$$

and for the 14% cold snake:

$$\begin{aligned} B &= 2.9835, \\ C_1 &= 17.7646, \\ C_2 &= 60.6398. \end{aligned}$$

With the operation of the two partial helical dipole snakes, a spin tune gap is generated as shown of the spin tunes as function of $G\gamma$ in Fig. 2.2. When the fractional parts of the betatron tunes are put into the spin tune gap during the energy ramping, both imperfection and intrinsic resonances can be avoided.

3.3 Coulomb-Nuclear Interference Polarimeter

A Coulomb-Nuclear Interference (CNI) polarimeter was installed in the C15 straight section in the AGS in 2003 with the goal of improving the diagnostics and ultimately increasing the polarization output to RHIC [26]. The CNI polarimeter is designed to measure the spin-dependent asymmetry δ of the proton-Carbon elastic scattering at very low momentum transfer in the Coulomb-Nuclear Interference region. The absolute beam polarization is given by $P = \delta/A_N$, where A_N is the analyzing power for pC elastic scattering [27], δ is the left-right or up-down asymmetry.

Table 3.2: Parameters of three CNI polarimeter targets.

Target	Moving direction	Thickness (mg/cm ²)	Width (μ m)
Target1	Horizontally	4	250
Target2	Vertically	4	618
Target3	Horizontally	4	600

The AGS CNI polarimeter uses thin carbon foil targets and silicon strip detectors (SSDs) that detect the energy and time of the recoil carbon nuclei. These carbon foil targets are 3-5 mg/cm² thick, 5 cm long and 250-600 μ m wide. During the AGS 2006 polarized proton run, three different carbon targets were used. Table 3.2 gives the parameters of the three targets.

All these targets are mounted on a moveable frame inside the polarimeter chamber. For each measurement, only one of the targets is moved into the beam line. The silicon detectors are segmented into 12 individual strips. Each strip is 2 mm wide and 10 mm long, and is oriented perpendicular to the beam direction. The 90 degree detectors are positioned directly to the left and to the right of the target at a distance of 32 cm. There are four SSDs used for the 2006 run, two in the left arm and two in the right arm. The two detectors in each arm are set to have the same acceptance of carbon recoil angle, but slightly offset in azimuthal angle.

The current pulses from the SSDs are processed by the polarimeter data acquisition (DAQ) system . After passing through a series of amplifiers, event pulses are analyzed by a waveform digitizer (WFD) system. The WFD modules extract timing, amplitude, and integrated charge from each event pulse. There are two criteria to be used to separate carbon events from background and to ensure overall data quality. One is based on the carbon time of flight (tof) to kinetic energy (E_{kin}) correlation (tof-energy correlation),

$$\text{tof} = l \sqrt{\frac{m_C}{2E_{kin}}}. \quad (3.3)$$

Here $l=32$ cm is the distance from the target to the detector and m_C is the carbon mass $11.18 \text{ GeV}/c^2$. The event cut is set to select events between ± 20 ns of the expected tof-energy correlation. Another criterion to select events is based on the kinematic range in momentum transfer. For pC elastic scattering, the momentum transfer, $-t$, is proportional to the kinetic energy of the scattered carbon,

$$-t = 2m_C E_{kin}. \quad (3.4)$$

During the AGS 2006 run, the momentum transfer cut was $0.004472 \text{ (GeV}/c)^2 \leq -t \leq 0.010062 \text{ (GeV}/c)^2$, which corresponds to approximately $400 \text{ keV} \leq E_{kin} \leq 900 \text{ keV}$. The events that pass the selection cuts are used to calculate the left-right asymmetry δ

$$\delta = \frac{\sqrt{L^\uparrow R^\downarrow} - \sqrt{L^\downarrow R^\uparrow}}{\sqrt{L^\uparrow R^\downarrow} + \sqrt{L^\downarrow R^\uparrow}}, \quad (3.5)$$

where $L^\uparrow (L^\downarrow)$ is the number of events of the up (down) polarization in the left arm, $R^\uparrow (R^\downarrow)$ is the corresponding events in the right arm. The advantage of using the square root relation to calculate the asymmetry is that the systematic errors due to the differences in the left and right detector acceptances, the difference in up and down polarization states and the fluctuation of beam intensity from pulse to pulse can be canceled to first order [28].

The analyzing power used for the AGS CNI polarimeter is based on the measurement from the AGS E950 experiment [29] at a beam energy of 21.7 GeV. Since the CNI polarimeter measurements happen at the AGS extraction energy of 24.3 GeV, the data from AGS E950 measurement are fit with theoretical constraints. The effective analyzing power at 24.3 GeV is determined by weighting the theoretical values with the measured event yields,

$$\langle A_N \rangle = \frac{\sum_{i=1}^{n_{bin}} (A_N^{th})_i N_i}{\sum_{i=1}^{n_{bin}} N_i}. \quad (3.6)$$

Here $(A_N^{th})_i$ is the theoretical value of the analyzing power for the i^{th} -t bin. N_i is the measured yield for the i^{th} bin, and n_{bin} is the number of -t bins used for the

measurement. For the 2006 AGS run, the effective analyzing power $\langle A_N \rangle = 0.01161$.

The beam polarization P in AGS measured by the CNI polarimeter was then calculated

$$P = \delta / \langle A_N \rangle \tag{3.7}$$

Chapter 4

Simulation and Experiment

As described in Chapter 2, with the two helical dipole partial snakes in the AGS the stable spin direction is tilted away from the vertical direction. The spin vector of the polarized proton will precess around the non-vertical stable spin direction during the whole acceleration. The interaction between the horizontal displacement and the vertical magnetic field can also perturb the spin vector away from the stable spin direction and cause polarization loss. When the spin precession frequency equals the frequency of the perturbing magnetic field, a horizontal intrinsic resonance occurs. The condition is $\nu_s = k \pm \nu_x$. The polarization loss due to the horizontal intrinsic resonances [8] was explored in both simulations and experiments. This chapter presents these results.

Additionally, in order to preserve the beam polarization, the vertical betatron tunes have been pushed inside the spin tune gap generated by the two helical partial snakes after $G\gamma = 5$ (see Fig. 4.6 and Fig. 4.7). However, two initial weak intrinsic resonances were still left uncorrected (for $G\gamma < 5$) because the vertical tunes could not be so high to maintain orbit stability of the lattice. Since the acceleration rate was also slow, the two weak resonances could cause polarization loss [30]. With the vertical tunes inside the spin tune gap after $G\gamma = 5$ during the energy ramping, another type

of depolarizing resonance called a partial snake resonance [31, 32, 33] could still occur at some values of the vertical betatron tune, resulting in a reduced available tune space with the two partial snakes. With vertical betatron tune close to the integer beam polarization was also very sensitive to any closed orbit distortion [33]. Therefore, experiments were developed to explore depolarization due to vertical motion, partial snake resonance and closed orbit distortion. These experimental explorations and data analyses will be discussed in this chapter.

4.1 Investigation of Horizontal Intrinsic Resonance

4.1.1 Simulation Results

The simulations of the horizontal intrinsic resonances were performed by two different methods: one was a simplified analytic model, and the other was multi-particle spin tracking using the program *SPINK* [34, 35]. Results were then compared to each other. Our first attempt was to find a connection between the analytic and the numerical model because the estimation of the horizontal resonance strength defined in the simplified analytic model can not be directly obtained in spin tracking using *SPINK*. In order to make a fair comparison, a special approach in the multi-particle spin tracking was introduced. This will be mentioned in the following description.

I Simplified Analytic Model

The simplified analytic model is based on Thomas Roser's estimate of each resonance occurring whenever $\nu_s = n \pm \nu_x$; if, as is the case, these resonances are very narrow and well separated, the overall depolarization factor is just the product of the effective Froissart-Stora factors for each of the resonances:

$$\frac{P_f}{P_i} = \prod_{n(\gamma)} \frac{1 - \frac{\pi|\epsilon(\gamma)|^2}{\alpha}}{1 + \frac{\pi|\epsilon(\gamma)|^2}{\alpha}}, \quad (4.1)$$

where the product is over all the values of γ where the resonance occurs, and $\epsilon(\gamma)$ is the resonance strength.

In this simple model the horizontal betatron motion is represented by a single kick at the strong cold snake. Because the effect of a second weaker snake modulates the resonance strength depending on the spin precession between the two snakes, resulting in canceling the effect on average over many resonances and being ignored in this model. The full horizontal oscillations in the rest of the ring have no effect on the spin since the spin precession commutes with the precession in the main dipoles. Note that this model therefore predicts that the horizontal resonances do not depend on the super-periodicity of the lattice but only depend on the lattice function at the snake. The horizontal resonance strength is given by the product of the horizontal component of the stable spin direction $P_h(G\gamma)$ calculated from the OTM and the rms value of the deviation of the total horizontal orbit angle Θ from 2π per turn at the cold snake:

$$\epsilon(\gamma) = \frac{G\gamma}{2\pi} \cdot P_h(G\gamma) \cdot \Theta = K(\gamma) \cdot \sqrt{\gamma}, \quad (4.2)$$

where $\Theta = \sqrt{\frac{(1+\alpha_x^2) \cdot I_{0x}}{\gamma\beta_x}} \cdot \sin(\pi\nu_x)$, I_{0x} is the normalized rms horizontal emittance, ν_x is the horizontal betatron tune, α_x and β_x are the Courant-Snyder parameters in front of the cold snake, $K(\gamma)$ is a factor determined by the lattice and has a weak energy dependence.

Identifying the $M = e^{-i\pi\nu_s\hat{n}_c\cdot\vec{\sigma}}$ with the OTM in front of the strong cold snake,

$$T = e^{-i\frac{1}{2}G\gamma(2\pi-\frac{2\pi}{3})\sigma_3} e^{-i\frac{\chi_w}{2}\sigma_2} e^{-i\frac{1}{2}G\gamma\frac{2\pi}{3}\sigma_3} e^{-i\frac{\chi_c}{2}\sigma_2}, \quad (4.3)$$

the three components $(\cos\Phi_1, \cos\Phi_2, \cos\Phi_3)$ of the stable spin direction \hat{n}_c along the radially outward, longitudinally forward and transversely vertical are obtained. The horizontal component of the stable spin direction $P_h(G\gamma)$ in front of the cold snake is calculated by

$$P_h(G\gamma) = \sqrt{(\cos\Phi_1)^2 + (\cos\Phi_2)^2}. \quad (4.4)$$

$P_h(G\gamma)$ is the function of beam energy $G\gamma$ and the strengths χ_c and χ_w of the two partial snakes. With the calculated $P_h(G\gamma)$ and $\epsilon(\gamma)$, the final polarization after crossing n horizontal intrinsic resonances is given by Eq. (4.1).

II *SPINK* Tracking

Currently the program *SPINK* is the primary code used to do spin tracking with a realistic AGS lattice. The general idea is to track a certain number of particles in a phase space through the AGS machine lattice. Each proton has four transverse coordinates, x, x', y, y' (x and y are the horizontal position along the radially outward direction and the vertical position of the proton, respectively), two longitudinal coordinates, $\delta\phi = \phi - \phi_s, \delta p = p - p_s$ (ϕ (ϕ_s), p (p_s) are the phase angle and momentum of the off-momentum particle (synchronous particle)), and three spin coordinates, S_x, S_y, S_s (where $S_x^2 + S_y^2 + S_s^2 = 1$). Given an initial condition, the consequent orbit and spin motion of each particle can be tracked using a transfer matrix of each accelerator component.

Three output files provided by *MAD8C* [36] are used by *SPINK*: one is the *.echo* file containing the first and second order 6×6 orbit transfer maps; one is the *.twiss* file containing the closed orbit distortion (COD), the Courant-Snyder parameters, phase advance and dispersion functions for each element; and one is the *.madout* file containing error tables. All of these files are read and combined by the *SPINK* preprocessor *madread* to create a file *.sy* that contains the 6×6 orbit transfer maps, Twiss function, COD and any information about misalignment or field errors of machine component. The transfer matrices are also simplified with the use of an iterative algorithm and routine due to F.Neri.

In the code, the particle orbit motion is transferred by the 6×6 symplectic matrices R [36] computed at the entrance and exit of each element in a planar accelerator as

following

$$\begin{pmatrix} x \\ x' \\ y \\ y' \\ -cdt \\ \Delta E/pc \end{pmatrix} = R \begin{pmatrix} x \\ x' \\ y \\ y' \\ -cdt \\ \Delta E/pc \end{pmatrix} \quad (4.5)$$

$$R = \begin{pmatrix} c_x & s_x & 0 & 0 & 0 & D_x \\ c'_x & s'_x & 0 & 0 & 0 & D'_x \\ 0 & 0 & c_y & s_y & 0 & 0 \\ 0 & 0 & c'_y & s'_y & 0 & 0 \\ -D'_x & -D_x & 0 & 0 & 1 & G \\ 0 & 0 & 0 & 0 & 0 & 1 \end{pmatrix}. \quad (4.6)$$

The explanation about the transfer matrix R is the following:

1. The subscripts of x and y correspond to the two transverse directions: the horizontal and the vertical.
2. $c_i = \cos(k_i l)$ and $s_i = \sin(k_i l)/k_i$ are calculated by the machine elements with k_i focusing (or defocussing) strength. c'_i and s'_i are the derivatives of c_i and s_i (Here $i = x, y$).
3. D_x is the element's dispersion component in the horizontal direction. $D'_x = \frac{dD_x}{ds}$ is the derivative of D_x .
4. $-D_x$ and $-D'_x$ represent the change of the longitudinal phase angle due to horizontal dispersion.
5. G represents the change of longitudinal phase angle due to the momentum spread.

In the *SPINK* program, the transverse motions x and y are transformed by the transfer matrices at different machine elements. Two methods can be used to describe the transformation in the longitudinal motion. One is using the 6×6 transfer matrices as mentioned above. The final phase angle is obtained not only from the momentum spread but also from the horizontal motion due to the dispersion function.

Alternatively, for an accelerator with small horizontal dispersion function, the longitudinal motion can also be simply tracked by using *Synchrotron Mapping Equations*,

$$\Delta E_{n+1} = \Delta E_n + eV(\sin \phi_n - \sin \phi_s), \quad (4.7)$$

$$\Delta \phi_{n+1} = \Delta \phi_n + \frac{2\pi h \eta}{\beta^2 E} \Delta E_{n+1}, \quad (4.8)$$

where $\Delta E_{n+1}(\Delta E_n)$ is the energy deviation of the non-synchronous particle with respect to the synchronous particle at its $(n+1)th$ (nth) passage through the RF cavity, $\Delta \phi_{n+1}(\Delta \phi_n)$ is the corresponding phase angle deviation with respect to the synchronous particle, $E = E_{0,n+1} = E_{0,n} + eV \sin \phi_s$ is the energy of the synchronous particle at its $(n+1)th$ passage through the RF cavity, $\eta = 1/\gamma_T^2 - 1/\gamma^2$ is the phase-slip factor. In this method, the RF electric field is treated as a single lumped element in a synchrotron. The particle gains or loses energy when it passes through the RF cavity, then the RF phase ϕ_{n+1} depends on the new off-energy coordinate ΔE_{n+1} . In reality, there are phase change due to the horizontal dispersion. However, the synchrotron mapping equations normally ignore this part for a synchrotron with small horizontal dispersion, like AGS. Therefore, the *Synchrotron Mapping Equations* are used during the spin tracking in this thesis.

For spin motion, the spin vector is transformed by the 3×3 matrix S_T ,

$$\begin{pmatrix} S_x \\ S_y \\ S_s \end{pmatrix} = S_T \begin{pmatrix} S_x \\ S_y \\ S_s \end{pmatrix}, \quad (4.9)$$

where $S_i (i = x, y, s)$ are three components of spin vector along the radially outward, vertical and longitudinally forward direction, S_T represents the spin matrix that is

constructed from the BMT equation (See Appendix E)

$$\frac{d\vec{S}}{ds} = \vec{S} \times \vec{w}, \quad (4.10)$$

with \vec{w} as a function of the magnetic field in the machine component calculated at the instantaneous position of the particle,

$$\vec{w} = \frac{h}{B\rho} [(1 + G\gamma)\vec{B} - G(\gamma - 1)(\vec{r}' \cdot \vec{B})\vec{r}'], \quad (4.11)$$

where $h = \sqrt{x'^2 + y'^2 + (1 + x/\rho)^2}$ and $\vec{r}' = \frac{\vec{v}}{v}$.

The spin matrix is given by [34]

$$S_T = \begin{pmatrix} 1 - (a_2^2 + a_3^2)Cs & a_1a_2Cs + a_3Sn & a_1a_3Cs - a_2Sn \\ a_2a_1Cs - a_3Sn & 1 - (a_1^2 + a_3^2)Cs & a_2a_3Cs + a_1Sn \\ a_3a_1Cs + a_2Sn & a_3a_2Cs - a_1Sn & 1 - (a_1^2 + a_2^2)Cs \end{pmatrix}. \quad (4.12)$$

Here

$$\begin{aligned} a_1 &= \frac{w_x}{w_0} = \cos \theta \sin \phi \\ a_2 &= \frac{w_y - 1/\rho}{w_0} = \sin \theta \\ a_3 &= \frac{w_s}{w_0} = \cos \theta \cos \phi \end{aligned} \quad (4.13)$$

with

$$w_0^2 = w_x^2 + (w_y - \frac{1}{\rho})^2 + w_s^2, \quad (4.14)$$

and

$$Cs = 1 - \cos w_0\delta s, \quad Sn = \sin w_0\delta s. \quad (4.15)$$

The components a_1, a_2, a_3 are the precession axis, the latitude θ is the angle between the vector and the horizontal plane, the azimuth ϕ is the angle formed by the projection of the \vec{w} with respect to \hat{s} , δs is the orbit path length through the machine element along the equilibrium orbit, and $\delta\Psi = w_0\delta s$ represents the spin rotation angle around its corresponding precession axis. *SPINK* has many entries of calculated spin matrices for different types of machine elements, such as dipole, quadrupole, snake etc.

There are two different ways to represent the Siberian snake and spin rotator:

1. Synthetic
2. Snake Map

A synthetic snake (same to spin rotator) is defined in *MAD* file as a marker that represents a thin element in orbit with a unit transfer map. The angle of spin rotation μ and angles of the rotation axis θ, ϕ are given in the input file. The result is that the snake only rotates the spin vector around the snake axis, while the orbit is not affected. In the snake map, the snake is treated as a thick element, optically represented by 6×6 snake transfer matrix. The snake transfer matrices are energy dependent and obtained by tracking the particle trajectory through the numerical field map calculated for the snake with the code OPERA. Therefore, in addition to the spin rotation, the snake maps also give a contribution to the orbital motion resulting in spin motion being revised due to the betatron phase.

III Comparison of Two Simulation Results

In the simplified analytic model, the product of the effective Froissart-Stora factors through all the resonances gives the final polarization along the stable spin direction. Once given the normalized rms horizontal emittance I_{0x} , the horizontal betatron tune ν_x , the Courant-Snyder parameters α_x, β_x in front of the cold snake and the strengths χ_c and χ_w of two partial snakes, the value of final polarization can be easily calculated.

However, the spin tracking using *SPINK* is more complicated because the magnetic field experienced by each particle in one beam bunch can be different due to the particle's trajectory. In order to simulate the real beam situation during the acceleration, spin tracking was carried out with 100 Gaussian distributed particles in the horizontal phase space and a rms momentum spread $\frac{\Delta p}{p} = 0.003$ initially. The spin motion of each particle in the distribution would be different due to the betatron motion. The final polarization was calculated as the average polarization of the 100 particles projected onto the stable spin direction.

Spin tracking was started from finding the stable spin direction at the original energy. This procedure was realized by setting the spin vector of the center particle along the vertical direction, tracking the spin motion at the initial energy without acceleration and averaging the three components of the spin vector respectively after several thousand turns. All of the 100 particles were aligned along this initial stable spin direction before tracking. In reality, the initial spin direction of each particle can be slightly different, but the difference is small for the polarized proton beam in the AGS and has little effect on the spin tracking.

To get more realistic simulation results, many preparations were done before tracking. First, since the AGS lattice changes during the acceleration, especially at the low energies due to the setup of two partial snakes, *MAD* was run at different energies to generate the lattices based on the real betatron tune. During spin tracking the lattice was updated, more frequently at low energies than at high energies. Second, the varied acceleration rates as shown in Chapter 3 Fig. 3.2 were extracted from the real machine operation. The varied strengths of the two partial snakes as shown in Fig. 3.4 and Fig. 3.5 respectively along the energy ramp were also obtained from the fits of designed snake maps. All of these conditions have been prepared and used in the simulations. In order to make a fair comparison, the Courant-Snyder parameters α_x and β_x in front of the cold snake at different energies were read out from the same lattices used in the *SPINK* tracking. This information was used in the simplified analytic model, which gave the final polarization from Eq. (4.1).

Figure 4.1 shows both simplified analytic model and spin tracking results for two partial snakes separated by 1/3 of the ring with two different snakes strength setups: the top plot is for a 10% cold snake and 5.9% warm snake, the bottom one for a 14% cold snake and 5.9% warm snake.

Zero vertical emittance was used to eliminate the residual polarization effect from the vertical motion, and the horizontal betatron tune was set at 8.72. In general, the polarization should stay constant or decrease monotonically if the components

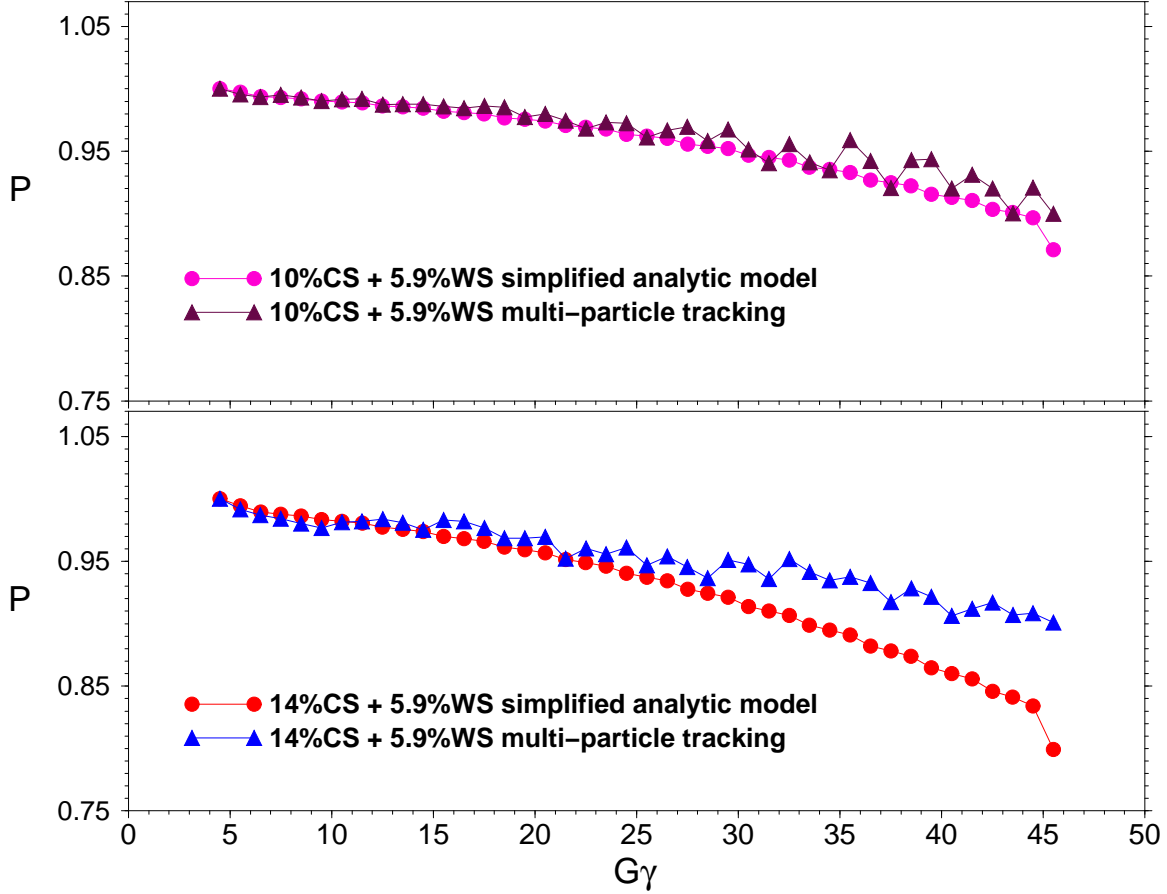


Figure 4.1: Simplified analytic model and multi-particle tracking with a Gaussian distribution in horizontal phase space. The upper plot is for 10% and 5.9% partial snakes; the lower one is for 14% and 5.9% partial snakes. Both simplified analytic model and simulation have the same normalized rms horizontal emittance, zero vertical emittance and 8.72 horizontal tune. The multi-particle tracking shows that the spin coherence results in less polarization loss comparing to the simplified analytic model.

of spin motion transverse to the stable spin direction completely decohere between resonance crossings. However, spin tracking shows spin coherence, which means spin components after one resonance may be affected by the previous resonances. As a result, the spin trackings give less polarization loss than the simplified analytic model. This coherence can be seen in Fig. 4.1 as an increase of polarization after some resonance crossings.

In order to compare the spin tracking to the simplified analytic model that treats the horizontal resonances as isolated resonances during the energy ramping, one approach has been artificially used to remove spin coherence effects in the multiparticle tracking by separating the spin tracking in several short energy ranges. Each time before the re-started spin tracking, the stable spin direction was calculated at the new start energy. All the particles were re-set along the stable spin direction. With this method, the spin coherence phenomenon was eliminated in multiparticle spin tracking. The final polarizations from the two models agrees well as shown in Fig. 4.2, the top plot is for 10% cold snake and 5.9% warm snake, the bottom one for 14% cold snake and 5.9% warm snake. This result implies that the horizontal resonances arise from the tilted stable spin direction with the partial snakes: more tilting away from the vertical direction for 14% and 5.9% snakes causes stronger horizontal intrinsic resonances resulting in more polarization loss. The sudden polarization drop at the last point is due to the slow acceleration rate, resulting from the current of the magnetic field ramping down after arriving at the top energy of AGS. The discrepancy between the spin tracking and the simplified analytic model in Fig. 4.1 is due to the spin coherence. The agreement confirms the existence of the horizontal intrinsic resonances in the AGS with two snakes by both methods. With this agreement, the $K(\gamma)$ value can be predicted from Eq. (4.2) given the snake strength and normalized emittance.

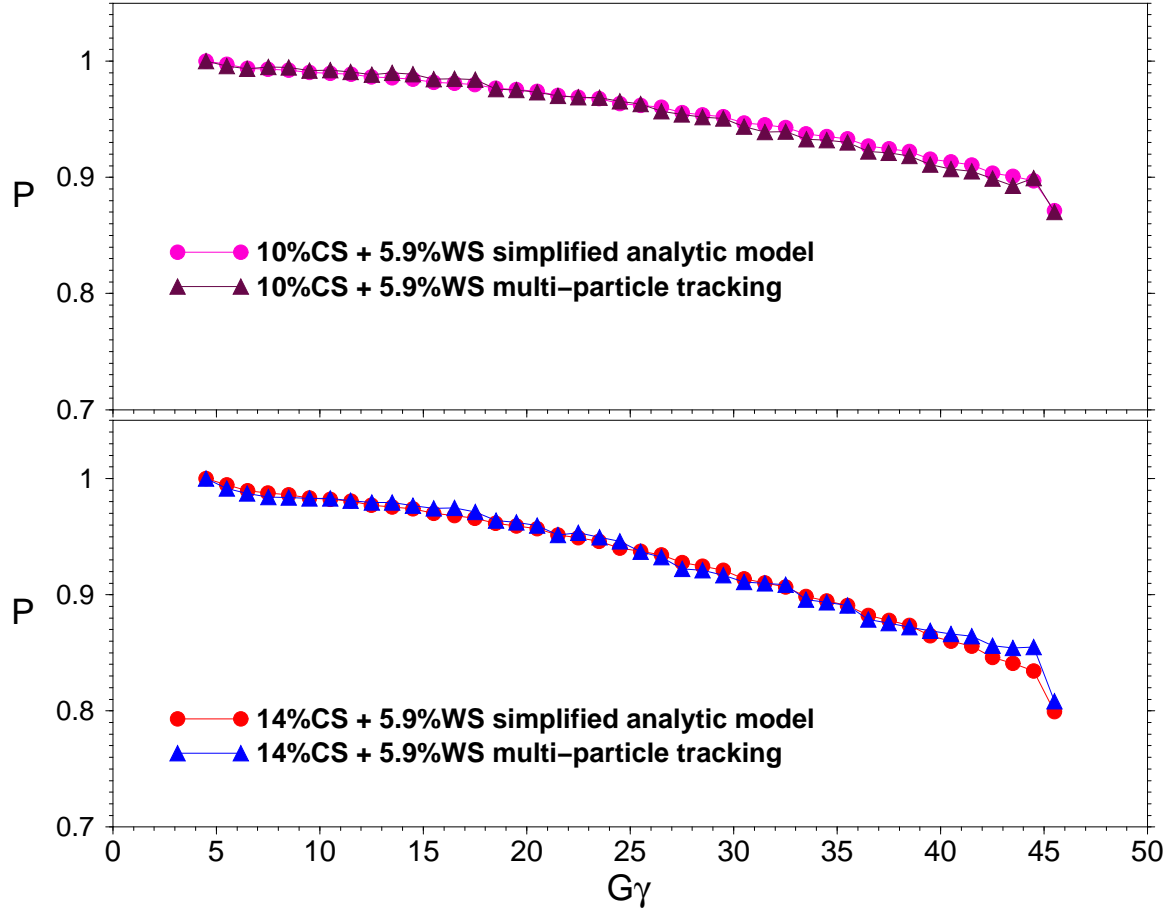


Figure 4.2: Spin tracking from both simplified analytic model and multi-particle with Gaussian Distribution. The upper plot is for 10% and 5.9% partial snakes; the lower one is for 14% and 5.9% partial snakes. Both simplified analytic model and simulation have the same normalized rms horizontal emittance, zero vertical emittance and 8.72 horizontal tune. The spin coherence is artificially removed from the multi-particle tracking.

4.1.2 Experimental Results

The exploration of horizontal intrinsic resonances was carried out in the AGS 2006 polarized proton run. Two types of experimental methods, horizontal polarization profile measurements and B-field scans, have been employed from the different points of view. The two methods and data analyses are described in the following.

I Horizontal Polarization Profile

The intrinsic resonance strength is proportional to the square root of the particle emittance I ,

$$|\epsilon(I)|^2 = |\epsilon(I_0)|^2 \frac{I}{I_0}, \quad (4.16)$$

where I_0 is the rms emittance of the beam, $\epsilon(I_0)$ is the rms value of resonance strength. For a beam with Gaussian distribution $\rho(I) = \frac{1}{2I_0} e^{-\frac{I}{2I_0}}$ in the phase space, the beam polarization after passing through an intrinsic resonance is given by the integral of the Froissart-Stora formula,

$$\left\langle \frac{P_f}{P_i} \right\rangle = \int_0^\infty [2e^{-\frac{\pi|\epsilon|^2}{2\alpha}} - 1] \rho(I) dI, \quad (4.17)$$

or

$$\left\langle \frac{P_f}{P_i} \right\rangle = \frac{1 - \frac{\pi|\epsilon(I_0)|^2}{\alpha}}{1 + \frac{\pi|\epsilon(I_0)|^2}{\alpha}}. \quad (4.18)$$

The final polarization strongly depends on the rms resonance strength $\epsilon(I_0)$. As shown in Eq. (4.16) and (4.17), higher polarization is expected for the particles with smaller emittance. Hence, a polarization profile in the horizontal plane, namely, different polarization for particle at different horizontal emittance, is produced due to the numerous horizontal spin resonances.

This horizontal polarization profile measurement was realized by using the CNI polarimeter vertical target 3 to take the polarization measurement. Target 3 is a vertically oriented thin target that moves horizontally. When the beam arrived at the "flattop" energy where the polarization was to be measured, the target 3 was

moved into the polarimeter vacuum chamber and was set at a certain horizontal position inside of the beam. For a complete polarization profile, a few polarization measurements were taken by placing the target 3 at different horizontal positions.

In order to get accurate measurements, a target scan was taken before the polarization measurement to find the beams center and width. The following target positions could be set at center or off-center by a few target steps, one target step equals 0.19 mm in the AGS 2006 run. Since polarization measurements were somewhat time consuming, usually for each profile only five polarization measurements were taken, two at each side of the beam center plus one at the beam center. The two target positions closest to the beam center were set around the location of beam rms size (1σ) that could be obtained from the target scan. In the AGS 2006 polarized proton run the horizontal rms beam size (1σ) was approximately 1 mm, corresponding to 5 target steps. Two more measurements were set at 2σ , which was 10 target steps.

The count rate detected by the SSDs of AGS CNI polarimeter is the number of events per elapsed time when the beam bunch crosses the carbon target. The total events are given by summing the product of count rate and the elapsed time. In 2006, a total of 40 million events are collected in each polarization measurement for data analysis in order to reduce the statistical error. Since in each beam bunch there are more particles around the beam center than away from the center, it takes less time to collect data when the target is set at beam center, and it takes more time when the target is away from the beam center. Hence, the display of the count rate per cycle at different target locations gives the beam profile or the distribution of the particles in the beam bunch. The beam profile verifies that the target was located at the correct position, as well as the beam size. Because only one proton bunch is injected every cycle, the intensity can be different for each cycle. In order to eliminate the effect of intensity variation on the count rate, the beam profile is plotted using the count rate normalized by the averaged beam intensity for each cycle.

Therefore, in each horizontal polarization profile, two correlations are created : one is the measured polarization as a function of the target position, and one for the normalized count rate as a function of the target position in millimeters.

Two horizontal polarization profiles were measured at the $G\gamma = 45.5$ for the different cold snake strengths of 10% and 14%. The warm snake strength was kept at 5.9% for both cases. The partial snake percentage quoted here is the strength at the top energy. For a fair comparison between the two profiles, the beam intensity was adjust to 1.0×10^{11} proton/bunch and the beam size was measured as the same.

In order to get more accurate results, several polarization measurements taken at the same target position were averaged. The statistic error was the least-squared error given by $\sigma = (\sum \frac{1}{(\sigma_i)^2})^{-\frac{1}{2}}$, where σ_i is the i th statistic error of the polarization measurement. Target scans were also done frequently to locate and verify the target was at the expected position. Table 4.1 lists the final values, which are graphed in Fig. 4.3. Dots represent the 10% cold snake plus 5.9% warm snake configuration, diamonds represent the 14% cold snake plus 5.9% warm snake configuration.

Table 4.1: Experimental data for horizontal polarization profile measurements with two partial snakes at 10% plus 5.9% and 14% plus 5.9%.

Target position (target unit)	Target position (mm)	Polarization	
		(10+5.9)% snakes	(14+5.9)% snakes
0	0	65.35 ± 0.89	59.39 ± 0.92
5	0.95	65.14 ± 1.26	57.36 ± 1.23
-5	-0.95	61.81 ± 0.95	53.49 ± 1.24
10	1.9	54.79 ± 1.44	46.95 ± 1.24
-10	-1.9	55.55 ± 1.27	45.00 ± 1.25

Many different distribution functions for beams have been used in accelerator physics. One needs to be chosen to give a reasonable description. Based on the figure measured from the IPM (Ionization Profile Monitor), which is used to measure the transverse profile of the circulating beam, a Gaussian distribution function is used to fit the beam profile,

$$\rho(x) = A \cdot e^{-\frac{(x-x_0)^2}{2\sigma^2}}, \quad (4.19)$$

where A is the normalized count rate at the beam center, x_0 is the beam center position, and σ is the horizontal rms beam size. Table 4.2 lists the fitting results.

Table 4.2: Fitted parameters from beam profiles. A is the normalized count rate at the beam center, x_0 is the beam center position, and σ is the horizontal rms beam size.

Fitting parameters	(10+5.9)% snakes	(14+5.9)% snakes
A	591332	602327
$x_0(\text{mm})$	0.228	0.
$\sigma(\text{mm})$	0.974	0.912

Based on the fitted rms beam size and the beam center position obtained from the beam profile, the following assumptions were assumed in the deriving of the polarization: (i) depolarization effects due to the vertical coupling motion do not show on the horizontal plane, (ii) the beam only crossed 82 isolated horizontal intrinsic resonances during the acceleration based on the Eq. (4.18), (iii) the horizontal resonance strength is proportional to the square root of the normalized horizontal beam emittance. Since we can only measure the polarization vs the horizontal position, we need to average the beam polarization over the conjugate phase space coordinate p_x :

$$\langle \frac{P_f}{P_i} \rangle = \int_0^\infty [2e^{-\frac{\pi K^2 \gamma}{2\alpha} \cdot \frac{(x^2 + p_x^2)}{\sigma^2}} - 1] \times \frac{1}{\sqrt{2\pi}\sigma} \cdot e^{-\frac{p_x^2}{2\sigma^2}} dp_x, \quad (4.20)$$

where $p_x = \beta x' + \alpha x$ is the normalized conjugate momentum and also has a Gaussian distribution function, Eq. (4.16) is replaced by

$$|\epsilon(I)|^2 = |\epsilon(I_0)|^2 \frac{I}{I_0} = K^2 \gamma \cdot \frac{(x^2 + p_x^2)}{\sigma^2}, \quad (4.21)$$

where (x, p_x) are the normalized conjugate phase-space coordinates, and $I = x^2 + p_x^2$ is the action. The energy independent factor $K = \frac{\epsilon(\gamma)}{\sqrt{\gamma}}$ is introduced in order to make a comparison with the simplified analytic model. After the integral over p_x and crossing the n isolated resonances, we obtain

$$\left\langle \frac{P_f}{P_i} \right\rangle = \prod_{n(\gamma)} [2 \cdot e^{-\frac{\pi K^2 \gamma (x-x_0)^2}{\alpha(\gamma) \cdot 2\sigma^2}} \cdot \sqrt{\frac{1}{\frac{\pi K^2 \gamma}{\alpha(\gamma)} + 1}} - 1], \quad (4.22)$$

where P_f is the measured final polarization after the acceleration, and P_i is the fitted initial polarization at injection. The relative polarizations shown in Fig. 4.3 are the values of P_f divided by the P_i . $\alpha(\gamma)$ is the acceleration rate extracted from the AGS cycle as shown in Chapter 3. x_0 and σ are determined by fitting the beam profile.

Table 4.3: Fitted parameters from horizontal polarization profiles.

P_i is the initial polarization at injection and $K = \frac{\epsilon(\gamma)}{\sqrt{\gamma}}$ is the energy independent factor.

Fitting parameters	(10+5.9)% snakes	(14+5.9)% snakes
P_i	68.49 ± 0.02	63.08 ± 0.02
K	$(2.17 \pm 0.15) \times 10^{-5}$	$(2.61 \pm 0.14) \times 10^{-5}$

Table 4.3 lists the fitting results for the initial polarization P_i and energy independent factor K . The error bars are from polarization statistical errors only. As expected, a stronger partial snake gives a stronger horizontal spin resonance and leads to more curvature in the polarization profile as shown on the polarization profile in Fig. 4.3.

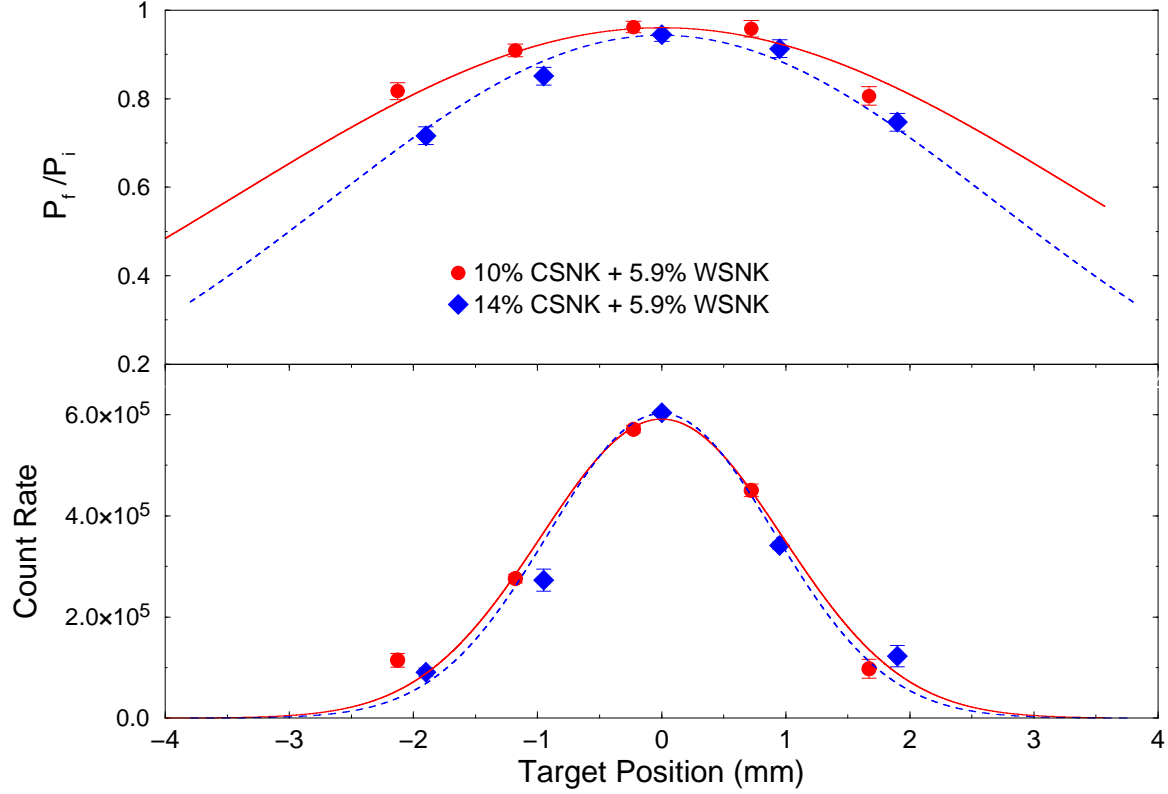


Figure 4.3: Horizontal polarization profiles (upper) and horizontal beam profiles (bottom) in the AGS for two different strength of the partial snakes. The solid curves are for 10% cold snake and 5.9% warm snake, and the dashed ones for 14% cold snake and 5.9% warm snake. The beam profile curves are fitted using Eq. (4.19) and polarization profile curves are fitted using Eq. (4.22) after crossing 82 isolated horizontal intrinsic resonances.

The averaged weak energy dependent factor $K(\gamma)$ can be calculated from the simplified analytic model. In order to get the rms beam size σ_β due to the betatron oscillation, the part due to dispersion should be subtracted from the measured beam size:

$$\sigma_\beta^2 = \sigma^2 - (d_x \frac{\Delta p}{p})^2, \quad (4.23)$$

where σ is given from the measured rms beam profile, d_x is the dispersion at the location of polarimeter, and $\frac{\Delta p}{p}$ is the momentum spread of the beam at the measurement energy. The normalized rms horizontal emittance ϵ_{Nrms} is obtained by:

$$\epsilon_{Nrms} = \beta\gamma \cdot \epsilon_{rms} = \beta\gamma \cdot \frac{\sigma_\beta^2}{\beta_x}. \quad (4.24)$$

Here β, γ are the Lorentz factors, β_x is the horizontal betatron amplitude at the CNI polarimeter. The values of d_x , $\frac{\Delta p}{p}$, β , γ and β_x used in the calculation of rms beam size σ_β are shown in Table 4.4. Therefore, the normalized rms horizontal emittance

Table 4.4: Beam parameters used in the calculation of rms beam size σ_β due to the betatron motion.

$d_x(\text{m})$	$\frac{\Delta p}{p}$	$\beta\gamma$	β_x
1.66	0.0003	25.36	9.2

Table 4.5: Comparison of K values between the calculation and the fitting for two different partial snakes configurations.

	(10+5.9)% snakes	(14+5.9)% snakes
Calculation	2.571×10^{-5}	3.358×10^{-5}
Fitting	$(2.171 \pm 0.15) \times 10^{-5}$	$(2.606 \pm 0.14) \times 10^{-5}$

was 1.79 mm-mrad for 10% cold snake and 1.46 mm-mrad for 14% cold snake. The

averaged $K(\gamma)$ can be calculated from Eq. (4.2) respectively. Table 4.5 shows the values of K from both calculation and fitting. Although the simplified model does not agree exactly with the real lattice spin tracking result quantitatively, it is useful to understand the polarization effect of the horizontal intrinsic resonances.

II B-field Scan

The magnetic rigidity of a beam is given by

$$B\rho[Tm] = 3.3357p[GeV/c], \quad (4.25)$$

which generates the relationship between the beam energy and the machine main dipole field. Here B is the main dipole field strength and ρ is the radius of curvature. As discussed in Chapter 2, the spin tune ν_s , an important quantity describing the spin motion, is determined by the beam energy. Since the spin tune characterizes the location of spin depolarization, the relationship between the spin tune and beam energy can be transferred to a relation between the spin tune and the machine's main dipole field B . Namely, by setting the main dipole magnetic field at different values, the spin depolarization condition will or will not be satisfied while keeping a constant vertical betatron tune. The result is that the measured beam polarization has a profile with respect to the different main dipole field values. The polarization drop happens when the resonance condition is satisfied. This B-field scan technique was employed to explore horizontal intrinsic resonances during the AGS 2006 polarized proton run.

Due to horizontal intrinsic resonances in the AGS, the depolarization happens when the spin tune satisfies the condition $\nu_s = k \pm \nu_x$, where ν_x is the horizontal betatron tune, and ν_s is energy dependent spin tune calculated as shown in Chapter 2 with two partial snakes. For instance, in the most time of AGS 2006 run, the horizontal betatron tune was set to 8.72 during the acceleration cycle. Therefore, horizontal intrinsic resonance locations were expected at $\nu_s = 4.72, 5.28, 5.72 \dots$

45.28, 45.72, 46.28 for the energy range $G\gamma = 4.5$ to 46.5. The polarization is usually measured at the AGS extraction energy, then a B-field scan can be carried out easily at the flat top energy around $G\gamma = 46.5$. At $G\gamma = 46.5$, the main dipole field strength B is usually set at 9.497 kGauss. The shift of dipole field can satisfy the depolarization condition resulting in the beam depolarized.

The values of $G\gamma$ at the flat top energy are calculated from the set main dipole field using the following formulas,

$$B\rho \text{ [Tm]} = 3.3357p \text{ [GeV/c]} \quad (4.26)$$

$$E = \sqrt{(pc)^2 + (E_0)^2}, \quad \gamma = E/E_0 \quad (4.27)$$

with the AGS radius of curvature $\rho = 85.378$ m, the mass of proton $E_0 = 0.93827$ GeV, and $G = 1.7928$ for the proton. In reality, for the real machine, the fluctuation of main dipole field and uncertainty of ring radius results a discrepancy between real value of $G\gamma$ and the calculated ones from the set main dipole field. Another approach to get the calibrated $G\gamma$ values is from the measured RF frequency f_{RF} and the AGS ring radius R_0 with the deviation ΔR_0 by

$$\begin{aligned} v &= 2\pi(R_0 + \Delta R_0)f_{RF}/h, \\ \gamma &= \frac{1}{\sqrt{1 - \beta^2}} = \frac{1}{\sqrt{1 - (v/c)^2}}. \end{aligned} \quad (4.28)$$

Here v is the particle's velocity, $h = 12$ the harmonic number of AGS and the ring average radius is 128.45798 m.

Some of the $G\gamma$ values calculated from the main dipole field and from RF frequency in one B-field scan are listed in Table 4.6, which also lists the set point of the main dipole fields, the measured RF frequencies, and the measured polarizations. The maximum of the discrepancy of $G\gamma$ from the two methods is less than 0.02, which is acceptable. Figure 4.4 shows all the data from the B-field scans: the measured beam polarizations as function of $G\gamma$ values, the black dots are for the calculated $G\gamma$ values and the red diamonds are for the calibrated $G\gamma$ values.

Table 4.6: Part of the B-field scan data.

Set B	$G\gamma$ from B	RF frequency	$G\gamma$ from RF freq.	diff. $G\gamma$	Polarization
9.2370	45.21	4.4537668	45.19954	0.01146	-40.50 ± 2.9
9.2570	45.31	4.4537816	45.30123	0.00750	-2.20 ± 2.9
9.2770	45.41	4.4537955	45.38869	0.01778	-53.90 ± 2.9
9.3170	45.60	4.4538253	45.58795	0.01400	-29.00 ± 2.9
9.3470	45.75	4.4538476	45.73255	0.01600	-47.00 ± 2.9
9.3870	45.94	4.4538773	45.92940	0.01463	-22.40 ± 2.9
9.4370	46.19	4.4539125	46.17603	0.01235	38.30 ± 2.9
9.4670	46.33	4.4539342	46.32216	0.01283	17.10 ± 2.9
9.5070	46.53	4.4539623	46.51187	0.01861	42.70 ± 2.9
9.5270	46.63	4.4539771	46.62001	0.00821	12.10 ± 2.9

¹The first column lists the set points of the main dipole field in unit of kG, the second column lists the calculated $G\gamma$ values using the set main dipole fields given in the first column, the third column lists the measured RF frequencies in unit of MHz, the fourth column lists the calibrated $G\gamma$ values using the RF frequencies, the fifth column shows the difference between the calculated and the calibrated $G\gamma$ values, the last two columns give the measured the polarizations and their statistical errors.

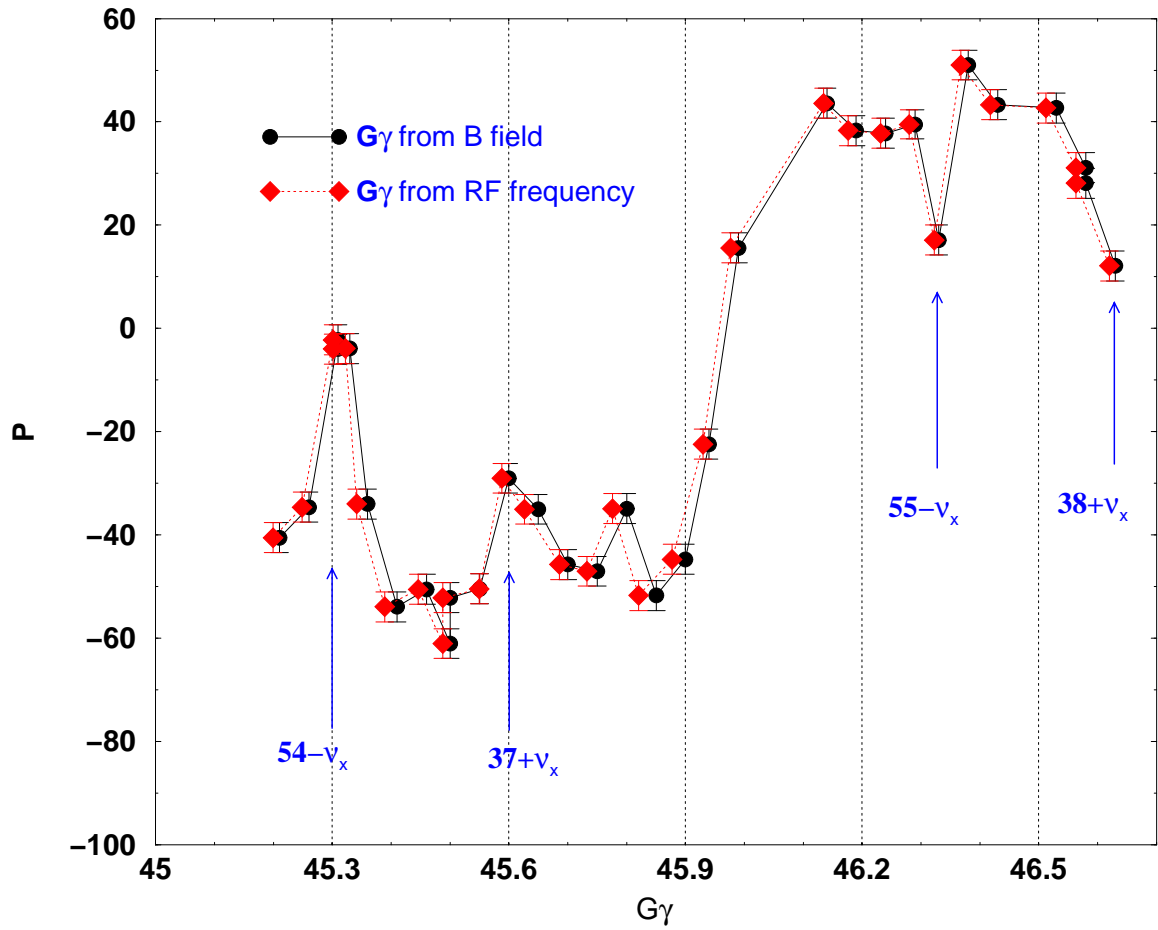


Figure 4.4: One B-field scan from the AGS 2006 polarized proton run. Black dots are for the calculated $G\gamma$ and red diamonds are for the calibrated $G\gamma$. The horizontal betatron tune was around 8.64.

Because the range of $G\gamma$ was between 45.2 to 46.7 and the measured horizontal betatron tune ν_x was around 8.64 during the B-field scan, the depolarization was expected to happen at $G\gamma = 45.36, 45.64, 46.36$ and 46.64 , which correspond to the horizontal intrinsic resonance locations: $G\gamma = 54 - \nu_x$, $G\gamma = 37 + \nu_x$, $G\gamma = 55 - \nu_x$ and $G\gamma = 38 + \nu_x$ respectively. The figure clearly shows polarization drops at these locations. Since the effect of the horizontal magnetic fields on the vertical component of the beam polarization has been eliminated by putting the vertical betatron tunes in the spin tune gap generated by the two partial snakes, only the vertical magnetic fields can depolarize the horizontal component of the polarization. Therefore, non-zero polarizations are expected at these resonance locations. However, the zero polarization can be obtained if there is a vertical and horizontal motion coupling or if some adjacent spin resonances are coherent to the horizontal intrinsic resonances, resulting in the complete depolarization.

4.2 Investigation of Other Depolarizing Sources

4.2.1 Residual Vertical Intrinsic Resonances

In order to overcome the imperfection and intrinsic resonances, the vertical betatron tunes have to be pushed inside the spin tune gap generated by the two helical partial snakes. However, it is difficult to get high vertical tunes below $G\gamma = 5$ since the partial snakes cause large orbit and optics distortions near injection energy, resulting in beam loss even with the compensation quadrupoles powered. The vertical betatron tunes were below 8.92 before $G\gamma = 5$, where two initial weak intrinsic resonances $(-4) + \nu_y$ and $14 - \nu_y$ were located. Because the acceleration rate was also slow, these two uncorrected weak resonances could cause some polarization loss. Therefore, in addition to the horizontal polarization profiles, a vertical polarization profile was also

measured to investigate the beam polarization loss due to the vertical motion.

The vertical polarization profile was carried out with 10% (2.1 T) cold snake and 5.9% (1.53 T) warm snake operation by using the horizontally oriented target 2 that moved up and down in the polarimeter vacuum chamber. The procedure of measurement was the same as for the horizontal profiles. Figure 4.5 shows one of the vertical polarization profile measurements, combined with the corresponding beam intensity profile from the normalized count rate. With the two helical partial snakes separated by $1/3$ of the ring, the generated spin tune gap is expected to be large enough to overcome both imperfection and intrinsic resonances if the vertical betatron tune during the acceleration cycle is completely moved inside the spin tune gap. The polarization should have no effect from the beam vertical motion, which means that the vertical polarization profile should be flat. However, the non-flat vertical polarization profile implies that depolarization due to the vertical betatron motion does exist during the acceleration in the machine.

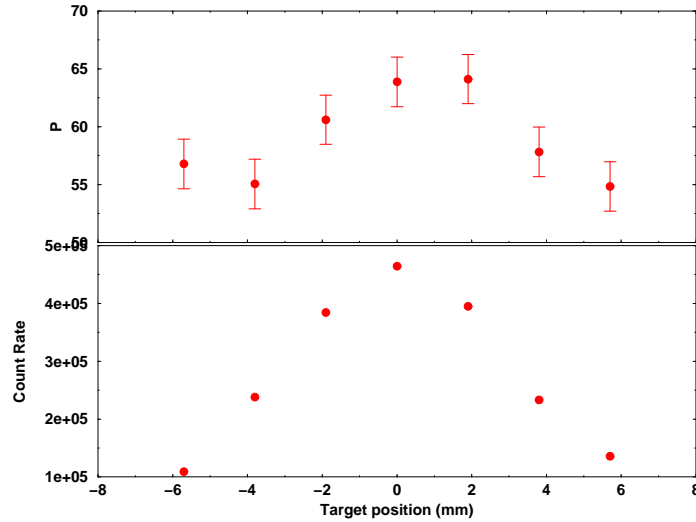


Figure 4.5: Vertical polarization profile (upper) and vertical beam profile (bottom) in the AGS for the 10% cold snake and 5.9% warm snake configuration.

To help identify the sources of depolarization shown in the vertical polarization profile, a vertical betatron tune scan was taken over the whole acceleration cycle as shown in Fig. 4.6. The plot shows both the fractional part of the measured vertical tune and the spin tune with a 10% (2.1 T) cold snake and 5.9% (1.53 T) warm snake as a function of $G\gamma$ for the whole energy ramp. There was difficulty for the vertical tune to be pushed into the spin tune gap before $G\gamma = 5$, which resulted in two initial intrinsic resonances outside the spin tune gap.

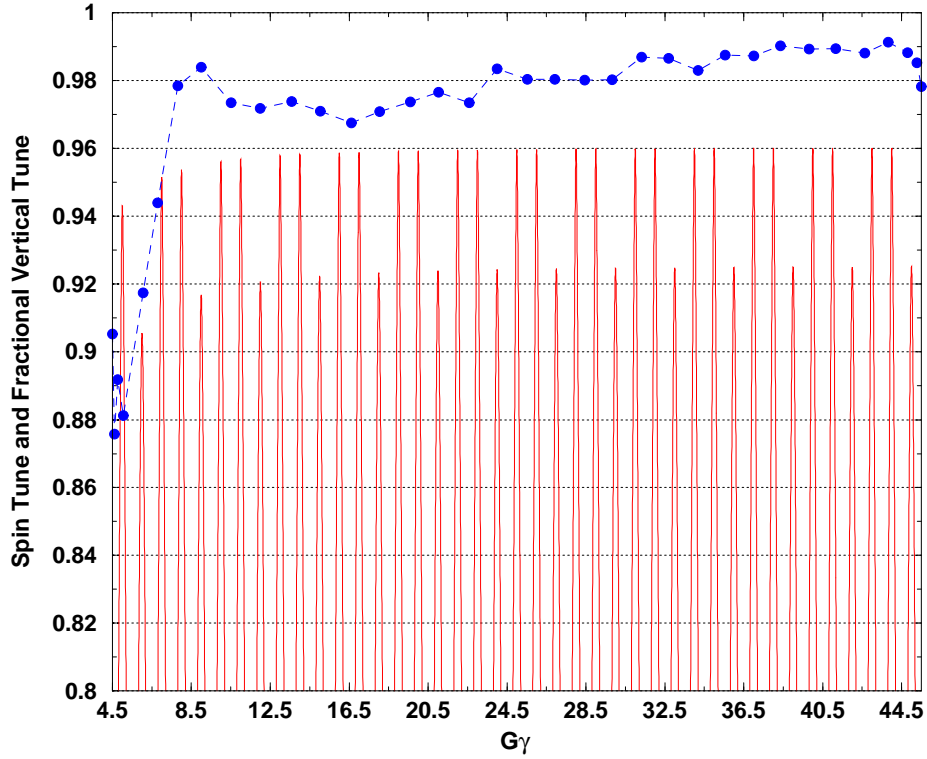


Figure 4.6: Fractional part of the measured vertical tunes (dots are connected by a dashed line) and spin tune with 10% cold snake and 5.9% warm snake as a function of $G\gamma$.

One more detailed tune scan at the beginning part of acceleration was performed to examine the vertical tunes in detail as shown in Fig. 4.7. At the two intrinsic

resonance locations $G\gamma = 4.92$ and $G\gamma = 5.08$, the vertical betatron tune was 8.896 and 8.904, which gave resonance strength of $\epsilon_1 = 1.3787 \times 10^{-4}$ and $\epsilon_2 = 1.0427 \times 10^{-4}$ as calculated by the program DEPOL [11, 37]. Treating the two intrinsic resonances as isolated and well separated, about 2% depolarization would be expected after passing through both resonances according to

$$P = \frac{1 - \frac{\pi|\epsilon_1|^2}{\alpha_1}}{1 + \frac{\pi|\epsilon_1|^2}{\alpha_1}} \times \frac{1 - \frac{\pi|\epsilon_2|^2}{\alpha_2}}{1 + \frac{\pi|\epsilon_2|^2}{\alpha_2}}. \quad (4.29)$$

Here $\alpha_1 = 1.10 \times 10^{-5}$ and $\alpha_2 = 1.50 \times 10^{-5}$ are the acceleration rate crossing the two intrinsic resonances, respectively.

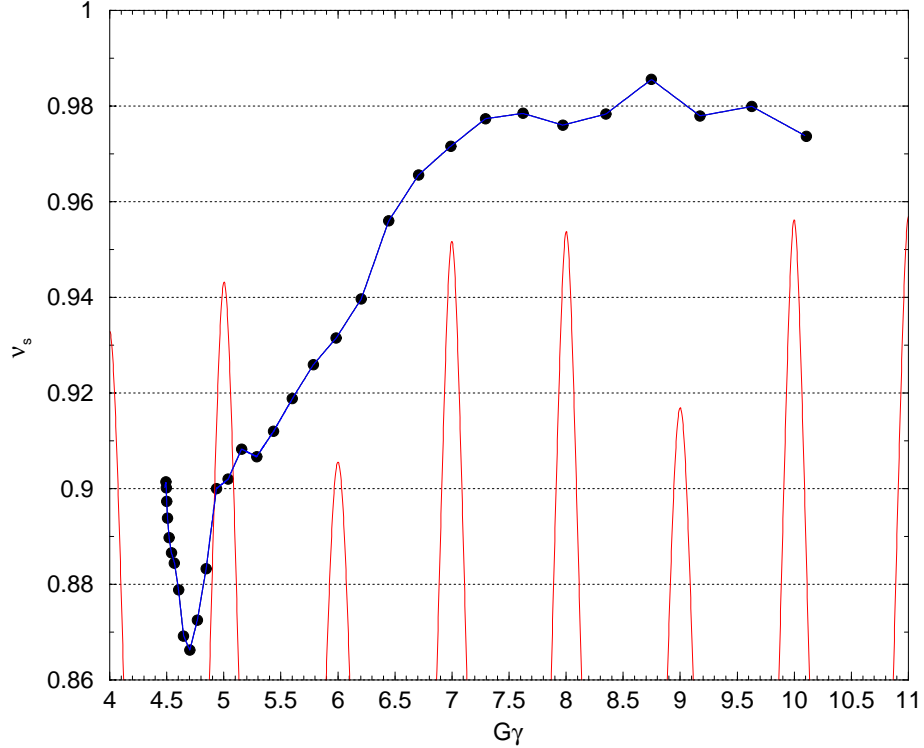


Figure 4.7: Fractional part of the measured vertical tunes (dots connected by a line) and spin tune with 10% cold snake and 5.9% warm snake at the early part of the energy ramp.

Spin tracking using *SPINK* also confirmed the depolarization from the two intrinsic resonances. The tracking was performed using 100 particles with Gaussian distribution in the vertical phase space with a normalized rms emittance 2.5 mm-rad, as well as a rms $\frac{\Delta p}{p} = 0.003$ momentum spread to eliminate the spin coherence phenomenon. The horizontal emittance was set to zero to avoid any depolarizing effect from the horizontal motion. The vertical tune path data came from Fig. 4.7, and the real acceleration rate was taken from Fig. 3.2. In order to get rid of the polarization loss from spin mismatching at injection, the spin direction was initialize to the stable spin direction at injection energy. Figure 4.8 shows the tracking result

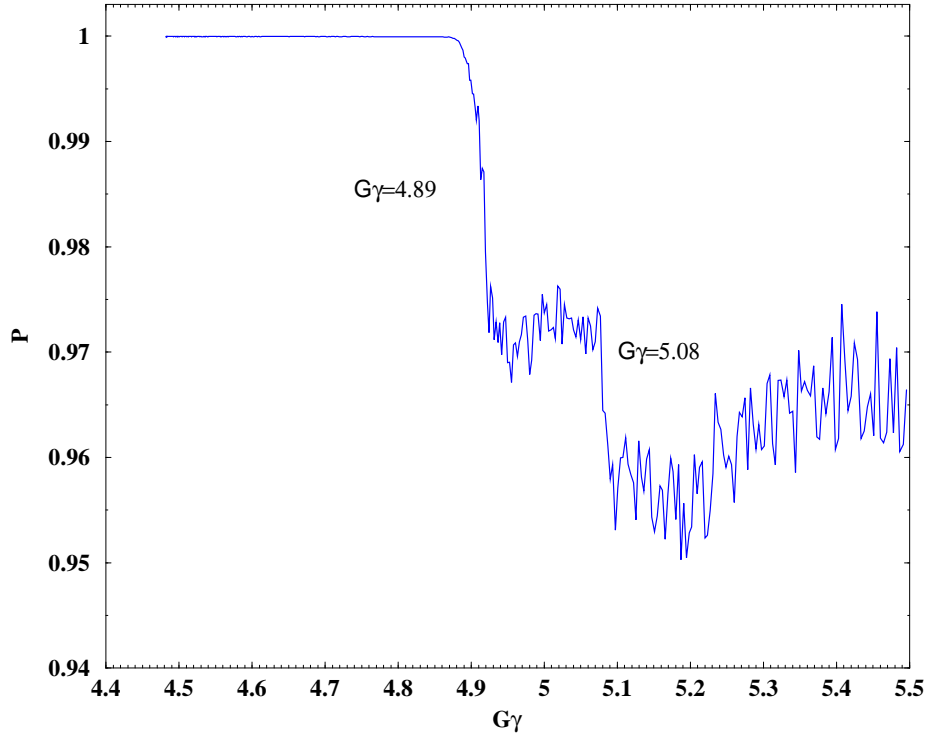


Figure 4.8: Spin tracking through the first two weak intrinsic resonances with 10% (2.1 T) cold snake and 5.9% (1.53 T) warm snake. The polarization is obtained along the stable spin direction.

after crossing the two intrinsic resonances at $G\gamma = 4.92$ and $G\gamma = 5.08$ with 10% (2.1 T) cold snake and 5.9% (1.53 T) warm snake. The polarization can lose 4% of the initial 100%, including a 3% loss due to the crossing of the first resonance and a 1% loss due to the second resonance. The strength of the two intrinsic resonances can also be estimated from Fig. 4.8 by

$$\frac{P_f}{P_i} = \frac{1 - \frac{\pi|\epsilon|^2}{\alpha}}{1 + \frac{\pi|\epsilon|^2}{\alpha}} \quad \text{to get} \quad \epsilon = \sqrt{\frac{1 - \frac{P_f}{P_i}}{1 + \frac{P_f}{P_i}}} \cdot \frac{\alpha}{\pi}, \quad (4.30)$$

where $\frac{P_f}{P_i}$ is the ratio of polarization after and before crossing the resonance. The resultant strengths of the two resonance are $\epsilon_1 = 2.1890 \times 10^{-4}$ and $\epsilon_2 = 1.1108 \times 10^{-4}$ respectively, larger than the values from the DEPOL [11, 37]. The difference can be explained by the following:

1. DEPOL is a code used to calculate the strength of the imperfection and intrinsic resonances from the integral in Eq. (2.13), which is calculated by breaking it up to sum over all the elements in the machine lattice. The vertical displacement, including closed orbit distortion or betatron motion at each element, is obtained from the information of the *MAD* output *.twiss* file. In the DEPOL program, the snake has been treated as a drift space with no contribution to the vertical orbit or spin precession, which in reality do change. Therefore, the resonance strength given by DEPOL is not exactly correct, and is smaller than the value that we have expected.
2. *SPINK* is a program that tracks the spin motion continuously during the energy ramping. As shown in Fig. 4.8, the spin resonance overlapping does not need to be considered since the separation of the two weak resonances satisfies $\Delta G\gamma = 0.17 \gg \max(|\epsilon_1|, |\epsilon_2|)$. However, the spin motion can still be affected by the resonance it passed due to coherence, especially when two adjacent resonances are not far away from each other. The depolarization effect can be enhanced

and cause more or less polarization loss, depending on the interference of the two resonances.

Therefore, the *SPINK* tracking is more realistic in describing spin motion during the energy ramp. Based on the spin tracking result of 4% loss for the initial 100%, the two resonances counted 3.4% loss to the injected 82% polarized proton beam in the AGS 2006 polarized proton run.

Except for providing an estimated polarization loss through the two weak intrinsic resonances, *SPINK* tracking provides a hint on how to reduce the depolarization by separating the two resonances as widely as possible to eliminate the spin coherence. Another important hint to reduce the polarization loss is to increase the effective resonance crossing rate α_c . If the vertical betatron tune keeps constant during the acceleration, the effective resonance crossing rate α_c equals the acceleration rate α . However, the α_c can be increased by changing the vertical betatron tune path during the energy ramping as follows

$$\alpha_c = \frac{d(G\gamma - \nu_y)}{d\theta} = \alpha - \alpha \cdot \frac{d\nu_y}{dG\gamma}. \quad (4.31)$$

Here α is the acceleration rate of AGS as mentioned before. The negative slope of $\frac{d\nu_y}{dG\gamma}$ expresses how much the α_c has benefited.

Several spin trackings with different vertical tune paths were done based on the above two ideas, as shown in Fig. 4.9, with 10% (2.1 T) cold snake and 5.9% (1.53 T) warm snake. Different colors represent different tune paths and the corresponding spin trackings crossing the two weak intrinsic resonances. The first vertical tune path (red color) is from the measured tunes in the AGS 2006 run and the others are simulation.

Some important parameters extracted from spin trackings are listed in Table 4.7. Using the lattice in each resonance, DEPOL gives the corresponding strengths of intrinsic resonances shown in Table 4.8.

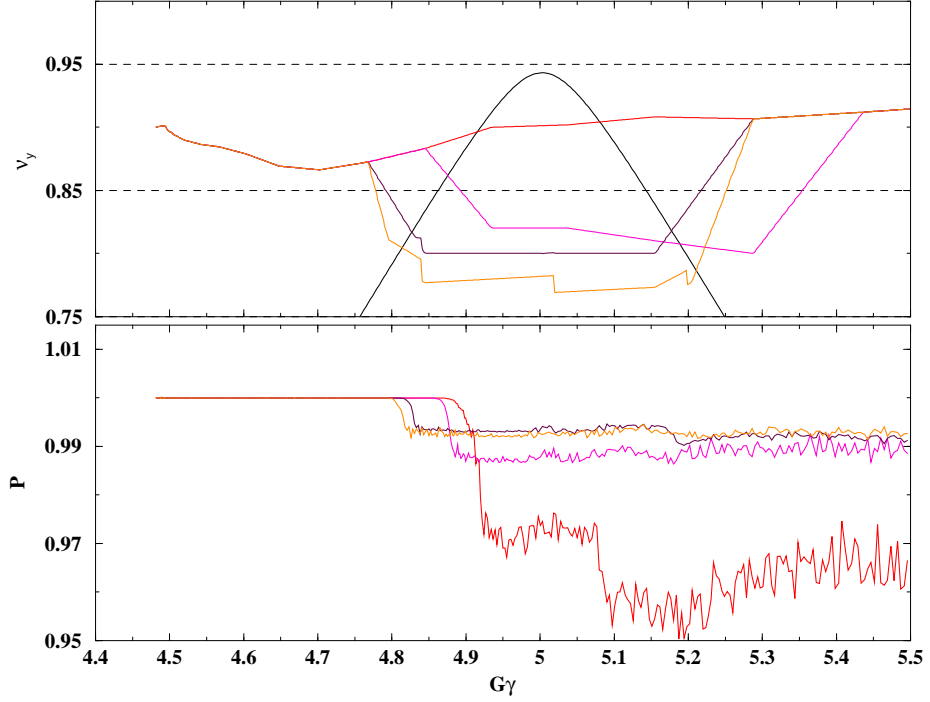


Figure 4.9: Spin trackings through the first two weak intrinsic resonances with different vertical tune paths. The polarization is obtained along the stable spin direction.

Table 4.7: Important parameters from four spin trackings with different vertical tune paths. Different colors represent different trackings as shown in Fig. 4.9.

Color	First Resonance					Second Resonance				
	$G\gamma$	P_f/P_i	α (10^{-5})	α_c (10^{-5})	ϵ (10^{-4})	$G\gamma$	P_f/P_i	α (10^{-5})	α_c (10^{-5})	ϵ (10^{-4})
red	4.915	0.973	1.10	1.10	2.1890	5.081	0.993	1.50	1.50	1.2950
magenta	4.875	0.987	0.67	1.15	1.5476	5.188	0.999	1.53	1.40	0.4722
maroon	4.827	0.993	1.00	2.00	1.4953	5.177	0.998	1.54	2.70	0.9275
orange	4.814	0.993	1.04	1.43	1.2644	5.211	0.999	1.57	4.05	0.8031

Table 4.8: Calculated strengths of the two intrinsic resonances from DEPOL with different vertical tune paths.

Color	First Resonance		Second Resonance		$\Delta G\gamma$
	$G\gamma$	$\epsilon(\times 10^{-4})$	$G\gamma$	$\epsilon(\times 10^{-4})$	
red	4.915	1.3787	5.081	1.0427	0.166
magenta	4.875	1.3193	5.188	0.8773	0.313
maroon	4.827	1.2682	5.177	0.8822	0.350
orange	4.814	1.2577	5.211	0.8645	0.397

The observations can be summarized as follows:

1. The calculated strengths of spin resonances from DEPOL are less than the values from spin tracking because of the treatment of snakes as drift spaces in the DEPOL program. This can lead to a maximum 1.6% difference of the polarization loss.
2. Both of the two intrinsic resonances are weak resonances and the second one is much weaker than the first one. All of four separations of the two resonances are large enough to eliminate the spin resonance overlapping, because of $\Delta G\gamma \gg \max(|\epsilon_1|, |\epsilon_2|)$, but may still leave the spin coherence effect, especially for the most realistic case (red color).
3. The strength of a spin intrinsic resonance close to an integer is larger than the one far from the integer.
4. With an appropriate vertical tune path, the polarization loss can be reduced by 2% after crossing the first intrinsic resonance comparing the first spin tracking (red color) to the fourth spin tracking (orange color). The large separation of the two resonances can reduce the spin coherence effect on the polarization while crossing the second resonance because there is more time for the components

perpendicular to the stable direction to decohere. At least 3% polarization can be rescued through the two weak intrinsic resonances.

Therefore, a modest reduction of polarization loss from crossing the first two weak intrinsic resonances can be obtained by selecting an appropriate vertical tune path if vertical betatron tune can not be placed inside the spin tune gap.

4.2.2 High Order Partial Snake Resonances

With two partial snakes in the AGS, the spin tune ν_s depends on energy and partial snake strengths as given in Eq. (2.37). Although the vertical tunes have been placed into the spin tune gap, the partial snakes themselves can still provide a mechanism for depolarization, called partial snake resonance [38, 39, 31, 32, 33]. The partial snake resonance occurs when

$$\nu_s + k\nu_y = \text{integer}, \quad (4.32)$$

where ν_y is the vertical betatron tune and $k > 1$ is an integer. The spin kick coherent to the condition of the partial snake resonance due to the fact that the intrinsic resonance strength in the tracking demonstration is non-zero. Therefore, the partial snake resonance strength is proportional to the strength of the intrinsic resonance strength. Table 4.9 lists the strengths of the four strong intrinsic resonances calculated

Table 4.9: Strengths of four strong intrinsic resonances calculated by DEPOL in the bare AGS machine assuming particle at a normalized rms emittance 2.5 mm-mrad.

P(GeV/c)	$G\gamma$	ϵ
4.871	$0 + \nu_y$	0.0075
11.565	$12 + \nu_y$	0.0026
15.208	$36 - \nu_y$	0.0069
24.951	$36 + \nu_y$	0.0133

using DEPOL assuming a single particle at a normalized rms emittance 2.5 mm-mrad ellipse in the bare AGS machine (“bare” means the machine lattice is constructed only by the combined function of bending magnets and the tune quadrupoles). The partial snake resonance can easily happen in the vicinity of the strongest intrinsic resonance at $36 + \nu_y$, and may also happen at the weakest one at $12 + \nu_y$.

Because the vertical betatron tunes have been moved into the spin tune gap at all four strong intrinsic resonances in the AGS, the intrinsic resonance at $k = 1$ can easily be avoided. However, the high order partial snake resonances can be experienced by the particle within the reduced tune space.

The measurements of polarization as a function of vertical tune, called vertical tune scans, were carried out to investigate the effect of high order partial snake resonance on the polarization. Beam polarizations were measured at the AGS extraction energy and the machine setup was kept similar during the tune scans. Figure 4.10 presents two tune scans at intrinsic resonance positions $12 + \nu_y$ and $36 + \nu_y$ with 14% (2.5 T) cold snake plus 5.9% (1.53 T) warm snake. More curvature has been shown at the tune scan around $36 + \nu_y$ location because the strength of the partial snake resonance is proportional to the strength of the intrinsic resonance. One more vertical tune scan at the moderately strong intrinsic resonance position $36 - \nu_y$ is shown in Fig. 4.11 (A tune scan at $12 + \nu_y$ is included for comparison).

The polarization drop with $\nu_y \leq 8.9$ appears when the vertical tune is moved outside of the spin tune gap. At the four strong intrinsic resonance locations $0 + \nu_y$, $12 + \nu_y$, $36 - \nu_y$, $36 + \nu_y$ with the two snakes, the high order partial snake resonance positions are listed in Table 4.10, and agree with the experimental results. The high order partial snake resonances do not show a significant effect on the polarization and the polarization reaches a plateau when the vertical tune is above 8.96 at $12 + \nu_y$ and $36 - \nu_y$. The strongest intrinsic resonance at $36 + \nu_y$ shows the effect of the polarization from the second, third and fourth order partial snake resonance. As expected, the higher order of the resonance, the less polarization dip due to the weaker resonance

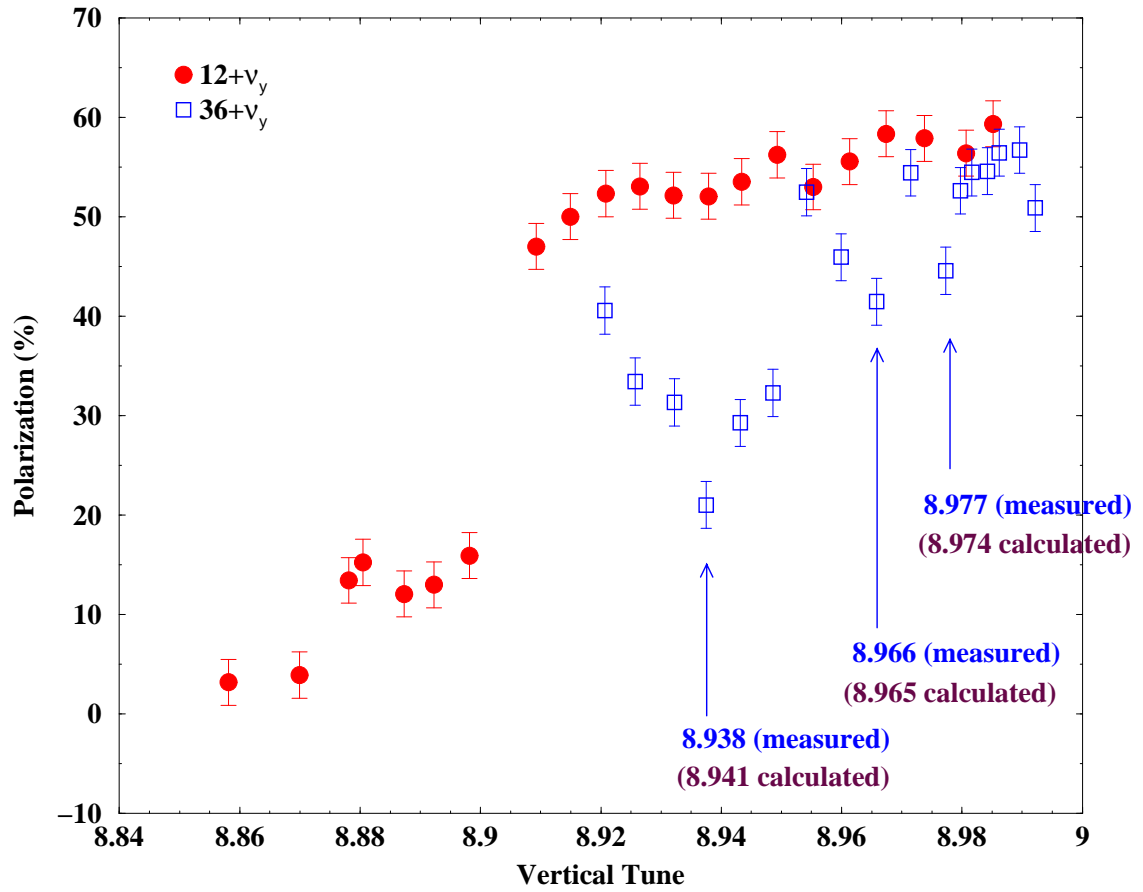


Figure 4.10: Vertical tune scan at $12 + \nu_y$ (weaker) and $36 + \nu_y$ (stronger) intrinsic resonance position for 14% (2.5T) cold snake plus 5.9% (1.53T) warm snake.

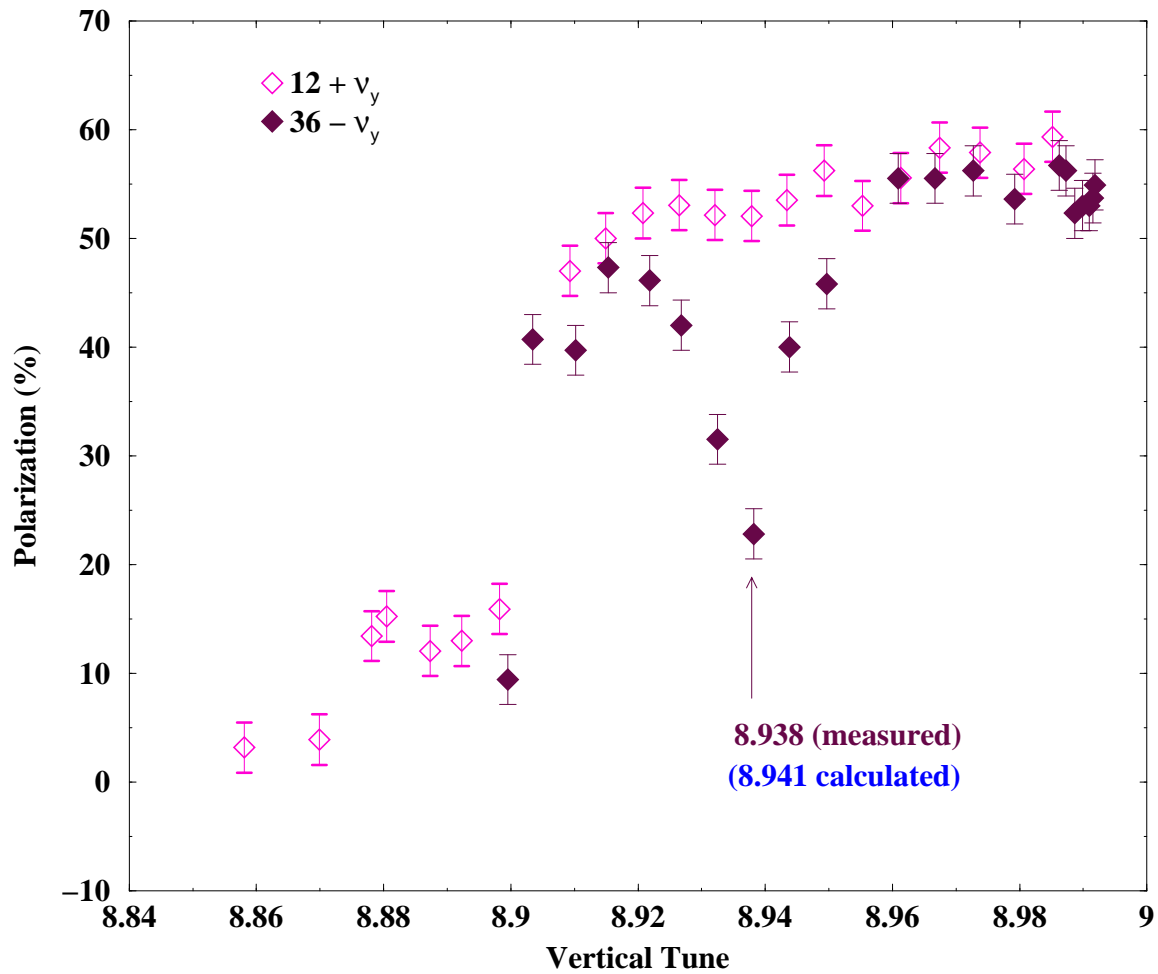


Figure 4.11: Vertical tune scan at $12 + \nu_y$ and $36 - \nu_y$ with 14% (2.5T) cold snake and 5.9% (1.53T) warm snake.

Table 4.10: High order partial snake resonance locations for both 10% (2.1 T) cold snake plus 5.9% (1.53 T) warm snake and 14% (2.5 T) cold snake plus 5.9% (1.53 T) warm snake conditions.

Condition		ν_y			
Snakes	Resonance Location	l=2	l=3	l=4	l=5
2.1T cold snake & 1.53T warm snake	$0 + \nu_y$	0.951	0.972	0.981	0.985
	$12 + \nu_y$	0.953	0.974	0.981	0.985
	$36 - \nu_y$	0.953	0.974	0.981	0.985
	$36 + \nu_y$	0.953	0.974	0.981	0.985
2.5T cold snake & 1.53T warm snake	$0 + \nu_y$	0.937	0.961	0.972	0.977
	$12 + \nu_y$	0.941	0.965	0.974	0.979
	$36 - \nu_y$	0.941	0.965	0.974	0.980
	$36 + \nu_y$	0.941	0.965	0.974	0.980

strength.

Spin trackings for the investigation of high order partial snake resonances at the strongest intrinsic resonance $36 + \nu_y$ are completed with the following conditions: (i) 100 particles with 2.5 mm-mrad normalized rms emittance for a Gaussian distribution in the vertical phase space only, (ii) the vertical betatron tunes are set at the third, fourth and fifth order partial snake resonance locations respectively, (iii) the energy ramping starts from $G\gamma = 43.5$ to $G\gamma = 46.5$, crossing the strong intrinsic resonance at $G\gamma = 36 + \nu_y$, (iv) realistic acceleration rate and machine lattice are used for spin tracking. The performance of the vertical component of polarization is shown in Fig. 4.12 with 14% cold snake and 5.9% warm snake and in Fig. 4.13 with 10% cold snake and 5.9% warm snake. The simulations confirm the existence of high order partial snake resonances at $36 + \nu_y$, and the polarization dip is negligible above the fifth order partial snake resonance when the vertical betatron tune is beyond 8.98 for 14% cold

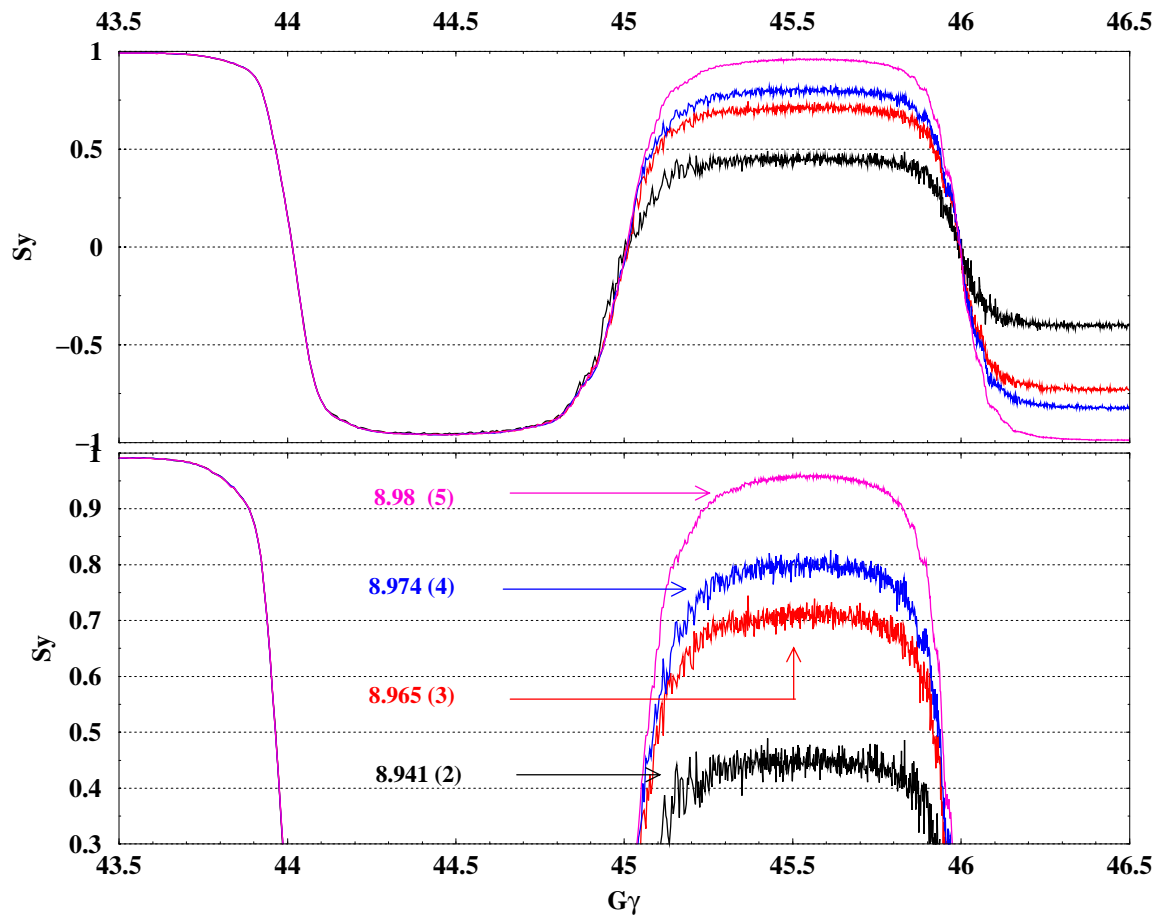


Figure 4.12: Spin tracking with constant vertical betatron tunes located at high order partial snake resonance locations with 14% (2.5T) cold snake and 5.9% (1.53T) warm snake.

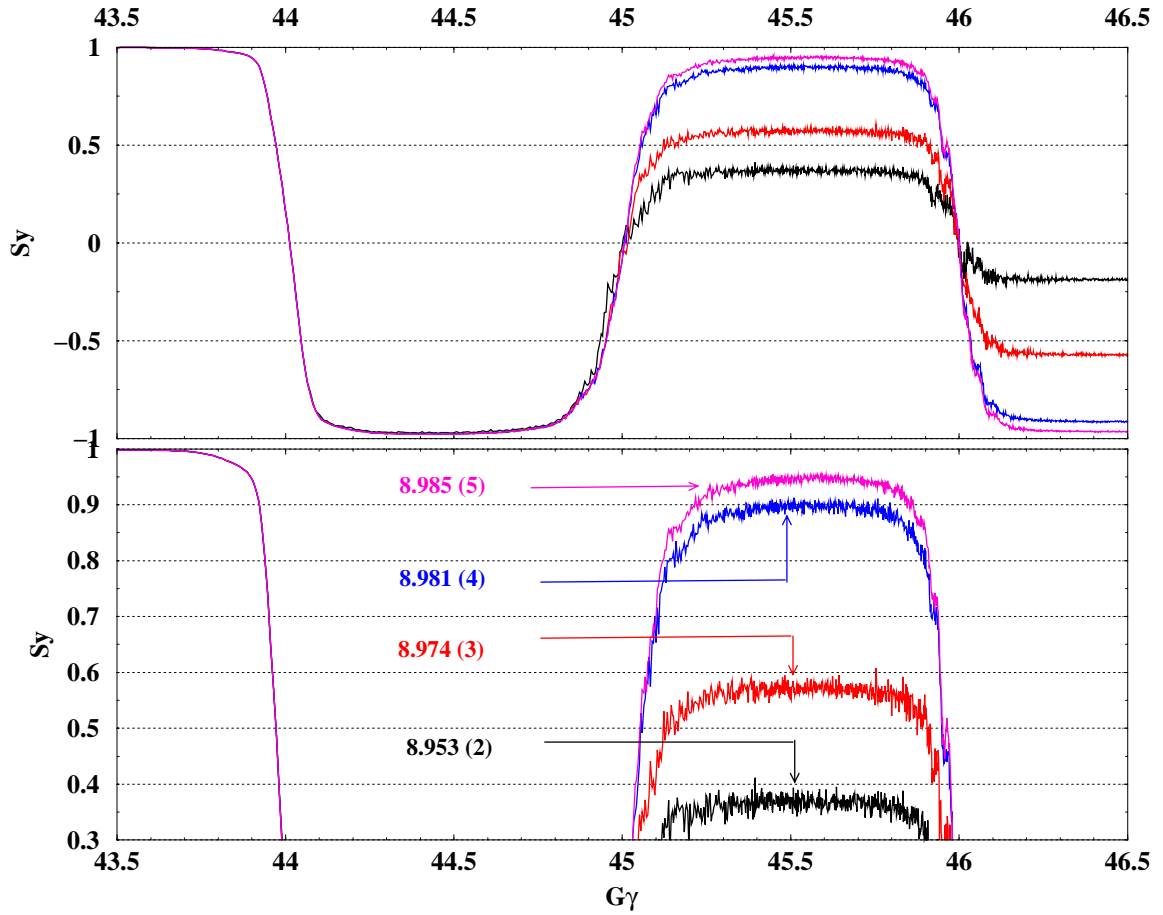


Figure 4.13: Spin tracking with constant vertical betatron tunes located at high order partial snake resonance locations with 10% (2.1T) cold snake and 5.9% (1.53T) warm snake.

snake and 8.985 for 10% cold snake.

Vertical tune scans at these strong intrinsic resonance locations, combined with the spin tracking simulations, give a guide where the vertical tune should be put to preserve the polarization with the reduced space limit. In conclusion, the vertical tunes have to be pushed above 8.98 at $36 + \nu_y$ and above 8.96 at $12 + \nu_y$ and $36 - \nu_y$ with 14% cold snake and 5.9% warm snake. However, with the vertical tune beyond 8.99, the associated orbit distortion is likely another reason to cause the polarization drop as discussed in the following section.

4.2.3 Closed Orbit Distortion

With the vertical betatron tune pushed close to integer 9 at the flat-top energy in the AGS, the beam polarization becomes sensitive to the associated large closed orbit distortion.

In an accelerator, the vertical closed orbit amplitude is given by

$$y_{co}(s_0) = \frac{\sqrt{\beta(s_0)}}{2 \sin \pi \nu_y} \oint \sqrt{\beta(s)} \cos(\pi \nu_y + \psi(s_0) - \psi(s)) \frac{\Delta B}{B\rho} ds. \quad (4.33)$$

Here $\beta(s_0)$ and $\psi(s_0)$ are respectively the β function and phase at the measured s_0 location. $\beta(s)$, $\psi(s)$ and $\frac{\Delta B}{B\rho} ds = d\theta$ are respectively the β function, phase and kick angle caused by the field error at s location. ν is the vertical betatron tune. As seen from Eq. (4.33), the closed orbit is greatly enhanced when the vertical betatron tune is close to an integer. Because the imperfection resonance

$$\epsilon_K = \frac{1 + G\gamma}{2\pi} \oint \frac{\partial B_z}{\partial x} y_{co}(s) e^{iK\theta} ds \quad (4.34)$$

is proportional to the closed orbit amplitude y_{co} and beam energy $G\gamma$, the imperfection resonance can still be an important depolarization source at high energy even with two partial snakes installed. The near integer vertical tune makes the effect of the 9^{th} harmonics much stronger. If the effect of partial snakes and a strong imperfection resonance is out of phase, the resulting effective strength is weakened, and

the spin tune gap becomes too small to preserve the polarization. The imperfection resonance with large orbit distortion can cancel the effect of the two partial snakes. Experimentally, we did observe polarization loss due to the closed orbit distortion. Measured Polarization as a function of $\sin 9\theta$ harmonic orbit amplitude at $36 + \nu_y$ is shown in Fig. 4.14.

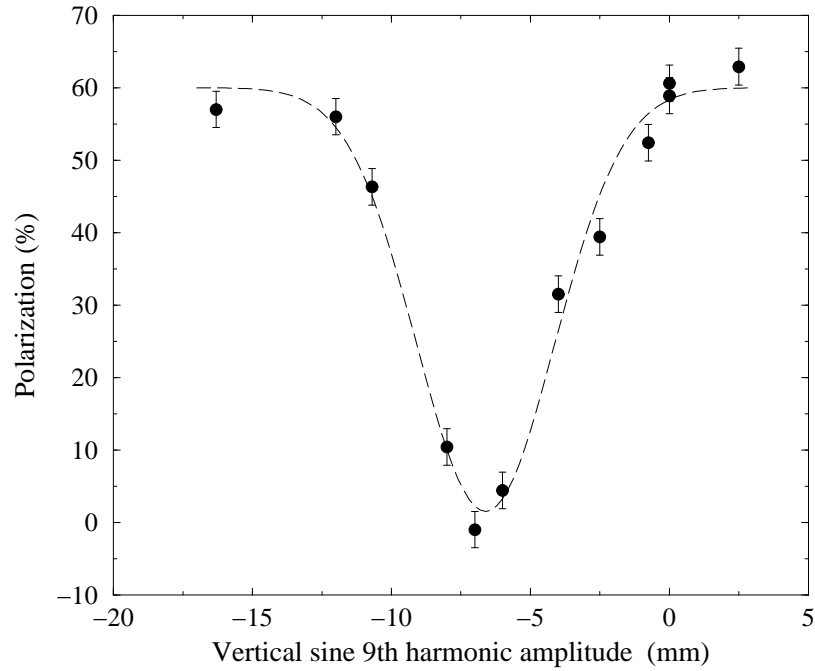


Figure 4.14: Measured polarization as a function of vertical $\sin 9\theta$ harmonic amplitude.

Estimated imperfection resonance strengths, around $G\gamma = 36 + \nu_y$ where the vertical tune is beyond 8.989, for the AGS lattice with different $\sin 9\theta$ harmonic amplitudes are given in Table 4.11 and shown in Fig. 4.15. The choice of $\sin 9\theta$ harmonic amplitudes comes from the experiment data and these resonance strengths can be strong enough to be comparable to the two partial snake strengths.

Spin tracking sweeping the energy at $G\gamma = 36 + \nu_y$ are used to investigate the beam polarization with these different closed orbit distortions of the $\sin 9\theta$ harmonic

Table 4.11: AGS imperfection resonance strengths calculated using DEPOL with different closed orbit distortions and vertical tune close to 9 at $G\gamma = 36 + \nu_y$.

The sin9th harmonic amplitude (mm)	Imperfection resonance strength ϵ_K at $G\gamma = 36 + \nu_y$	rms orbit distortion (mm)
-16	0.04512540	10.4863
-12	0.08325239	7.7819
-10.5	0.08786251	6.5573
-8.2	0.06274099	5.8790
-6.4	0.04938734	4.6127
-4.0	0.03112522	2.8979
-2.4	0.01874080	1.7426
-0.6	0.00469420	0.4362
0	0	0
2.5	0.01952357	1.8153

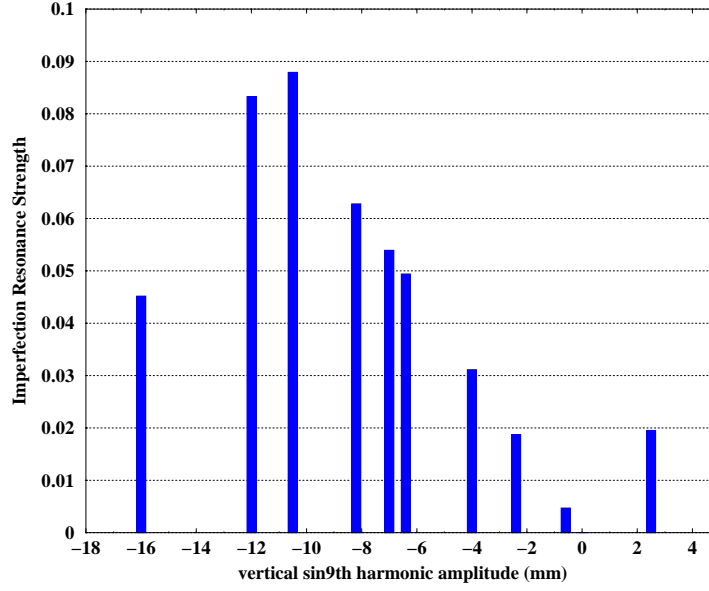


Figure 4.15: Imperfection resonance strengths calculated using DEPOL as a function of different vertical $\sin 9\theta$ harmonic amplitude at $36 + \nu_y$.

amplitudes. 100 particles with normalized rms emittance 2.5 mm-mrad in the vertical phase space and rms momentum spread $\frac{\Delta p}{p} = 0.001$ in the longitudinal phase space were chosen for these simulations. These spin trackings were from $G\gamma = 44.5$ to $G\gamma = 45.5$, only crossing the imperfection resonance at $G\gamma = 45$. The comparison of the polarization as a function of vertical $\sin 9\theta$ harmonic amplitude crossing the imperfection resonance at $G\gamma = 45$ between the spin trackings and experiments is shown in Fig. 4.16. The relative polarization is given by P_f/P_i , where P_f and P_i are the polarization after and before resonance. Depolarization happens with the amplitude expected from the calculation. The disagreement of the relative polarizations at some amplitudes comes from the complexity of the real closed orbit distortions, which also have the contribution from other n^{th} harmonic amplitudes.

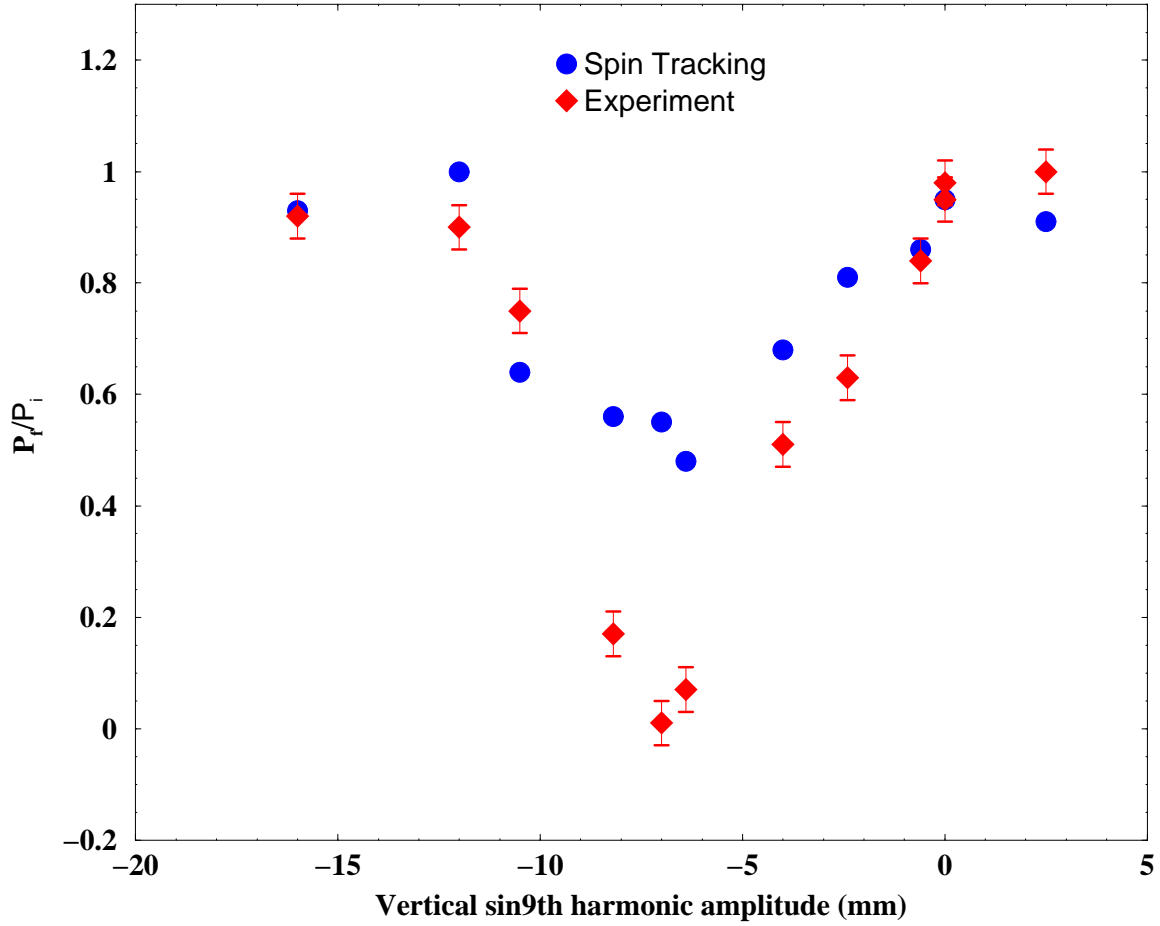


Figure 4.16: Comparison of the polarization vs. the vertical $\sin 9\theta$ harmonic amplitude while crossing the imperfection resonance at $G\gamma = 45$ between spin tracking and experiment. The vertical axis is the ratio of polarization after and before resonance, the horizontal axis is the vertical $\sin 9\theta$ harmonic amplitude. The locations of polarization dip agree well between the simulation and experiment.

Chapter 5

Summary and Solution

5.1 Summary

Polarized proton beam can lose their beam polarization when encountering spin depolarizing resonances in a synchrotron. Two main resonances are classified as imperfection resonances when the spin tune equals an integer, and intrinsic resonances when the spin tune equals $nP \pm \nu_y$, where P is the super periodicity of the accelerator and ν_y is the vertical betatron tune. Special approaches have to be introduced to overcome these spin resonances and maintain the beam polarization. One solution is to use *Siberian snake*. The rotation of spin vector caused by *Siberian snakes* breaks up the resonance conditions, resulting in the preservation of the polarization.

For a full Siberian snake precessing the particle spin by 180° about an horizontal axis, the spin tune becomes $\frac{1}{2}$. This particular spin tune can avoid the two spin resonance conditions caused by the magnetic field error. Since the depolarizing resonance strength in a medium energy synchrotron is not very strong, a strong enough partial snake, which needs less space, can generate a large enough spin tune gap to overcome both imperfection and intrinsic resonance, as long as the vertical tune is placed inside the spin tune gap. The only challenge is to maintain the betatron tune close to an

integer. The use of two partial helical dipole snakes, called warm partial snake and cold partial snake respectively, in the AGS has proved this concept.

The intention of using *two* partial snakes separated by $1/3$ of the ring comes from two considerations:

1. One strong partial snake can introduce non-negligible polarization loss due to the spin direction mismatching at the injection and extraction energies. An additional partial snake can reduce the spin direction mismatching and also increase the effective partial snake strength if its position is chosen properly.
2. Separating the two partial snakes by $1/3$ of the ring introduces a periodicity of three units in the spin tune dependence of $G\gamma$. Since both the super- periodicity of the AGS ($P = 12$) and the vertical betatron tune ($\nu_y \sim 9$) are divisible by three, the spin tune gap is largest at $G\gamma = 3n$ where the strong intrinsic resonances are located.

With the 10% (2.1 T) cold partial snake and 5.9% (1.53 T) warm partial snake, the polarization at AGS extraction reached the high polarization of 65% with the injected 82-86% in 2006 polarized proton run. However, there was still a 20% polarization loss. Several depolarizing sources, existing in the current AGS machine status, are classified as following:

1. *Horizontal Intrinsic Resonance* — Generally, the spin intrinsic resonance only happens at $G\gamma = nP \pm \nu_y$, associated with the vertical betatron tune ν_y where the vertical polarization is affected by the horizontal magnetic fields. However, the stable spin direction will not be vertical any more with the presence of the partial snakes. Therefore, the perturbing fields that rotate the spin away from the stable spin direction have vertical as well as horizontal component. Particles undergoing horizontal betatron oscillation encounter vertical field deviation at the horizontal oscillation frequency. As a result, the spin resonance occurs

whenever the spin tune satisfies $\nu_s = n \pm \nu_x$, and this type of resonance is called horizontal intrinsic resonance.

2. *Residual Vertical Intrinsic Resonance* — Four compensation quadrupoles for each partial snake have been added to eliminate the lattice distortion caused by the partial snake magnets especially at the low energies, with the result that the vertical betatron tunes can only be pushed into the spin tune gap after $G\gamma = 5$. Although two remaining intrinsic resonances below $G\gamma = 5$ are weak, they are enhanced by the slow acceleration rate at the beginning of the ramp and can account for at least 4% polarization loss. The spin coherence between the two adjacent resonances may enhance the depolarizing effect, resulting in more depolarization after crossing them.
3. *High Order Partial Snake Resonance* — Partial snake resonances happen at $\nu_s \pm K\nu_y = \text{integer}$, where ν_s is the spin tune with the partial snake(s), ν_y is the vertical betatron tune and K is an integer. Since the vertical betatron tunes have been moved into the spin tune gap after $G\gamma = 5$, the intrinsic resonance (or called the first order partial snake resonance) can easily be avoided. However, higher order partial snake resonances can still cause depolarization the beam, especially in the vicinity of the strong intrinsic resonances, because the snake resonance strength is proportional to the strength of the nearby intrinsic resonance. The polarization gets much worse when the vertical tune meets these high order partial snake resonance conditions during the energy ramp.
4. *Enhanced Imperfection Resonance* — When the vertical betatron tune is beyond 8.99, the closed orbit distortion is greatly enhanced. Since the imperfection resonance strength is proportional to the closed orbit distortion and beam energy, an imperfection resonance can cancel the effect of two partial snakes resulting in a significant polarization drop.

The above spin sources of depolarization have been investigated during AGS 2006 polarized proton run. Horizontal polarization profile measurements were used to explore the horizontal intrinsic resonance; vertical polarization profile measurements were used to explore polarization loss due to the beam vertical motion; vertical tune scans in the vicinity of the strong intrinsic resonances were employed to explore the high order partial snake resonance, and a vertical 9th harmonic amplitude scan was carried out to explore the enhanced imperfection resonance due to the large closed orbit distortion when the vertical betatron tune was close to the integer 9. All of the relationships between the polarization and the depolarizing source were clearly observed in these experiments as described in Chapter 4.

To quantify these polarization losses, more realistic spin trackings were done for the different cases. In order to explore the depolarization due to the horizontal intrinsic resonance, the particles were given a Gaussian distribution only in the horizontal phase space with a momentum spread to eliminate the spin coherent phenomenon. A similar condition was given to explore spin depolarization due to vertical motion, except the particles were distributed in vertical phase space. For the investigation of partial snake resonances, the spin trackings were focused at the top energy range where the vertical betatron tunes were moved into the spin tune gap.

In summary, spin trackings show $\sim 6\%$ polarization loss due to the horizontal intrinsic resonance, $\sim 4\%$ due to the residual vertical intrinsic resonance, $\sim 3\%$ due to the high order partial snake resonance with a 10% (2.1 T) cold snake and 5.9% (1.53 T) warm snake. In addition, there were 2 $\sim 3\%$ polarization loss due to the spin mismatching at injection. The effect of closed orbit distortion on the polarization can be overcome in the machine operation.

5.2 Solution

Although the historically highest polarization of 65% has been achieved by the installation of the two partial helical dipole snakes in the AGS, the stated goal of 70% polarization is required by the RHIC spin program. A further study will focus on overcoming all causes of beam depolarization. Different schemes have been proposed aiming at different depolarizing mechanisms as described below and several will be carried out in the future runs. Before that, preliminary simulations have also been developed to give guidance.

1. To overcome the horizontal intrinsic resonance, the horizontal betatron tunes need to be also pushed up inside the spin tune gap generated by the two partial helical dipole snakes. One simple spin tracking was done by putting one particle at 2.5π mm-mrad normalized emittance ellipse in the horizontal phase space and zero vertical emittance to eliminate the effect on the polarization due to the vertical motion. The horizontal tune was set at 8.985 inside the spin tune gap generated by 10% (2.1 T) cold snake and 5.9% (1.53 T) warm snake. Spin tracking results are shown in Fig. 5.1. The blue straight line is the polarization projected to the stable spin direction, the red curve exhibits the vertical component of the polarization following the stable spin direction with three unit periodicity. The results indicate that there is no polarization loss during the energy ramping with the horizontal tune inside the spin tune gap.

In reality, the challenge for AGS to push the horizontal tune high enough is the limit of the current in the family of 12 tune quadrupoles. A higher betatron tune demands higher current. The maximum available current in the horizontal quadrupoles is 700 A that constraints the maximum horizontal tune to be about 8.83 at the top energy. This problem can be solved (partially) by adding 12 unused quadrupoles to the vertical quadrupoles string. With increased tolerance of vertical betatron tune, the horizontal betatron tune can be pushed from 8.82

to 8.95. [40]. In addition, the radius shift [41] towards the inside of the ring enhances the increase of the horizontal tune.

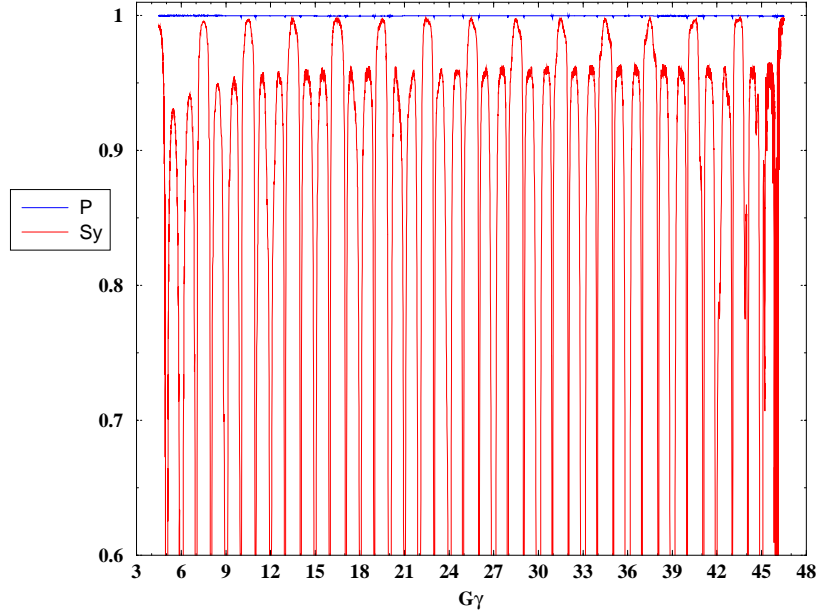


Figure 5.1: A simple spin tracking by putting one single particle at the normalized rms emittance 2.5π mm-mrad ellipse in the horizontal phase space. The horizontal tune was set at 8.985 inside the spin tune gap generated by 10% (2.1 T) cold snake and 5.9% (1.53 T) warm snake. The tracking result shows no depolarization.

2. To overcome two weak intrinsic resonances before $G\gamma = 5$, the most direct method is to push the vertical tunes high enough to be in the spin tune gap. However, this approach is difficult at injection because the large lattice and orbit distortions caused by the partial snakes do not allow a vertical tune above 8.95 with beam survival, even though four compensation quadrupoles for each of partial snake have been added for optics correction. Another approach to reduce the polarization loss can be increasing the acceleration rate based on the

Froissart-Stora formula. This is also not practical because a quick acceleration rate needs a change of the ramping magnet function, which is not reasonable for the AGS power supply. A more flexible approach is to lower the vertical tunes when the beam crosses the two resonances. One advantage of this is to separate the two resonances far away from each other to eliminate any spin coherence effect, and another is to raise the effective resonance crossing rate. A simulation of 100 particles with Gaussian distribution in the vertical phase space was performed with the lower vertical tune path set as shown in Fig. 5.2. The polarization loss after crossing the two weak intrinsic resonances should be reduced to less than 1%.

3. Since the second and third order partial snake resonances in the vicinity of strong intrinsic resonance $36 + \nu_y$ are still strong enough to cause a modest polarization loss, the vertical betatron tune should be pushed as high as possible inside the spin tune gap. In the AGS 2006 polarized proton run, the vertical tunes have been pushed above 8.98 after $G\gamma = 7.5$, even beyond 8.99 at $36 + \nu_y$ strong intrinsic resonance position in order to preserve the polarization.
4. When the vertical tune is above 8.99 at $36 + \nu_y$ that is close to the imperfection resonance at $G\gamma = 45$, the associated large orbit distortion can contribute to polarization loss as described in Chapter 4. The depolarization due to the closed orbit distortions can be eliminated with harmonic orbit correction. Local bumps at $G\gamma = 36 + \nu_y$ have been used to correct the orbit distortion. As long as the $\sin 9\theta$ harmonic orbit amplitude is less than 3 mm, polarization is preserved.

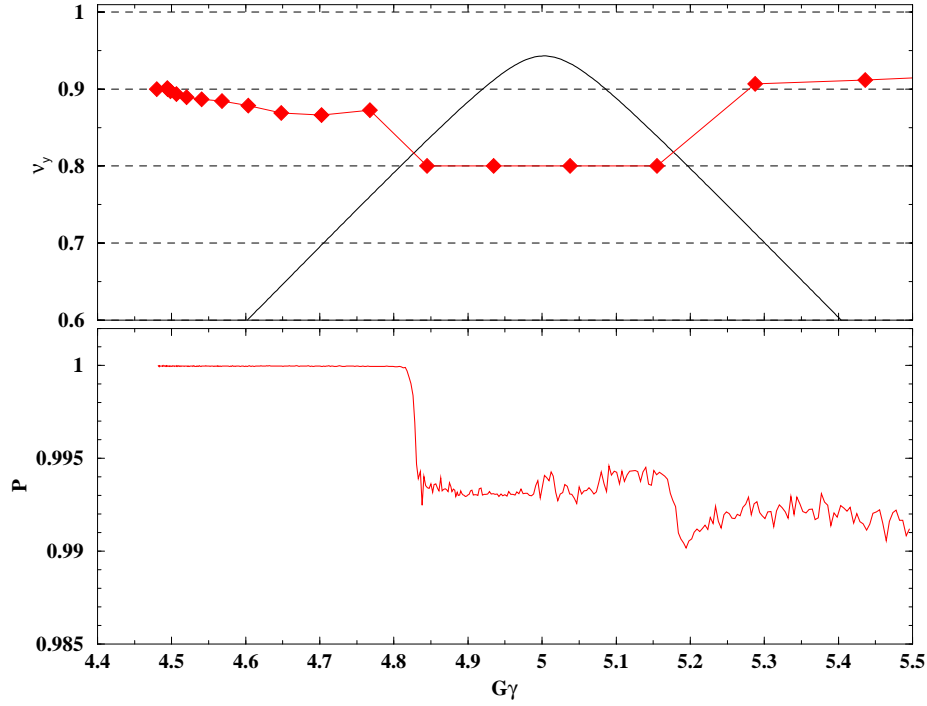


Figure 5.2: Spin tracking of 100 particles with Gaussian distribution in the vertical phase space. The normalized rms vertical emittance was set at 2.5π mm-mrad, and zero for the horizontal emittance. The upper plot is the vertical tune path. The bottom plot is the tracking result, which shows significantly less depolarization comparing to Fig.4.8.

Appendix A

Transverse and Longitudinal Component of Magnetic Field with Respect to the Beam Direction

The particle motion in an accelerator can be expressed in the Frenet-Serret coordinate system $(\hat{x}, \hat{s}$ and $\hat{y})$ as

$$\vec{r} = \vec{r}_0(s) + x\hat{x} + y\hat{y}. \quad (\text{A.1})$$

Here ρ is the local radius of curvature of the reference orbit.

Then the velocity and the derivative of the velocity of a particle is given by

$$\vec{v} = \frac{d\vec{r}}{dt} = \frac{ds}{dt} [x' \hat{x} + (1 + \frac{x}{\rho}) \hat{s} + y' \hat{y}] \approx v(x' \hat{x} + \hat{s} + y' \hat{y}), \quad (\text{A.2})$$

$$\vec{v}' = v[(x'' - \frac{1}{\rho}) \hat{x} + \frac{x'}{\rho} \hat{s} + y'' \hat{y}]. \quad (\text{A.3})$$

Here the prime denotes differentiation with respect to the coordinate s . The magnitude of the particle velocity is

$$v = \frac{ds}{dt} [(1 + \frac{x}{\rho})^2 + x'^2 + y'^2]^{1/2} \approx \frac{ds}{dt} (1 + \frac{x}{\rho}), \quad (\text{A.4})$$

A. Transverse and Longitudinal Component of Magnetic Field with Respect to the Beam Direction

86
and

$$\frac{ds}{dt} = \frac{v}{(1 + \frac{x}{\rho})}. \quad (\text{A.5})$$

Using the relation

$$m\gamma \frac{d\vec{v}}{dt} = e\vec{v} \times \vec{B}, \quad B\rho = \frac{\gamma mv}{e}, \quad (\text{A.6})$$

we have

$$\begin{aligned} \vec{B}_\perp &= \frac{1}{v^2}(\vec{v} \times \vec{B}) \times \vec{v} = \frac{1}{v^2} \frac{m\gamma}{e} \frac{d\vec{v}}{dt} \times \vec{v} = \frac{1}{v^2} \frac{m\gamma}{e} \frac{ds}{dt} \frac{d\vec{v}}{ds} \times \vec{v} \\ &= \frac{1}{v^2} \frac{m\gamma}{e} \frac{v}{(1 + \frac{x}{\rho})} v^2 [(x'' - \frac{1}{\rho})\hat{x} + \frac{x'}{\rho}\hat{s} + y''\hat{y}] \times [v(x'\hat{x} + \hat{s} + y'\hat{y})] \\ &= B\rho(1 - \frac{x}{\rho})[(x'' - \frac{1}{\rho})\hat{y} - (x'' - \frac{1}{\rho})y'\hat{s} + \frac{x'y'}{\rho}\hat{x} - \frac{x'^2}{\rho}\hat{y} + y''x'\hat{s} - y''\hat{x}] \\ &\approx B\rho(1 - \frac{x}{\rho})[(x'' - \frac{1}{\rho})\hat{y} + \frac{1}{\rho}y'\hat{s} - y''\hat{x}]. \end{aligned} \quad (\text{A.7})$$

Here the high order terms have been ignored.

The contribution to longitudinal component of magnetic field come from two sources: one is from the variance of radius curvature and the other from the vertical orbit. Since the dipole guide field is given by $B_z = -\frac{B\rho}{\rho}$, the magnetic field parallel to the particle orbital direction is given by

$$\vec{B}_\parallel = (B_s + y'B_y)\hat{s} = (-B\rho y(\frac{1}{\rho})' - y'\frac{B\rho}{\rho})\hat{s} = -B\rho(\frac{y}{\rho})'\hat{s} \quad (\text{A.8})$$

Appendix B

Effective Froissart-Stora Formula for a Gaussian Distribution Beam

Given a beam bunch has Gaussian distribution

$$\rho(I) = \frac{1}{2I_0} e^{-\frac{I}{2I_0}}, \quad (\text{B.1})$$

and the intrinsic resonance strength is proportional to the square root of the particle emittance I

$$|\epsilon(I)|^2 = |\epsilon(I_0)|^2 \frac{I}{I_0}, \quad (\text{B.2})$$

88 B. Effective Froissart-Stora Formula for a Gaussian Distribution Beam

where I_0 is the rms emittance of the beam, $\epsilon(I_0)$ is the rms value of resonance strength, the polarization after passing through a resonance is given by

$$\begin{aligned}
 \langle \frac{P_f}{P_i} \rangle &= \int_0^\infty [2e^{-\frac{\pi|\epsilon|^2}{2\alpha}} - 1] \rho(I) dI \\
 &= \int_0^\infty [2e^{-\frac{\pi|\epsilon(I_0)|^2}{2\alpha} \frac{I}{I_0}} - 1] \frac{1}{2I_0} e^{-\frac{I}{2I_0}} dI \\
 &= \frac{1}{2I_0} \left[\int_0^\infty 2e^{-(\frac{\pi|\epsilon(I_0)|^2}{\alpha} + 1) \frac{I}{2I_0}} dI - \int_0^\infty e^{-\frac{I}{2I_0}} dI \right] \\
 &= \frac{1}{2I_0} \left[2 \frac{-2I_0}{1 + \frac{\pi|\epsilon(I_0)|^2}{\alpha}} e^{-(\frac{\pi|\epsilon(I_0)|^2}{\alpha} + 1) \frac{I}{2I_0}} \Big|_0^\infty + 2I_0 e^{-\frac{I}{2I_0}} \Big|_0^\infty \right] \\
 &= \frac{-2}{1 + \frac{\pi|\epsilon(I_0)|^2}{\alpha}} (0 - 1) + (0 - 1) \\
 &= \frac{1 - \frac{\pi|\epsilon(I_0)|^2}{\alpha}}{1 + \frac{\pi|\epsilon(I_0)|^2}{\alpha}} \tag{B.3}
 \end{aligned}$$

Appendix C

Spinor Equation

The spin vector \vec{S} with three components (S_1, S_2, S_3) can be expressed by a two-component spinor Ψ as

$$S_i = \langle \Psi | \sigma_i | \Psi \rangle = \Psi^\dagger \sigma_i \Psi, \quad (\text{C.1})$$

where σ_i , $i = 1, 2, 3$ are the Pauli matrices.

Assume the spinor satisfies the Hamiltonian equation:

$$\frac{d\Psi}{d\theta} = -\frac{i}{2}H\Psi, \quad \frac{d\Psi^\dagger}{d\theta} = \frac{i}{2}\Psi^\dagger H, \quad (\text{C.2})$$

where H is a Hermitian operator satisfying $H = H^\dagger$, then

$$\begin{aligned} \frac{dS_i}{d\theta} &= \frac{d\Psi^\dagger}{d\theta} \sigma_i \Psi + \Psi^\dagger \sigma_i \frac{d\Psi}{d\theta} \\ &= \frac{i}{2} \Psi^\dagger (H \sigma_i - \sigma_i H) \Psi \\ &= \frac{i}{2} \Psi^\dagger [H, \sigma_i] \Psi. \end{aligned} \quad (\text{C.3})$$

Since any 2×2 unitary matrix can be expressed as a linear combination of the three Pauli matrices as

$$\frac{d\Psi}{d\theta} = -i\frac{\lambda}{2}(\vec{\sigma} \cdot \hat{n})\Psi, \quad (\text{C.4})$$

where \hat{n} is a unit vector and λ is a θ independent factor, it has $H = \lambda(\vec{\sigma} \cdot \hat{n})$. Then

Eq.(C.3) is rewritten as

$$\frac{dS_i}{d\theta} = \frac{i}{2}\Psi^\dagger[\lambda(\vec{\sigma} \cdot \hat{n}), \sigma_i]\Psi = \frac{i}{2}\lambda\Psi^\dagger[\vec{\sigma} \cdot \hat{n}, \sigma_i]\Psi. \quad (\text{C.5})$$

With the relationships

$$\begin{aligned} \sigma_i \sigma_j &= 1, \quad \text{for } i = j; \\ \sigma_i \sigma_j &= i\epsilon_{ijk}\sigma_k, \quad \text{for } i \neq j, \end{aligned}$$

we have

$$\begin{aligned} [\sigma_i, \sigma_j n_j] &= [\sigma_i, \sigma_j] n_j = 0, \quad i = j; \\ [\sigma_i, \sigma_j n_j] &= [\sigma_i, \sigma_j] n_j = 2i\epsilon_{ijk} n_j \sigma_k = 2i(\hat{n} \times \vec{\sigma})_i, \quad i \neq j. \end{aligned}$$

Then Eq.(C.5) becomes

$$\frac{dS_i}{d\theta} = \frac{i}{2}\lambda\Psi^\dagger[2i(\hat{n} \times \vec{\sigma})]\Psi = (\lambda\hat{n} \times \Psi^\dagger \vec{\sigma} \Psi)_i = (\lambda\hat{n} \times \vec{S})_i = (\vec{S} \times (-\lambda\vec{n}))_i. \quad (\text{C.6})$$

Comparing with $\frac{d\vec{S}}{d\theta} = \vec{S} \times \vec{F}$ (Eq. (2.8)) , we can obtain

$$\vec{F} = -\lambda\hat{n}, \quad H = -\vec{\sigma} \cdot \vec{F}. \quad (\text{C.7})$$

Therefore, the spinor equation is

$$\begin{aligned} \frac{d\Psi}{d\theta} &= -\frac{i}{2}H\Psi = \frac{i}{2}\vec{\sigma} \cdot \vec{F}\Psi \\ &= -\frac{i}{2}[G\gamma\sigma_3 - F_2\sigma_2 - F_1\sigma_1]\Psi \\ &= -\frac{i}{2} \begin{pmatrix} G\gamma & F_1 - iF_2 \\ -(F_1 + iF_2) & -G\gamma \end{pmatrix} \Psi \\ &= -\frac{i}{2} \begin{pmatrix} G\gamma & \xi \\ -\xi^* & -G\gamma \end{pmatrix} \Psi. \end{aligned} \quad (\text{C.8})$$

Appendix D

Horizontal Component of the Stable Spin Direction

Considering two partial snakes separated by $1/3$ of the ring with χ_c and χ_w spin rotation angles respectively, the OTM is given by

$$T = e^{-i\frac{1}{2}G\gamma(2\pi-\frac{2\pi}{3}-\theta)\sigma_3} e^{-i\frac{\chi_w}{2}\sigma_2} e^{-i\frac{1}{2}G\gamma\frac{2\pi}{3}\sigma_3} e^{-i\frac{\chi_c}{2}\sigma_2} e^{-i\frac{1}{2}G\gamma\theta\sigma_3}, \quad (\text{D.1})$$

where θ is the orbital angle between the measurement location and the χ_c partial snake.

With the algebraic relations of the Pauli matrices

$$\begin{aligned} \sigma_i \sigma_j &= 1, \quad \text{for } i = j; \\ \sigma_i \sigma_j &= i\epsilon_{ijk}\sigma_k, \quad \text{for } i \neq j \end{aligned}$$

and

$$e^{-i\frac{\vec{\sigma}\cdot\vec{b}}{2}} = I \cos \frac{b}{2} - i\vec{\sigma} \cdot \hat{n} \sin \frac{b}{2} \quad (b = |\vec{b}|, \hat{n} = \frac{\vec{b}}{b}),$$

we have

$$\begin{aligned}
e^{-i\frac{G\gamma\theta}{2}\sigma_3} &= I \cos \frac{G\gamma\theta}{2} - i\sigma_3 \sin \frac{G\gamma\theta}{2}, \\
e^{-i\frac{\chi_c}{2}\sigma_2} &= I \cos \frac{\chi_c}{2} - i\sigma_2 \sin \frac{\chi_c}{2}, \\
e^{-i\frac{G\gamma\theta}{2}\frac{2\pi}{3}\sigma_3} &= I \cos \frac{G\gamma}{2}\frac{2\pi}{3} - i\sigma_3 \sin \frac{G\gamma}{2}\frac{2\pi}{3}, \\
e^{-i\frac{\chi_w}{2}\sigma_2} &= I \cos \frac{\chi_w}{2} - i\sigma_2 \sin \frac{\chi_w}{2}, \\
e^{-i\frac{G\gamma\theta}{2}(2\pi-\frac{2\pi}{3}-\theta)\sigma_3} &= I \cos \frac{G\gamma\theta}{2}(2\pi-\frac{2\pi}{3}-\theta) - i\sigma_3 \sin \frac{G\gamma\theta}{2}(2\pi-\frac{2\pi}{3}-\theta).
\end{aligned} \tag{D.2}$$

Multiplying all of the terms in Eq.(D.2) in order, the OTM becomes

$$\begin{aligned}
T = & \cos \frac{\chi_c}{2} \cos \frac{\chi_w}{2} \cos G\gamma - \sin \frac{\chi_c}{2} \sin \frac{\chi_w}{2} \cos \frac{\pi}{3} G\gamma - \\
& i\sigma_3 [\cos \frac{\chi_c}{2} \cos \frac{\chi_w}{2} \sin G\gamma - \sin \frac{\chi_c}{2} \sin \frac{\chi_w}{2} \sin \frac{\pi}{3} G\gamma] - \\
& i\sigma_2 [\sin \frac{\chi_c}{2} \cos \frac{\chi_w}{2} \cos (\theta - \pi) G\gamma - \cos \frac{\chi_c}{2} \sin \frac{\chi_w}{2} \cos (\frac{\pi}{3} - \theta) G\gamma] + \\
& i\sigma_1 [\sin \frac{\chi_c}{2} \cos \frac{\chi_w}{2} \sin (\pi - \theta) G\gamma - \cos \frac{\chi_c}{2} \sin \frac{\chi_w}{2} \sin (\frac{\pi}{3} - \theta) G\gamma].
\end{aligned} \tag{D.3}$$

The OTM expressed as a 2×2 matrix is then

$$T = \begin{pmatrix} A & B \\ C & D \end{pmatrix}, \tag{D.4}$$

where A, B, C, D are

$$\begin{aligned}
A &= \cos \frac{\chi_c}{2} \cos \frac{\chi_w}{2} e^{-iG\gamma} - \sin \frac{\chi_c}{2} \sin \frac{\chi_w}{2} e^{-i\frac{\pi}{3}G\gamma}, \\
B &= \sin \frac{\chi_c}{2} \cos \frac{\chi_w}{2} e^{i(\pi-\theta)G\gamma} + \cos \frac{\chi_c}{2} \sin \frac{\chi_w}{2} e^{i(\frac{\pi}{3}-\theta)G\gamma}, \\
C &= \sin \frac{\chi_c}{2} \cos \frac{\chi_w}{2} e^{-i(\pi-\theta)G\gamma} + \cos \frac{\chi_c}{2} \sin \frac{\chi_w}{2} e^{-i(\frac{\pi}{3}-\theta)G\gamma}, \\
D &= \cos \frac{\chi_c}{2} \cos \frac{\chi_w}{2} e^{iG\gamma} - \sin \frac{\chi_c}{2} \sin \frac{\chi_w}{2} e^{i\frac{\pi}{3}G\gamma}.
\end{aligned} \tag{D.5}$$

Identifying the OTM to

$$\begin{aligned}
T &= e^{-i\pi\nu_s \hat{n}_{co} \cdot \vec{\sigma}} = I \cos \pi\nu_s - i\vec{\sigma} \cdot \hat{n}_{co} \sin \pi\nu_s \\
&= I \cos \pi\nu_s - i(\sigma_1 \cos \Psi_1 + \sigma_2 \cos \Psi_2 + \sigma_3 \cos \Psi_3) \sin \pi\nu_s \\
&= \begin{pmatrix} \cos \pi\nu_s - i \cos \Psi_3 \sin \pi\nu_s & -i(\cos \Psi_1 - i \cos \Psi_2) \sin \pi\nu_s \\ -i(\cos \Psi_1 + i \cos \Psi_2) \sin \pi\nu_s & \cos \pi\nu_s + i \cos \Psi_3 \sin \pi\nu_s \end{pmatrix}
\end{aligned} \tag{D.6}$$

where ν_s represents the spin tune, $(\cos \alpha_1, \cos \alpha_2, \cos \alpha_3)$ are the stable spin direction \hat{n}_{co} directional cosines along the radially outward, longitudinally forward and vertically transverse axes respectively.

Finally, we can get the expression of spin tune and spin stable spin direction with the two partial snakes as

$$\nu_s = \frac{1}{\pi} \arccos \left(\cos \frac{\chi_c}{2} \cos \frac{\chi_w}{2} \cos [G\gamma\pi] - \sin \frac{\chi_c}{2} \sin \frac{\chi_w}{2} \cos [G\gamma \frac{\pi}{3}] \right), \quad (D.7)$$

$$\cos \alpha_1 = \frac{-1}{\sin \pi \nu_s} \left(\cos \frac{\chi_w}{2} \sin \frac{\chi_c}{2} \sin [G\gamma(\pi - \theta)] + \sin \frac{\chi_w}{2} \cos \frac{\chi_c}{2} \sin [G\gamma(\frac{\pi}{3} - \theta)] \right), \quad (D.8)$$

$$\cos \alpha_2 = \frac{1}{\sin \pi \nu_s} \left(\cos \frac{\chi_w}{2} \sin \frac{\chi_c}{2} \cos [G\gamma(\pi - \theta)] + \sin \frac{\chi_w}{2} \cos \frac{\chi_c}{2} \cos [G\gamma(\frac{\pi}{3} - \theta)] \right), \quad (D.9)$$

$$\cos \alpha_3 = \frac{1}{\sin \pi \nu_s} \left(\cos \frac{\chi_w}{2} \cos \frac{\chi_c}{2} \sin [G\gamma\pi] - \sin \frac{\chi_w}{2} \sin \frac{\chi_c}{2} \sin [G\gamma \frac{\pi}{3}] \right). \quad (D.10)$$

Appendix E

Spin Rotation for Spin Tracking

Start from the BMT equation:

$$\frac{d\vec{S}}{dt} = \frac{e}{m\gamma} \vec{S} \times \vec{F}, \quad (\text{E.1})$$

where

$$\vec{F} = (1 + G\gamma)\vec{B}_\perp + (1 + G)\vec{B}_\parallel + (G\gamma + \frac{\gamma}{\gamma + 1})\frac{\vec{E} \times \vec{\beta}}{c}. \quad (\text{E.2})$$

Assuming $\vec{E} = 0$ for the negligible electric field in the machine and the convenience of discussion, express the components of magnetic field \vec{B}_\perp and \vec{B}_\parallel in terms of magnetic field \vec{B} as

$$\vec{B}_\perp = \frac{1}{v^2}(\vec{v} \times \vec{B}) \times \vec{v} \quad (\text{E.3})$$

and

$$\vec{B}_\parallel = \frac{1}{v^2}(\vec{v} \cdot \vec{B})\vec{v}. \quad (\text{E.4})$$

Then the \vec{F} vector becomes

$$\begin{aligned}
\vec{F} &= (1 + G\gamma)\vec{B}_\perp + (1 + G)\vec{B}_\parallel \\
&= (1 + G\gamma)\frac{1}{v^2}(\vec{v} \times \vec{B}) \times \vec{v} + (1 + G)\frac{1}{v^2}(\vec{v} \cdot \vec{B})\vec{v} \\
&= (1 + G\gamma)\frac{1}{v^2}[(\vec{v} \cdot \vec{v})\vec{B} - (\vec{v} \cdot \vec{B})\vec{v}] + (1 + G)\frac{1}{v^2}(\vec{v} \cdot \vec{B})\vec{v} \\
&= (1 + G\gamma)\frac{\vec{v} \cdot \vec{v}}{v^2}\vec{B} - (1 + G\gamma)(\vec{v} \cdot \vec{B})\vec{v} + (1 + G)\frac{1}{v^2}(\vec{v} \cdot \vec{B})\vec{v} \\
&= (1 + G\gamma)\vec{B} - G(\gamma - 1)(\vec{v} \cdot \vec{B})\vec{v}.
\end{aligned} \tag{E.5}$$

Because of

$$\vec{v} = \frac{d\vec{r}}{dt} = \frac{ds}{dt}[x'\hat{x} + (1 + \frac{x}{\rho})\hat{s} + y'\hat{y}], \tag{E.6}$$

the amplitude of the velocity of the particle is

$$v = \frac{ds}{dt}[x'^2 + (1 + \frac{x}{\rho})^2 + y'^2]^{1/2}. \tag{E.7}$$

Therefore, the differentiation with respect to the coordinate t can be transformed to the differentiation with respect to s by

$$\frac{d}{dt} = \frac{d}{ds} \frac{v}{\sqrt{x'^2 + y'^2 + (1 + x/\rho)^2}}. \tag{E.8}$$

Using Eq.(E.8) and

$$\frac{e}{m\gamma} = \frac{v}{B\rho} \tag{E.9}$$

Eq.(E.1) becomes

$$\frac{d\vec{S}}{ds} = \vec{S} \times \vec{w}, \tag{E.10}$$

with

$$\vec{w} = \frac{h}{B\rho}[(1 + G\gamma)\vec{B} - G(\gamma - 1)(\vec{r}' \cdot \vec{B})\vec{r}'], \tag{E.11}$$

where $h = \sqrt{x'^2 + y'^2 + (1 + x/\rho)^2}$ and $\vec{r}' = \frac{\vec{v}}{v}$.

Expressing Eq.(E.11) in terms of three components, we have

$$\begin{aligned}
S'_x &= w_s S_y - (w_y - \frac{1}{\rho})S_s \\
S'_y &= w_x S_s - w_s S_x \\
S'_s &= (w_y - \frac{1}{\rho})S_x - w_x S_y.
\end{aligned} \tag{E.12}$$

The system generates three identical linear equation for the three components of the spin

$$S''' + w_0^2 S' = 0, \quad (\text{E.13})$$

where $w_0^2 = w_x^2 + (w_y - \frac{1}{\rho})^2 + w_s^2$. The general solution of Eq.(E.13) is

$$S = C_1 + C_2 \cos w_0 \delta s + C_3 \sin w_0 \delta s. \quad (\text{E.14})$$

Here δs is the orbit length along the reference orbit, C_1, C_2, C_3 are the constants that can be obtained as a function of the initial values of the three components of the spin using the original and second derivative system. The spin transfer matrix is given by

$$S_T = \begin{pmatrix} 1 - (a_2^2 + a_3^2)Cs & a_1 a_2 Cs + a_3 Sn & a_1 a_3 Cs - a_2 Sn \\ a_2 a_1 Cs - a_3 Sn & 1 - (a_1^2 + a_3^2)Cs & a_2 a_3 Cs + a_1 Sn \\ a_3 a_1 Cs + a_2 Sn & a_3 a_2 Cs - a_1 Sn & 1 - (a_1^2 + a_2^2)Cs \end{pmatrix}. \quad (\text{E.15})$$

Here

$$a_1 = \frac{w_x}{w_0}, \quad a_2 = \frac{w_y - 1/\rho}{w_0}, \quad a_3 = \frac{w_s}{w_0}, \quad (\text{E.16})$$

and

$$Cs = 1 - \cos w_0 \delta s, \quad Sn = \sin w_0 \delta s. \quad (\text{E.17})$$

Bibliography

- [1] Ya.S.Derbenev and A.M.Kondratenko, Dokl. Akad. Nauk SSSR 223, 830, (1975);
Sov. Phys. Dokl. 20, 562 (1976).
- [2] T.Roser, AIP Conference Proceedings, 187, 1442 (1988).
- [3] H.Huang et al., Phys. Rev. Lett. 73, 2982 (1994).
- [4] H.Huang, Ph.D. Thesis, Indiana University (1995).
- [5] T.Roser, et al., Proceedings of EPAC 2004 p.1577, Lucerne, Switzerland (2004);
T.Roser, et al., Proceedings of SPIN 2004 p.687, Trieste, Italy (2004).
- [6] E.Willen et al., Proceedings of PAC 2005 p.2935, Knoxville, Tennessee (2005).
- [7] J.Takano et al., Journal of Instrumentation, 1, 11002 (2006).
- [8] F.Lin et al., Phys. Rev. STAB 10, 044001 (2007).
- [9] L.H.Thomas, Phil. Mag. 3, 1 (1927) ; V.Bargmann, L.Michel, V.L.Telegdi, Phys.
Rev. Lett. 2, 435 (1956).
- [10] S.Y.Lee, *Spin Dynamics and Snakes in Synchrotrons*, Singapore: World Scientific (1997).
- [11] E.D.Courant and R.Ruth, BNL report, BNL-51270 (1980).

-
- [12] E.D.Courant, S.Y.Lee and S.Tepikian p.174 and S.Y.Lee p 189 in Proc. of Workshop on Polarized Beam at SSC, AIP Conf. Proc. No.145 p.174 (AIP, N.Y., 1985).
 - [13] M.Froissart and R.Stora, Nucl.Inst.Meth. 7, 297 (1960).
 - [14] A.Zelenski, et al., Proc. of the 9th Inter. Conf. on Ion Sources, Rev. Sci. Inst., Vol. 73, No.2, p.888 (2002)
 - [15] F.Z.Khiari et al., Phys. Rev. D80, 45 (1989).
 - [16] M.Bai et al., Phys. Rev. Lett. 80, 4673 (1998).
 - [17] M.Bai, Ph.D. Thesis, Indiana University (1999).
 - [18] V.I.Ptitsyn and Yu.M.Shatunov, Proc. 3rd Workshop on Siberian Snake and Spin Rotators, BNL (1994)
 - [19] T.Roser et al., AGS/RHIC/SN-72/BNL (1998)
 - [20] E.D.Courant, SPIN2002 15th International Spin Physics Symposium, AIP Con. Proc., No. 675 p.799 (2002)
 - [21] A.U.Luccio and T.Roser BNL/C-AD/AP/167 (2004)
 - [22] VECTOR FIELDS, LTD: Opera-3d Reference Manual. Technical report, England, January 2002
 - [23] A.U.Luccio, Technical Report AGS/RHIC/SN No.03 BNL (1996)
 - [24] J.P.Blewett and R.Chasman, Journal of Appl. Phys., 48, 2692 (1977)
 - [25] A.U.Luccio, KEK Report 2005-11, January 2006 A (2006)
 - [26] J.J.Wood, Ph.D. Thesis, University of California Los Angeles (2005)

- [27] G.G.Ohlsen and P.W.Keaton,Jr., Nucl. instrum. Methods, 109, 41 (1973)
- [28] H.Spinka et al., C-A/AP/108, BNL (2003)
- [29] J.Tojo et al., Phys. Rev. Lett., 89, 052302 (2002)
- [30] F.Lin et al., Proc. of 2007 Particle Accelerator Conference p.3534, Albuquerque, New Mexico, USA (2007)
- [31] R.A.Phelps, et al., Phys. Rev. Lett., 78, 2772 (1997)
- [32] V.H.Ranjbar, et al., Phys. Rev. Lett., 91, 03480 (2003)
- [33] H.Huang et al., accepted by Phys. Rev. Lett. (2007)
- [34] A.U.Luccio, BNL/AGS/AD/96-1 (1995); A.U.Luccio, Proceedings of the Adriatico Research Conference on Trends in Collider Spin Physics p.235 Trieste, Italy (1995).
- [35] A.U.Luccio, C-A/AP/283, BNL (2007)
- [36] F.C.Iselin, Report No. CERN/SL/92 (1994)
- [37] V.H.Ranjbar, Ph.D. Thesis, Indiana University (2002)
- [38] S.Tepikian, Ph.D. Thesis, State University of New York at Stony Brook (1986)
- [39] S.Y.Lee and S.Tepikian, Phys. Rev. Lett., 56, 1635 (1986)
- [40] H.Huang, RHIC Retreat 2007, BNL (2007)
- [41] Discussion in Spin Meeting at BNL CAD (2007)

CURRICULUM VITAE

Fanglei Lin

Physics Department, Indiana University
729 E 3rd Street, Bloomington, IN 47405
Email: linf@indiana.edu

• EDUCATION

DEGREE	MAJOR	INSTITUTION
Ph.D. (08/2007)	Accelerator Physics	Indiana University
M.S. (08/2005)	Accelerator Physics	Indiana University
M.S. (08/2003)	Optics Physics	U of Sci.&Tech. of China
B.S. (08/2000)	Physics	Shandong Normal Uni.

• RESEARCH

Brookhaven National Lab Collider-Accelerator Department 2004-2007

- Hands-on experience with acceleration operation. Have taken many shifts for AGS/RHIC setup and commissioning. Focused on increasing the polarization of the polarized proton by varying the tune, orbit and chromaticity.
- Revised the spin tracking program SPINK, carried out lots of spin trackings with the AGS operation lattice parameters.
- Focused on one project to explore of the horizontal intrinsic resonance in AGS with numerical simulation, theoretical calculation and experiment.
- Investigated the polarization drop in the AGS due to other causes: residual vertical intrinsic resonance, partial snake resonance, closed orbit distortion.
- Attended the theoretical derivation of the dispersion in NSLS II partially.

- **EXPERIENCE**

Dissertation TOWARDS FULL PRESERVATION OF POLARIZATION OF PROTON BEAM IN THE AGS 2007

Research Assistant Brookhaven National Laboratory 2005-2007

- Machine Operation: Shift trainee in RHIC Run2005; Shift leader in AGS Run2006.
- Exploration of Spin Horizontal Intrinsic Resonance of the Polarized Proton in the AGS and toward full preservation of polarization of proton beam in the AGS

Teaching Assistant Indiana University 2003-2004

Course: General Physics

Research Assistant U. of Science & Technology of China 2001-2003

Dissertation: Theoretical Study of Photonic Crystal

Teaching Assistant U. of Science & Technology of China 2000-2001

Course: Optics Physics

- **PUBLICATIONS**

- H.Huang, L.A.Ahrens, M.Bai, K.A.Brown, E.D.Courant, C.Gardner, J.W.Glenn, F.Lin, A.U.Luccio, W.W.MacKay, M.Okamura, V.Ptitsyn, T.Roser, J.Takano, S.Tepikian, N.Tsoupas, A.Zelenski, K.Zeno, “Overcoming Depolarizing Resonances with Dual Partial Helical Siberian Snakes”, Physical Review Letters, 99, 154801 (2007)
- F.Lin, L.A.Ahrens, M.Bai, K.A.Brown, E.D.Courant, C.Gardner, J.W.Glenn, H.Huang, S.Y.Lee, A.U.Luccio, W.W.MacKay, V.Ptitsyn, T.Roser, J.Takano, S.Tepikian, N.Tsoupas, A.Zelenski, K.Zeno, “Exploration of Horizontal In-

- trinsic Spin Resonances with Two Partial Siberian Snakes”, Physical Review Special Topics - Accelerators and Beams, 10, 044001 (2007)
- F.Lin, L.A.Ahrens, M.Bai, K.A.Brown, E.D.Courant, C.Gardner, J.W.Glenn, H.Huang, S.Y.Lee, A.U.Luccio, W.W.MacKay, T.Roser, N.Tsoupas, “Investigation of Residual Vertical Intrinsic Resonances with Dual Partial Siberian Snakes in the AGS”, Proceedings of 2007 Particle Accelerator Conference p.3534, Albuquerque, New Mexico, USA (2007)
 - F.Lin, W.Guo, Samuel Krinsky, “Dispersion Tolerance calculation for NSLS-II”, Proceedings of 2007 Particle Accelerator Conference p.1341, Albuquerque, New Mexico, USA (2007)
 - H.Huang, L.A.Ahrens, M.Bai, K.A.Brown, C.Gardner, J.W.Glenn, F.Lin, A.U.Luccio, W.W.MacKay, T.Roser, S.Tepikian, N.Tsoupas, K.Yip, K.Zeno, “Overcoming Depolarizing Resonances in the AGS with Two Helical Partial Siberian Snakes”, Proceedings of 2007 Particle Accelerator Conference p.748, Albuquerque, New Mexico, USA (2007)
 - H.Huang, L.A.Ahrens, M.Bai, A.Bravar, K.A.Brown, E.D.Courant, C.Gardner, J.W.Glenn, F.Lin, A.U.Luccio, W.W.MacKay, V.Ptitsyn, T.Roser, S.Tepikian, N.Tsoupas, J.Wood, K.Yip, A.Zelenski, K.Zeno, M.Okamura, J.Takano, “Polarized Proton Acceleration in the AGS with Two helical Partial Snakes”, Proceedings of the 17th International Spin Physics Symposium SPIN2006 Conference, Kyoto, Japan (2006)
 - H.Huang, L.A.Ahrens, M.Bai, A.Bravar, K.A.Brown, E.D.Courant, C.Gardner, J.W.Glenn, F.Lin, A.U.Luccio, W.W.MacKay, V.Ptitsyn, T.Roser, S.Tepikian, N.Tsoupas, J.Wood, K.Yip, A.Zelenski, K.Zeno, M.Okamura, J.Takano, “Acceleration of Polarized Protons in the AGS with Two helical Partial Snakes”, Proceedings of 2006 European Particle Accelerator Conference p.273, Edinburgh, UK (2006)

- H.Huang, L.A.Ahrens, M.Bai, K.A.Brown, E.D.Courant, C.Gardner, J.W.Glenn, R.C.Gupta, F.Lin, A.U.Luccio, W.W.MacKay, V.Ptitsyn, T.Roser, S.Tepikian, N.Tsoupas, E.Willen, A.Zelenski, K.Zeno, M.Okamura, J.Takano, “Acceleration of Polarized Protons in the AGS with Two helical Partial Snakes”, Proceedings of 2005 Particle Accelerator Conference p.1404, Knoxville, Tennessee, USA (2005)
- M.Bai, H.Huang, W.W.MacKay, V.Pitisyn, T.Roser, S.Tepikian, S.Y.Lee, F.Lin, “Observations of Snake Resonance in RHIC”, Proceedings of 2005 Particle Accelerator Conference p.2839, Knoxville, Tennessee, USA (2005)

• **PRESENTATION**

“Exploration of Horizontal Intrinsic Spin Resonances in the AGS”, 2006 APS April Meeting, Dallas, Texas, USA

• **FELLOWSHIPS AND GRANTS**

PAC2007 Graduate Student Grant

PAC2005 Graduate Student Grant

Indiana University Teaching Fellowship	2004-2005
--	-----------

Indiana University Teaching Fellowship	2003-2004
--	-----------

• **AWARDS AND HONORS**

PAC2007 Student Poster Award Winner (sponsored by IEEE-NPSS)	2007
--	------

Indiana University Award \$5000	2004-2005
---------------------------------	-----------

Indiana University Award \$5000	2003-2004
---------------------------------	-----------

Shandong Normal University “Excellent Student”	1998-1999
--	-----------

Shandong Normal University “Excellent Student”	1997-1998
--	-----------

Shandong Normal University “The Second-class Scholarship”	1998-1999
---	-----------

Shandong Normal University “The First-class Scholarship”	1997-1998
Shandong Normal University “The Second-class Scholarship”	1996-1997